Fakultät für Medizin

der Technischen Universität München

Interconnection of the metabolic syndrome and allergic lung inflammation through changes in thermogenic adipocytes

Ruth Karlina

Vollständiger Abdruck der von der Fakultät für Medizin der Technischen Universität München zur Erlangung des akadamischen Grades eines Doktors der Naturwissenschaften (Dr. rer. nat) genehmigten Dissertation.

Vorsitzender: Prof. Dr. Carsten Schmidt-Weber

Prüfer der Dissertation: 1. TUM Junior Fellow Dr. Siegfried Ussar

2. Prof. Dr. Claudia Traidl-Hoffmann

Die Dissertation wurde am 26.11.2020 bei der Technischen Universität München eingereicht und durch die Fakultät für Medizin am 08.06.2021 angenommen.

Abstract

Energy balance has dominated the conceptual framework of scientific study in obesity throughout the twentieth century. The fundamental thermodynamic law based on energy, that it cannot be destroyed and only can be transferred to another form, has emphasized excessive caloric intake and inadequate physical activity as the main determinant factors leading to obesity. Most obese subjects develop metabolic syndrome, which is implicated in various comorbidities. Asthma is strongly correlated to obesity and metabolic syndrome, and sedentary lifestyle has been detected as one of the triggers to develop allergic asthma, primarily caused by the house dust mite (HDM) allergen. In this work, metabolic syndrome and allergy-induced lung inflammation were simultaneously provoked in order to disentangle the interconnection between two diseases and their implications on each other's conditions. To accomplish this, C57BL/6J wild-type mice were chronically sensitized with HDM intranasally and fed with high fat diet. We found that prolonged exposure to HDM and high fat diet feeding attenuate the progression of both lung inflammation and the metabolic phenotype. These beneficial traits are partly caused by the increase of browning in subcutaneous fat, which contributes to higher energy expenditure and basal metabolic rate. Additionally, obese sensitized mice showed increases in Vegfa and Glut1 expressions, which might contribute to more glucose tolerance. Brown adipose tissue (BAT) is known to play a role in the regulation of body weight and its activation is strongly associated with improved metabolic health. Its health promoting effect is mostly described by Ucp1 via glucose and fatty acid utilization, resulting in heat production. Unfortunately, translation from murine BAT data to humans is limited because of putative differences in cellular composition between species. At room temperature, morphology of murine BAT appears homogeneous, while human BAT consists of a mixture of white and brown adipocytes. However, recently subsets of low and high Ucp1 expressing brown adipocytes were also identified in murine BAT, but the

developmental origin has not been studied. To this end, using single-cell RNA sequencing we observed distinct differentiation stages of brown preadipocyte clusters, but not distinct preadipocyte lineages. Furthermore, 67 brown preadipocyte and adipocyte clones were characterized, with various expressions of brown, beige and white adipocyte marker genes. Statistical and computational analysis of RNA sequencing data from preadipocyte and adipocyte clones identified stable expressed markers distinguishing brown adipocyte lineages. We confirmed the presence of Eif5, Tcf25 and Bin1, distinct gene markers for precursor and brown adipocyte subsets, *in vivo*. Furthermore, Bin1 marks a dormant type of brown adipocyte, since the loss of Bin1 enhances the expression of thermogenic genes and mitochondrial uncoupling in brown adipocytes. In summary, the interconnection between metabolic syndrome and lung allergy inflammation result in browning of subcutaneous fat and increased glucose uptake and creatine synthesis in brown fat. Furthermore, identifying multiple brown adipocyte lineages in murine BAT could ease the translation of murine data to humans.

Zusammenfassung

Das Energiegleichgewicht dominierte den konzeptionellen Rahmen wissenschaftlicher Studien zu Adipositas im 20. Jahrhundert. Das zugrundeliegende thermodynamische Gesetz besagt, dass Energie nicht zerstört, sondern nur in eine andere Form übertragen werden kann. Daraus ergibt sich, dass eine übermäßige Kalorienaufnahme und unzureichende körperliche Aktivität zwangsläufig zu Übergeweicht und Adipositas führt. Die meisten übergewichtigen Personen entwickeln das metabolische Syndrom, welches mit verschiedenen Komorbiditäten in Verbindung gebracht wird. Asthma steht im engen Zusammenhang mit Fettleibigkeit und dem metabolischen Syndrom. Des Weiteren ist ein immobiler Lebensstil einer der Auslöser für die Entwicklung von allergischem Asthma welches hauptsächlich durch Hausstaubmilbenallergene (HDM) verursacht wird. In dieser Arbeit wurden die Interaktion zwischen dem metabolischen Syndrom und einer allergieinduzierten Entzündung der Lunge untersucht, um die Verbindung zwischen den zwei Erkrankungen und ihre Auswirkungen aufeinander zu beschreiben.

Um dies zu erreichen, wurden C57BL/6J Wildtypmäuse chronisch intranasal mit HDM sensibilisiert und einer Hochfettdiät (HFD) ausgesetzt. Eine längere Exposition mit HDM bei gleichzeitiger Fütterung einer HFD schwächte sowohl die Progression der Lungenentzündung als auch des metabolischen Phänotyps ab. Diese vorteilhaften Eigenschaften wurden zum Teil durch die Zunahme von thermogenen Adipozyten im subkutanen Fettgewebe verursacht, was zu einem höheren Energieverbrauch und Grundumsatz beitrug. Darüber hinaus könnte eine stärkere Vaskularisierung im braunen Fettgewebe adipöser allergischer Mäuse zu einer erhöhten Glut1 vermittelten Glukoseaufnahme führen. Es ist bereits bekannt, dass braunes Fettgewebe eine Rolle bei der Regulierung des Körpergewichts spielt und dessen Aktivierung stark mit einer verbesserten metabolischen Gesundheit verbunden ist. Die gesundheitsfördernde Wirkung ist

hauptsächlich auf Ucp1 vermittelte mitochondriale Entkopplung bei Verwendung von Glukose und Fettsäuren zurückzuführen, was zur Wärmeerzeugung führt. Kürzlich wurden Untergruppen von braunen Adipozyten mit niedrigem und hohem Ucp1-Gehalt identifiziert, aber der Ursprung dieser Untergruppen im Laufe der Entwicklung wurde noch nicht untersucht. Dazu beobachteten wir mittels *single-cell RNA* Sequenzierung unterschiedliche Differenzierungsstadien von braunen Preadipozyten, jedoch keine unterschiedlichen Preadipozytenlinien. Darüber hinaus charakterisierten wir 67 braune Preadipozyten- und Adipozytenklone mit heterogener Expressionen von braunen, beigen und weißen Adipozyten-Markern. Die statistische Analyse der RNA-Sequenzierungsdaten identifizierte stabil exprimierte Marker, welche helfen können braune Adipozytenlinien zu unterscheiden. Wir bestätigten *in vivo* das Vorhandensein von Eif5, Tcf25 und Bin1, positiver brauner Adipozyten. Darüber hinaus konnte gezeigt werden, dass Bin1 einen ruhenden Typ brauner Adipozyten markiert, da der Verlust von Bin1 die thermogene Gene expression und die mitochondriale Entkopplung in braunen Adipozyten erhöht. Zusammenfassend lässt sich sagen, dass in den hier untersuchten Modellen die Interaktion zwischen dem metabolischen Syndrom und der Entzündung der Lunge, hervorgerufen durch Allergene, die Pathologien beider Erkrankungen verbesster, wobei dies maßgeblich auf erhöhter thermogener Fettaktivität zurückzuführen ist. Bei der Betrachtung thermogenen Fetts ist jedoch wichtig das dies auch bei Mäusen aus unterschiedlichen braunen Adipozytensubtypen zusammengesetzt ist, was für die Übertragung der Forschungsdaten aus Mäusen auf den Menschen von großer Bedeutung sein kann.

Table of Contents

List of Figures

List of Figures

List of Figures

List of Tables

Abbreviation

Table 1: List of abbreviation

Abbreviation	Meaning
AAMac	Alternatively activated macrophage
ADIPOQ	Adiponectin
ADR	Periadrenal
ADRB	B-adrenergic receptor
BAL	Bronchoalveolar lavage
BAT	Brown adipose tissue
BCAA	Branched-chain amino acid
Bdnf	Brain-derived neurotropic factor
Bin1	Bridging integrator 1
BMI	Body mass index
BMR	Basal metabolic rate
Cidea	Cell death-inducing DEFA-like effector A
CL	CL 316,243
COPD	Chronic obstructive pulmonary disease
CVD	Cardiovascular disease
EE	Energy expenditure
Eif5	Eukaryotic translation initiation factor 5
eNOS	Endothelial nitric oxide synthase
FACS	Fluorescence-activated cell sorting
FFA	Free fatty acids
FKPM	Fragments per kilobase of transcript per million reads mapped
Gamt	Guanidinoacetate N-methyltransferase
Gatm	Glycine amidinotransferase
GEMs	Gene expression modules
Glut1	Glucose transporter 1
Glut4	Glucose transporter 4
GTT	Glucose tolerance test
GWAS	Genome-wide association studies
H&E	Hematoxylin and eosin
HDM	House dust mites
HF	High fat
i.n.	Intranasal
i.p.	Intraperitoneal

Abbreviations

Igf1	Insulin-like growth factor 1
IL-1β	Interleukin 1β
IL-6	Interleukin 6
ILC2s	Type 2 innate lymphoid cells
iNKT	Invariant natural killer T cells
IRS1	Insulin receptor substrate 1
ITT	Insulin tolerance test
IVC	Individually ventilated cages
LF	Low fat
Lxrα	Liver x receptor α
MC4R	Melanocortin 4 receptor
Metrnl	Meteorin-like protein
NAFLD	Non-alcoholic fatty liver disease
Ngf	Nerve growth factor
NHANES	National Health and Nutrition Examination Survey
NK	Natural killer
NKTII	Type II natural killer T cells
Nrg4	Neuregulin 4
Nulp1	Nuclear localized protein 1
OCR	Oxygen consumption rate
ORO	Oil red O
PAS	Periodic acid Schiff
Pdgfra	Platelet-derived growth factor receptor a
Pepck	Phophoenolpyruvate carboxykinase
pgWAT	Perigonadal white adipose tissue
PPARG	Peroxisome proliferator-activated receptor gamma
Ppargc1a	Peroxisome proliferator-activated receptor gamma coactivator 1a
RT qPCR	Real-time quantitative poly chain reaction
SCLV	Supraclavicular
scRNAseq	Single-cell RNA sequencing
SCT	Subcutaneous
scWAT	Subcutaneous white adipose tissue
SNPs	Single nucleotide polymorphisms
SVF	Stromal vascular fraction
T2DM	Type 2 diabetes mellitus
Tbp	TATA-binding protein
Tcf25	Transcription factor 25
Tmem26	Transmembrane 26

Abbreviations

Tnfa	Tumor necrosis factor a
Tregs	Regulatory T cells
UCP	Uncoupling protein
Vegf	Vascular endothelial growth factor
WAT	White adipose tissue
WHO	World Health Organization

1. Introduction

1.1 Obesity & metabolic syndrome: a problem of energy imbalance

The first law of thermodynamic says, “Energy cannot be created or destroyed, it can only be transformed from one form to another”. For human physiology this means that excessive caloric intake and insufficient physical activity result in weight gain and obesity [1, 2]. In other words, obesity is a disease of energy imbalance, in which the amount of energy intake is greater than the energy expended, thus resulting in weight gain [2].

Food, as the source of human energy intake, is mostly affected by its availability, accessibility and type. In this modern era of the 21st century, the price of food relative to income has declined [3]. Moreover, the availability and access to food has improved, in turn promoting weight gain [4]. In part, obesity has resulted from changes in caloric quantity and quality of food. This is often related to an industrialized food system that has produced and marketed convenient and highly processed foods. Such foods are mostly calorie-dense meals and engineered to have appetite-driving properties, which contain high fat, salt, refined sugar and additives with low fiber [5]. Since 1997, it is known that high fat foods are associated with a positive palatability, thus overconsumption often occurs [6]. A 17-year longitudinal study from 1991-2008, including more than 2,700 adults, showed an increase in the proportion of energy intake coming from fat [7], which was in parallel with a significant increase in the prevalence of obesity in this population [8]. Therefore, this behavior overtime will lead to obesity.

Exposure during early life stages to the causal factors, leads to childhood obesity, which is a major risk in developing metabolic syndrome in adulthood [9]. Metabolic syndrome often occurs as a consequence of obesity, characterized by glucose intolerance, hyperinsulinemia, hypertension and hyperlipidemia [10, 11]. These

abnormalities are often linked to insulin resistance and found in subjects with abdominal obesity [12]. Therefore, insulin resistance is considered the driving force of metabolic syndrome.

1.1.1 Insulin resistance

In 1998, World Health Organization (WHO) defined insulin resistance as a mandatory element to diagnose a person with metabolic syndrome, besides other criteria, like dyslipidemia and hypertension [13]. Excessive caloric intake, represented by high sugar and fat consumption, may cause over production of insulin in order to compensate for high blood sugar levels as a homeostatic response. Chronically, insulin-sensitive tissues become unresponsive to insulin due to an alteration in receptor binding or post-receptor mechanisms, which is called insulin resistance [14], causing hyperglycemia or high circulating blood glucose level.

Insulin is responsible to increase glucose uptake, reduce blood glucose and convert glucose into storable forms, like glycogen or fat, mostly in skeletal muscle, liver and adipose tissue [15]. In the muscle and adipose tissue, insulin stimulates glucose uptake by translocation of glucose transporter 4 (Glut4) to the cell surface. Meanwhile, insulin triggers glycogen synthesis from glucose and inhibits glycogenolysis in the muscle and liver. Moreover, insulin decreases hepatic gluconeogenesis in the liver and inhibits lipolysis in the adipose tissue [16]. Therefore, when the system is impaired, systemic insulin resistance occurs.

1.2 Obesity is a multifactorial disease

Obesity and its morbidities have become a major health problem worldwide over the last decades. Obesity is defined by a body mass index (BMI) of 30 kg/m^2 or higher, and overweight when the BMI is 25 kg/m^2 or higher. Nevertheless, the BMI criteria are recognized to be unfit in some ethnicities and races. For example, BMI reference underestimates body fat in South Asian children, while overestimating body fat in African American children [17]. Discrepancies in obesity prevalence are apparent in the early life and affected by various factors.

However, it is a complex and multifactorial disease, implicating a combination and interaction of genetic and environmental factors [18].

1.2.1 Genetic factor

Genetic predisposition is an inherited factor to develop obesity [19]. Modern research tools and extensive studies, such as genome-wide association studies (GWAS), facilitate an understanding of gene interactions leading to obesity. GWAS has successfully identified monogenic and polygenic causes of obesity. Monogenic obesity is caused by single nucleotide polymorphisms (SNPs) that occur primarily in the leptin-melanocortin pathway as a key regulator of energy intake [20]. The cases are rare and often found in early-onset from childhood with a very severe phenotype [21]. Genes that are involved in monogenic obesity, such as leptin, leptin receptor, proopiomelanocortin and melanocortin 4 receptor (MC4R) [22], are implicated in endocrine disorders and abnormal feeding behavior causing hyperphagia.

In many cases, genetic predisposition to obesity is a combination effect of polygenic variants. Polygenic obesity, so-called common obesity, is triggered by multiple DNA polymorphisms that co-occur in different genes [23]. However, these gene variants by themselves do not result in the development of obesity, but cause the disease in combination with other variants [24, 25]. One of the first obesity-susceptible loci identified by GWAS is the fat mass obesity associated gene, which was also highlighted for type 2 diabetes mellitus (T2DM) and holds the strongest effect on obesity phenotypes to date [26, 27]. Polymorphisms in other genes, such as peroxisome proliferator-activated receptor γ-2 (PPARG2), adiponectin (ADIPOQ), MC4R [28], β-adrenergic receptor family (ADRB1-3) [29-32] and uncoupling proteins (UCP1-3) [33-35], are involved in either children, adolescent, or adult obesity.

A more recent obesity study found a correlation of obesity with environmental changes that affect energy intake and expenditure [36]. Meta-analysis of SNPs related to age interaction by GWAS discovered 11 out of 15 loci that have a greater effect on BMI in individuals below 50

years old [37]. This reflects on the increase in obesogenic environmental factors [38]. Interaction between gene and environment might be mediated by epigenetics through DNA methylation and various types of histone modifications, which affects gene expression without altering the principal base pair sequence, thus inheritable and reversible [39, 40]. Environment factors, including diet [41], physical activity [42, 43], smoking [44] and socioeconomic status [45] are known to have influence on obesity-related genes.

1.2.2 Environmental factor

Looking at the rapid increase in obesity over the past 30 years, strongly suggests that environmental factors, such as, socio-economic status, lifestyle and behavior, including cultural beliefs towards food and activities, are responsible for this trend [46], aside from its impact on obesogenic genes. Environmental factors play a role in the imbalance of energy by inducing excessive caloric intake and a sedentary lifestyle [1]. A more affordable energy dense food option in combination with a reduction in physical activity related to transportation for commuting, contribute to a positive energy balance [47]. Preferences to consume fast food have increased due to its convenience, costs, taste and availability [48]. In addition, the comfort of living in a modern era enables people to accomplish and receive most things via online and delivery services, causing people to be immobile and stay indoors. Lack of physical activity is strongly associated with obesity [49] and a higher risk for its comorbidities [50, 51]. Moreover, individual environmental factors, such as temperature [52] and microbiome [53] have been attributed as risk factors for obesity.

1.3 Allergy

Allergies occur in different forms caused by certain substances that are recognized by the body immune system as harmful. These substances are known as allergens, including medicine, food, dust, latex, mold,

insects, pets and pollen. The immune response is mediated by IgE antibodies, which bind to mast cells and basophils, thus releasing histamine granules and cause inflammation [54]. The type of hypersensitivity reaction towards these allergens is called type I hypersensitivity or anaphylactic response. Type I hypersensitivity reactions are comprised of bronchial asthma, allergic rhinitis and dermatitis, food allergy and anaphylactic shock, which are also highly correlated to obesity and metabolic syndrome as mentioned above.

Lung allergy is most defined by allergic asthma, which causes inflammation and intermittent airway obstruction, thus resulting in coughing and dyspnea (shortness of breath) [55]. Consequently, asthma deteriorates quality of life and contributes to a health economic burden. The severity of allergic asthma may vary from coughing to respiratory failure, which is a life-threatening sequence [56]. Therefore, though the symptoms seem mild, the progressive decline in respiratory function has to be taken care of seriously.

Allergic asthma is mostly induced by exposure to environmental inhalant allergens. One of the most common triggers is house dust mites (HDM), which are abundantly found in warm and humid household conditions [57]. HDM can be found in bedding materials, like sofas, carpets and beds, around the world, except Antarctica [58]. They are microscopic organisms, measuring between 0.2 – 0.4 mm, and they feed on human skin and hair [59], hence they are easily inhaled. Chronic and prolonged exposure to HDM can dramatically impact the health of people with asthma or those particularly allergic to HDM. Moreover, HDM sensitization in the early life affects lung function significantly and in long term inflicts respiratory health [60].

HDM is an indoor allergen, thereby it highly inflicts inactive people, or people who spend most of their time inside the house. This shares the same environmental factors as obesity and metabolic syndrome, which is a sedentary lifestyle. In addition, obesity and metabolic syndrome are major risk factors to develop asthma [61, 62], thus the co-occurrence of both conditions might exacerbate the prognosis of allergic asthma.

1.4 Correlation between obesity and metabolic syndrome with the occurrence of allergy

According to WHO, worldwide obesity has tripled since 1975, affecting 13% of adults aged 18 years and older in 2016, and 38 million children below 5 years old in 2019, thus It is projected to increase in the future [63]. Meanwhile, a steady increase of allergic diseases in the world population has been observed. Approximately 30-40% of the population is affected by one or more allergic conditions, and it is still rising dramatically in developed and developing countries [64]. Inflicted allergic diseases, such as allergic rhinitis, asthma, atopic eczema, food allergy, insect allergy and skin allergy, have increased worldwide [65]. Hersoug and Linneberg hypothesized that the decrease in immunological tolerance induced by obesity results in the increase of allergic diseases [66]. They proposed that the immunological changes induced by adipokines, like leptin and adiponectin, and cytokines, like IL-6 and Tnfa, secreted by WAT skews the immune system towards a Th2 cytokine profile and reduces immunological tolerance to antigens [66].

A study involving 98 children analyzed the relationship between IgE levels and obesity with the immunomodulatory effect of ghrelin and leptin, as hunger and satiety hormones, respectively. Increased adipose tissue in obese subjects is related to a rise in leptin. Leptin, a satiety hormone made by adipose tissue, is found higher in the airways among asthmatics [67, 68]. It is believed that the abundance of leptin receptor in visceral fat has been related to bronchial hyperresponsiveness, which leads to the concept that obesity-induced asthma is a disease of peripheral adipose tissues [69]. There was also a strong negative correlation between plasma ghrelin and serum IgE levels, indicating ghrelin may suppress IgE production [70]. Ghrelin levels are found lower in obese subjects [71], thus relating obesity with higher levels of IgE. National Health and Nutrition Examination Survey (NHANES) 2005-2006 results showed that IgE levels and odds ratio for atopy are found highest

among obese children compared to normal weight children, which is largely driven by an allergic sensitization to food [72]. These studies suggest that there is a link between obesity and allergic disease caused by immunological changes in obese subjects.

1.5 Complications of obesity and metabolic disease

Prolonged and untreated metabolic syndrome will lead to various complications and damage different organs. Obesity and metabolic disorder are strongly associated with abnormally high blood glucose level, so-called hyperglycemia, and insulin resistance, in which is correlated with T2DM [73, 74]. T2DM is described as a combination of peripheral insulin resistance and low amounts of insulin that is produced by pancreatic β-cells [75]. Furthermore, diabetes and insulin resistance are predictors of cardiovascular disease (CVD) [76]. It arises from several mechanisms, such as: a) dyslipidemia that promotes atherosclerosis, which is defined as plaque on the artery walls caused by the accumulation of fat, cholesterol, calcium and other substances, thus overtime hardening and narrowing the arteries [15, 77]; b) hypertension or high blood pressure [78]; c) high pro-inflammatory cytokines cause an increase in oxidative stress and a decrease in endothelial nitric oxide synthase (eNOS) bioactivity, thus inducing endothelial cell apoptosis [79]. In addition, metabolic syndrome itself is a major risk factor for CVD [80].

Obesity and metabolic syndrome have been linked to the increase risk of several types of malignancies, including cancer in gastrointestinal, such as esophagus, gastric, colorectal, gallbladder, biliary, and pancreatic carcinoma [81], kidney [82], even prostate [83] and breast cancer [84]. One of the mechanisms is by hyperinsulinemia, which is a major anabolic hormone to stimulate cancer cell proliferation via insulin/insulin-like growth factor 1 (Igf1) signaling [85, 86]. Moreover, there is increasing evidence that proves obesity and metabolic syndrome are correlated with many neurodegenerative diseases, such as Alzheimer's disease, Parkinson's disease and Huntington's disease, with caloric

restriction thought to be the preventive step against these diseases [87, 88]. In DIO, the inability of adipose tissue to store lipid causes an increase in of free fatty acids (FFA) mobilization; one of the targets is the liver. This results in hepatic insulin resistance and *de novo* hepatic lipogenesis, thus accumulating more triglycerides in the hepatocytes and causing non-alcoholic fatty liver disease (NAFLD) [89]. The progression of NAFLD may lead to liver cirrhosis and carcinoma, and is correlated with obesity and metabolic syndrome [90].

Obesity directly interferes with respiratory function by increasing gastric and esophagus pressure, thereby decreasing lung volume and lung compliance [91]. Additionally, individual components of metabolic syndrome, such as dyslipidemia, abdominal obesity and hypertension, are associated with lung function impairment, with abdominal obesity as the strongest relation [92, 93]. In relation to that, obesity and metabolic disease are major risk factors for asthma and chronic obstructive pulmonary disease (COPD) [94]. For instance, the increase in leptin levels in obese subjects may modulate immune reaction in the airways towards a Th1 phenotype [95], since leptin receptors are present on bronchial epithelial cells [96]. Other potential mechanisms for metabolic disorder to affect lung function are described in Figure 4. Therefore, obesity and metabolic disease leads to type 2 diabetes mellitus, CVD, certain cancers, neurodegenerative diseases, NAFLD and lung diseases [97], which has become a serious burden in the society.

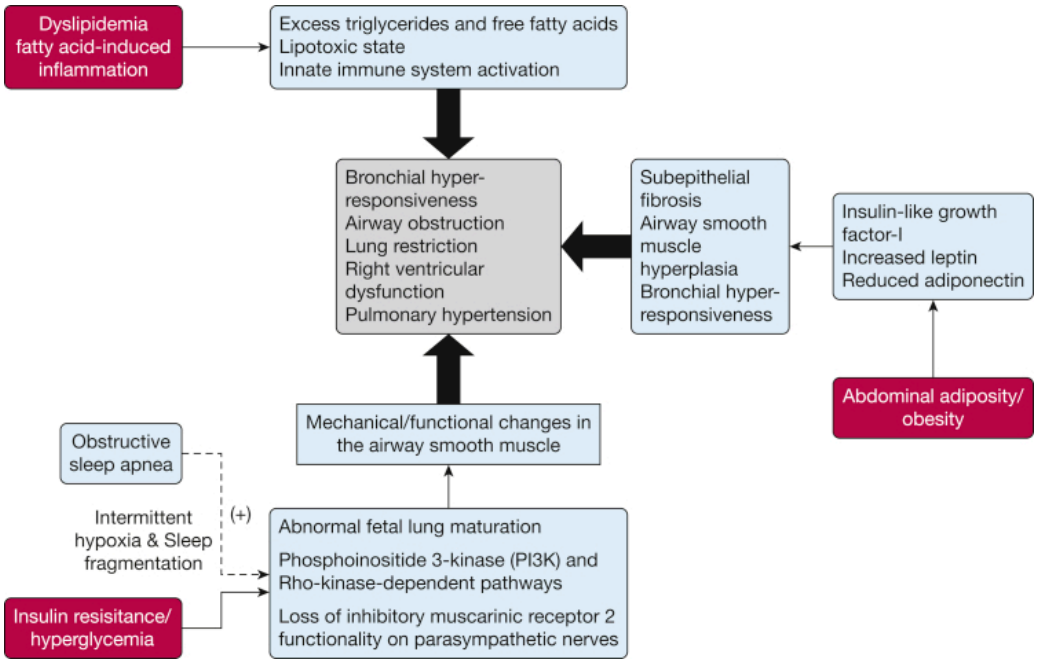

Figure 1: Potential mechanisms of metabolic syndrome affecting lung function. Multiple pathways, including changes in leptin, adiponectin, growth hormone and Igf1, hyperglycemia and hyperinsulinemia, hyperlipidemia causing fatty acid-induced inflammation and abdominal obesity, play a role in influencing lung function. This image is taken from [98]

1.6 Role of white adipose tissue (WAT) in metabolic syndrome and obesity

Both, obesity and metabolic syndrome are strongly associated with an increase in body fat, so-called white adipose tissue, as energy storage [99]. Upon chronic nutrient excess, WAT undergoes expansion, brought about by an increase in adipocyte size (hypertrophy) and number (hyperplasia). In addition, exceeding the lipid storage capacity of adipocytes results in adipocyte death and lipid spillover into other organs such as muscle and liver, resulting in local and systemic insulin resistance [100]. Humans possess several WAT depots, and depending on the location, it serves different endocrine and immunological functions. In terms of gene expression profiling, expandability and inflammation, human visceral (omental) fat is resembled in mouse perigonadal (pgWAT) fat, while subcutaneous (scWAT) is anatomically and functionally similar between human and mice (Figure 1) [101-104].

In the context of metabolic syndrome, the problematic fat accumulation occurs mainly in the abdominal cavity (Figure 1) [105], which is highly correlated to pro-inflammatory cytokines secreted by visceral WAT, such as Tnfa, IL-6 and interleukin 1β (IL-1β) [106]. Adipocyte enlargement causes hypoxia by increasing the distance between adipocytes to the vasculature for oxygenation [107]. Chronic hypoxia leads to cell death, which triggers macrophage infiltration to the adipose tissue, thus magnifying inflammatory signals that shift immune cell populations [108]. In a healthy lean subject, immune cells in WAT maintain an anti-inflammatory state, primarily through regulatory T cells (Tregs) [109] and ILC2s [110]. Furthermore, ILC2s activate M2 macrophages and eosinophils that promote anti-inflammatory responses [110]. Besides, Tregs produce IL-10 that suppresses Th1 T cell function, which attenuates pro-inflammatory responses [111]. On the other hand, in obese subjects, pro-inflammatory cytokines are provoked, resulting in polarization of immune responses into M1 macrophages, Th1 ($CD4^+$ and $CD8^+$) T cells and Th17 with reduction in Tregs and ILC2s (Figure 3) [109, 112].

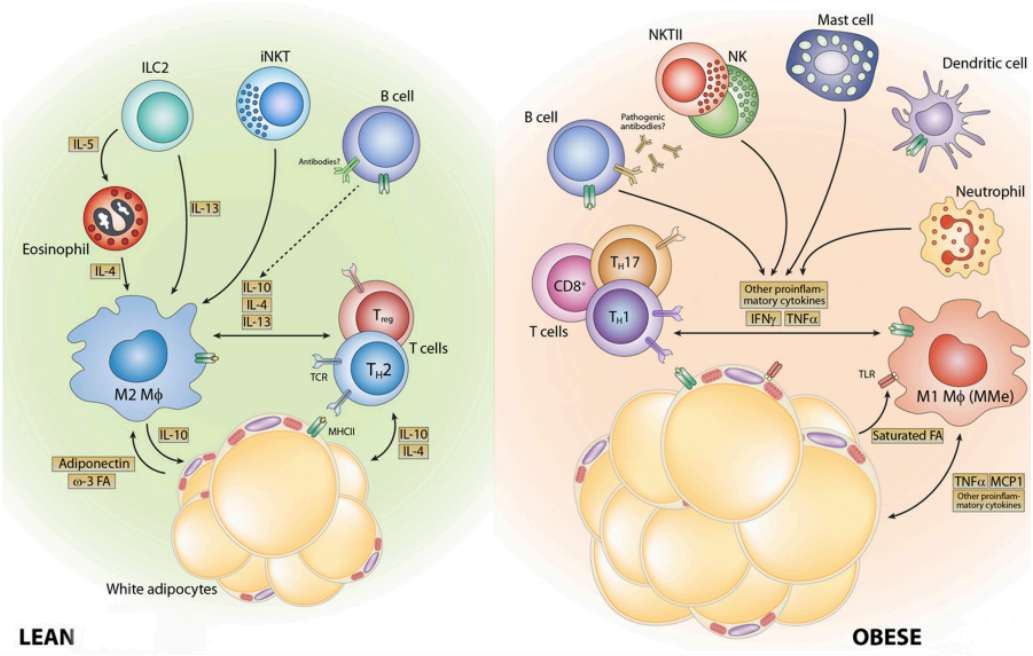

Figure 2: Immune cell regulation in white adipose tissue from lean and obese subjects.
A healthy expansion of WAT in lean subjects recruits a Th2 type, an anti-inflammatory immune response via ILC2s to release eosinophils. In turn, IL-4 is released and secreted by eosinophils, Treg and invariant natural killer T cells (iNKT). This results in

activation of M2 macrophages, which then produces IL-10 and Th2 type cytokines. In contrast, obese WAT resembles a Th1 type immune response by recruiting M1 macrophages and other innate immune cells, like neutrophils, natural killer (NK) cells, type II NKT (NKTII) cells, mast cells and dendritic cells, which promote the release of pro-inflammatory cytokines. As a result, there is a local increase of B cells, $CD4^+$ and $CD8^+$ T cells, which contribute to inflammation by secreting more pro-inflammatory cytokines. Image is taken from [113].

1.7 Role of adipose tissue in energy balance

Energy homeostasis is crucial for the survival. Body size and composition, environment temperature, food intake and physical activity determine the energy expenditure (EE) in humans. Generally, higher fat-free mass, colder environment temperature, higher food intake and more exercise boost body metabolism, resulting in greater energy expenditure [114]. In adulthood, the main contributor to total EE is the amount of energy required for body maintenance under resting state, so-called basal metabolic rate (BMR). Nonetheless, people have a high variability in EE, independent of body size and composition. Since 1990, resting muscle metabolism has been known to be responsible for the variance in EE [115]. Therefore, it was predicted to play a role in the pathogenesis of obesity.

1.7.1 Brown adipose tissue (BAT)

In obesity, adipose tissue or fat has claimed a bad reputation, since its excessive accumulation leads to many detrimental effects on systemic metabolism. In contrast, the discovery of BAT to increase EE arises as a potential target to combat obesity. Increasing BAT activity improves metabolic health by inducing weight loss [116, 117], increasing glucose tolerance and insulin sensitivity [118, 119]. It was long believed that BAT is absent in humans after the first year of life, until 2009, FDG-PET scanned an area with high glucose uptake and it contained uncoupling protein 1 (Ucp1), indicating active BAT in adult humans [120]. Humans possess several BAT depots (Figure 1), with the highest activation in the supraclavicular and paravertebral region [121]. The amount and activity of BAT greatly varies among individuals, with higher levels found in

younger, leaner subjects [120, 122] or triggered by stimuli, such as cold exposure [123] and β3-adrenergic receptor agonists [124, 125]. When activated, Ucp1 allows BAT to dissipate energy in the form of heat via mitochondrial uncoupling [126, 127] utilizing glucose, fatty acid [128-130] and branched-chain amino acid (BCAA) as energy substrates [131]. Therefore, the important role of BAT in regulating metabolic health is inevitable, and reduction in BAT function induces obesity [132].

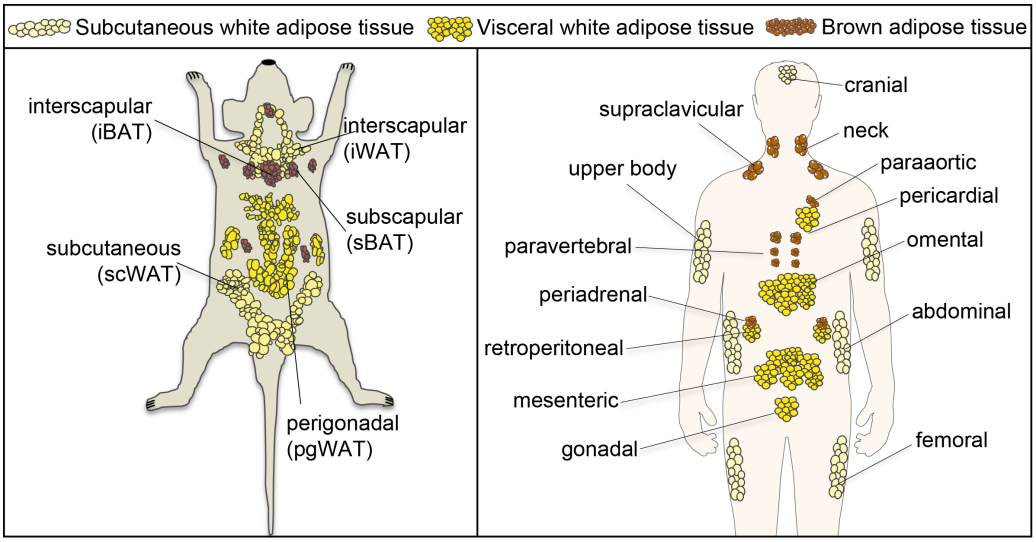

Figure 3: Brown and white adipose tissue depots in mice and human.
White adipose tissue (WAT) in mice and humans are divided into subcutaneous (scWAT) and visceral (perigonadal in mice; pgWAT). Subcutaneous fat is located under the skin and visceral fat is found in the abdominal cavity (inside peritoneum). In contrast, BAT is mainly in the neck and shoulder region (interscapular and subscapular in mice, supraclavicular in humans), paravertebral and periadrenal. This figure is adapted and simplified from [104].

To utilize BAT as therapeutic target for obesity, it is essential to understand BAT on the molecular level. Previous studies showed that the molecular identity of human brown adipocytes resembles beige adipocytes in mice [133, 134], yet its mRNA profile expresses classic brown fat markers [135]. Furthermore, immortalized single cell clones derived from human BAT express heterogeneous Ucp1 levels [136], indicating human BAT is a heterogeneous tissue. Depending on the location of BAT depots, human BAT shows different histological and functional features, with potentially distinct developmental origins [137-140]. These discrepancies highlight the same question for murine BAT, if

it is derived from a single brown adipocyte lineage as commonly believed, which is Myf5^{+} cells [141], or multiple lineages. A recent study identified low- and high-Ucp1 brown adipocyte subpopulations that exist in murine BAT [142]. Moreover, housing mice at thermoneutrality, mimics the histology and physiological state of human BAT, which consists of a mixtures of unilocular and multilocular adipocytes, corresponding to white and brown adipocytes, respectively [143]. Nonetheless, a thorough understanding of the developmental origins of murine brown adipocytes is crucial to foster the translation of murine BAT research data to human physiology, especially as a therapeutic target for obesity.

1.7.2 White adipose tissue browning

The emergence of brown-like adipocytes expressing Ucp1 upon cold exposure and other stimuli in the white adipose tissue is called beige adipocytes [144]. Similar to brown fat, beige adipocytes contain small and many lipid droplets (multilocular), are loaded with mitochondria and express key thermogenic genes like Ucp1, cell death-inducing DEFA-like effector A (Cidea) and peroxisome proliferator-activated receptor gamma co-activator 1a (Ppargc1a). In addition, its thermogenic capacity is inducible by various stimuli [145]. However, at the basal state, beige adipocytes express significantly lower thermogenic capacity than brown adipocytes [134], yet they are still a potent target to increase EE upon stimuli, like cold exposure and β3-adrenergic agonists [146]. Beige adipocytes can be found in several WAT depots, but most prominently in the inguinal scWAT. Beige adipocytes are derived from distinct precursor cells unlike brown adipocytes (see review [145]), with Cd137 and transmembrane 26 (Tmem26) as novel beige fat-specific markers [147].

1.7.3 Crosstalk in brown and beige fat

However, crosstalk with other cell types, like preadipocytes, neurons, vascular endothelial cells and immune cells, affects the expansion and thermogenic activity in beige and/or brown adipocytes. For instance, innervation in BAT is highly associated with its browning activity, since denervation upon cold exposure and high fat diet causes a reduction in Ucp1 levels, mitochondrial activity and glucose uptake [148, 149]. In WAT, the density of sympathetic nerves is positively correlated with the development of beige adipocytes [150].

In addition, vascular endothelial growth factor (Vegf), a major angiogenic factor is highly expressed in BAT compared to WAT and its expression is increased upon cold stimulation, thus allowing BAT to receive the necessary oxygen supply and substrate for thermogenesis fuel [151-153]. Outside of BAT, but Vegf overexpression also induces beige fat differentiation and leads to metabolic improvements [154]. In contrast, high fat and high sucrose diet results in a reduction in Vegf levels and a decrease in vessel density in BAT, thus further causing mitophagy and whitening of BAT [155].

Resident immune cells in adipose tissue play a substantial role in regulating metabolic homeostasis. In diet-induced obesity (DIO), monocytes are recruited into adipose tissue and differentiated into pro-inflammatory M1 macrophages, which produce inflammatory cytokines, like tumor necrosis factor a (Tnfa). Inflammatory cytokines are able to block insulin action in adipocytes, as well as impair preadipocyte differentiation, and induce apoptosis in brown adipocytes [156, 157]. Conversely, in lean healthy animals, M2 macrophages emit anti-inflammatory cytokines, such as IL-4 and IL-10, which promote insulin sensitivity and adipocyte differentiation [158]. Moreover, eosinophils maintain activated M2 macrophages [159], enhance lipolysis, beiging in WAT and BAT thermogenesis via catecholamine secretion. Furthermore, type 2 innate lymphoid cells (ILC2s) are found less in the adipose tissue of obese subjects, while ILC2s promote WAT beiging by producing Met-encephalin peptides, which then increase the expression of Ucp1 in

adipocytes (Figure 2) [160, 161]. Taken together, there are inevitable factors that contribute to the thermogenesis capacity of beige and brown adipocytes, thereby increasing EE and promoting metabolic health.

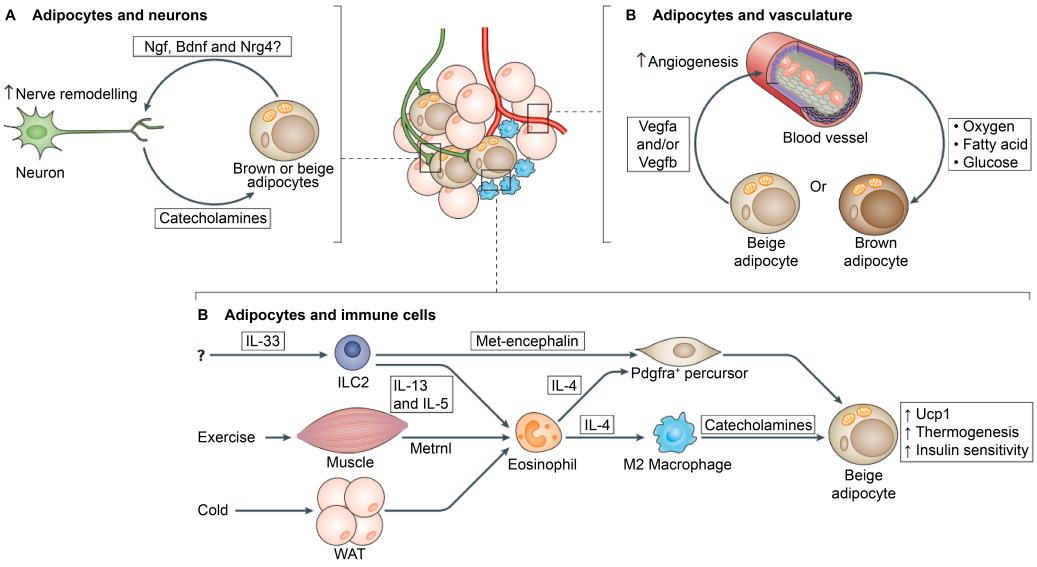

Figure 4: Crosstalk in brown and beige adipocytes.
(A) Adipocytes and nerve cells. Catecholamines are secreted by sympathetic nerve fibers and regulate thermogenic function in brown and beige adipocytes. Brown or beige adipocytes might induce nerve remodeling by producing neurotropic factors, like nerve growth factor (Ngf), brain-derived neurotropic factor (Bdnf) and neuregulin 4 (Nrg4). (B) Adipocytes and vasculature. Vegf, secreted by adipocytes, increases vasculature to promote nutrition and oxygen flux for thermogeneis in beige and brown adipocytes, thus promoting energy expenditure and insulin sensitivity. (C) Beige adipocytes and immune cells. ILC2s, activated by IL-33, secrete IL-13 and IL-5, which activate eosinophils. IL-4 is secreted by eosinophils then induces differentiation of M2 macrophages, which serves as an important source of catecholamines for beige fat activation. Alternatively, IL-4 acts directly on platelet-derived growth factor receptor a $(Pdgfra)^{+}$ precursor cells to increase the proliferation and differentiation into beige adipocytes. Met-encephalin peptides, secreted by ILC2s, promote beige adipocyte differentiation. Moreover, muscle and WAT secrete meteorin-like protein (Metrnl), which activates eosinophils to drive beige adipocyte development. This image is taken from [145].

1.8 Aim of work

The increased prevalence of obesity, metabolic syndrome and airway allergies have brought up the question of whether there is/are any interconnection between those conditions. Preliminarily, the mouse model to study this interconnection was tested. BALB/c mice are protected against DIO, thus C57BL/6J mice were chosen to be the mouse model. In this experimental setup, we dissect the effect of acute lung allergic inflammation on metabolic impaired condition, in the context of metabolic parameter and inflammation in the lungs. Furthermore, to mimic physiological condition on the development of metabolic syndrome and HDM allergy, a chronic and simultaneous exposure to high fat diet and HDM sensitization were performed. The aim was to uncover the effect of one condition on the other and *vice versa*. The phenotype that was observed directed the underlying mechanism to the activation of brown adipose tissue. During observation, we found an uneven distribution of uncoupling protein 1, thus further becoming the basis to study the heterogeneity in mice BAT. The importance of translational purposes from murine to human physiology brought up the idea to identify distinct lineages in mice brown adipocyte. Thus, we characterize marker genes to distinguish brown precursor and adipocyte subsets with their function in regulating thermogenic genes in BAT.

2. Material & Methods

2.1 Material

2.1.1 Chemicals & compounds

Table 2: List of chemicals

Product	Company	Catalog #
2-3, 3'-5 Triiodothyronine sodium salt (T3)	Calbiochem	64246-250MG
2,4-DInitrophenol (DNP)	Sigma-Aldrich	34334-250MG
2-Deoxy-D-glucose	Alfa Aesar	207338
3-Isobuthyl-1-methylxanthin (IBMX)	Sigma-Aldrich	I5869-1G
Acetic acid	AppliChem	A0661
Agarose	Sigma-Aldrich	A9539-500G
Agarose, low gelling temperature	Sigma-Adrich	A9414-100G
Ammonium persulfate (APS)	Serva	13375.01
Antimycin A	Sigma-Aldrich	A8674-25mg
Beta-mercaptoethanol	Carl Roth	4227.3
Bovine serum albumin (BSA) fraction V	Carl Roth	T844.2
Bovine serum albumin essentially fatty acid free	Sigma	A6003
Chloroform	Carl Roth	4423.1
Chromotrope II R (Eosin)	Alfa Aesar	A17519.14
CL 316243 disodium salt	R&D Systems	1499/10
Collagenase D	Roche Diagnostics GmbH	11088866001
Collagenase type IA	Sigma-Aldrich	C9891
Collagenase type IV	Life Technologies	17104019
Dako fluorescence mounting medium	Agilent Technologies	S302380-2
Dermatophagoides farinae extract	Citeq Biologies	
Dexamethasone	Sigma	D4902
D-glucose	Sigma-Aldrich	49159-1KG
Diff-Quik staining	Dade Behring	
Dimethyl sulfoxide (DMSO)	Carl Roth	A994.3
Dithiothreitol (DTT)	VWR Lifesciences	0281-5G
DMEM, high glucose, GlutaMAX™, pyruvate	Life Technologies	31966021

DMEM, no glucose, L-glutamine, phenol red, sodium pyruvate, sodium bicarbonate, powder	Sigma-Aldrich	D5030-10X1L
eBioscience™ 1x RBC lysis buffer	Invitrogen™	00-4333-57
EDTA disodium salt dihydrate	Carl Roth	8043.1
Ethanol (absolute)	Merck Millipore	1.009.832.500
EZ-RUN Recombinant Protein Ladder	Fischer Scientific	10785674
FBS	Life Technologies	10270-106
Formaldehyde solution 37%	Carl Roth	4979.1
Glucose solution 20%	B.Braun	4164483
Glucose strips	Abbott GmbH	0435991
Glycin Pufferan	Carl Roth	3908.2
HEPES	Gibco	15630106
Hydrochloric acid (HCl 37%)	Sigma-Aldrich	30721-1L-GL
Immobilon™ Western Chemiluminescent HRP substrate	Merck Millipore	WBKLS0500
Indomethacin	Santa Cruz Biotechnology	Sc-200503A
Insulin (Actrapid Penfill)	Novo Nordisk	00536427
Insulin (cell culture)	Sigma-Aldrich	I9278-5ml
Isopropanol	Sigma-Aldrich	33539-2.5L
Isoproterenol hydrochloride	Sigma-Aldrich	16504
iTaq Universal SYBR® Green Supermix	BioRad	172-5124
Ketamine	Pharmanovo GmbH	
L-glutamine	Sigma-Aldrich	G7513-100ML
Mayer's solution (Hematoxylin)	Merck	1092490500
Methanol	Merck Millipore	1-06009.2500
MOPS Pufferan R	Carl Roth	6979.4
MTT, Thiazolyl blue	Serva	20395.03
Normocin™	InvivoGen	Ant-nr-1
NP-40	Abcam	Ab142227
Nuclease-free water	Qiagen GmbH	129114
Oil Red O powder	Alfa Aesar	A12989
Oligomycin	Sigma	O4876
Paraffin wax	Leica Surgipath	39601006
Paraformaldehyde	Carl Roth	0335.2
Penicillin/Streptomycin	Life Technologies	15140-122
Percoll®	GE Healthcare	17-0891-01
Phosphatase inhibitor cocktail II	Sigma-Aldrich	P5726-1ml

Phosphatase inhibitor cocktail III	Sigma-Aldrich	P0044-5ml
Phosphate buffer saline (PBS)	Life Technologies	14190-094
Polyfect	Qiagen GmbH	301107
Potassium dihydrogen phosphate (KH_2PO_4)	Carl Roth	3904.2
Potassium chloride (KCl)	Carl Roth	6781.1
Protease inhibitor cocktail	Sigma-Aldrich	P8340-5ml
Puromycin hydrochloride	Biomol	Cay13884-500
QIAzol	Qiagen GmbH	79306
Rosiglitazone	Santa Cruz Biotechnology	Sc-202795
Rotenone	Sigma-Aldrich	R8875-1G
Roti®-Histokitt II	Carl Roth	T160.1
Rotiphorese® Gel 30	Carl Roth	3029.2
Sample buffer 4x	Life Technologies	NP0008
Sodium chloride (NaCl)	Carl Roth	3957.1
Sodium chloride solution 0.9%	Fresenius Kabi Deutschland GmbH	808765
Sodium dodecyl sulfate (SDS)	Carl Roth	CN30.3
Sodium hydroxide (NaOH)	Carl Roth	6771.3
Sodium phosphate (Na_2HPO_4)	Acros Organics	204855000
Sodium pyruvate solution	Sigma-Aldrich	S8636-100ML
Temed	AppliChem	A1148.0100
Thermo Scientific™ Restore™ PLUS Western Blot Stripping Buffer	ThermoFischer Scientific	10016433
Tri-sodium citrate dehydrate	Carl Roth	4088.3
TRIS Pufferan	Carl Roth	4855.1
Triton™ X-100	Sigma-Aldrich	N150
Trypan blue solution	Sigma-Aldrich	93595
Trypsin, 0.05% EDTA, phenol red	Life Technologies	11580626
Tween-20	Santa Cruz Biotechnology	Sc-29113
Xylacin as hydrochloride (20mg/ml)	Proxylaz	
Xylol	Carl Roth	9713.5

2.1.2 Kits

Table 3: List of kits

Product	Company	Catalog #
High-Capacity cDNA Reverse Transcription Kit	ThermoFischer Scientific	4368813
LEGENDplex™ MU Th Cytokine Panel	Biolegend	741043
Pierce™ BCA™ Protein-Assay	ThermoFischer Scientific	23225
QuickExtract™ RNA Extraction Kit	Lucigen	QER090150
RNeasy Mini Kit	Qiagen GmbH	74106
Seahorse XF24 FluxPak	Agilent Technologies	100850-001
Seahorse XFe96 FluxPak	Agilent Technologies	102416-100
Triglyceride Quantification Kit	BioVision	K622
Ultra Sensitive Mouse Insulin ELISA Kit	Crystal Chem	90080

2.1.3 Primers

Table 4: List of qPCR primers 5' – 3'

Gene	Forward sequence	Reverse sequence
Agrp	CTGACCAGGCTCTGTTCCC	ACTTCTTCTGCTCGGTCTGC
Asc1	AGTGTTCCAGGACACCCTTG	GGGTGGCACTCAAGAAAGAG
B2m	TTCTGGTGCTTGTCTCACTGA	CAGTATGTTCGGCTTCCCATTC
Bin1	GGCTACCATCCCCAAGTCC	CCTTGGATGGGGTGTGTTTG
Cd137	GCCGAACTGTAACATCTGCA	TTCAATGCACTCACACTCCG
Cd68	TCACCTTGACCTGCTCTCTC	AGGCCAATGATGAGAGGCAG
Cidea	CGGGAATAGCCAGAGTCACC	TGTGCATCGGATGTCGTAGG
Eif5	GTACCGAGGCATGCTTGAC	TCTTTCCTGTACCAATGTCACT
Glut1	AACTGGGCAAGTCCTTTG	TTCTTCTCCCGCATCATCTG
Glut4	TGATTCTGCTGCCCTTCTGT	GGACATTGGACGCTCTCTCT
Ifnγ	GCCAGTTCCTCCAGATATCCA	CCACGGCACAGTCATTGAAA
IL-1β	CTGAAAGCTCTCCACCTCAA	CCCAAGGCCACAGGTATTTT
IL-4	TCAGTGATGTGGACTTGGAC	GAGCTGCAGAGACTCTTTCG
IL-6	GTCGGAGGCTTAATTACACATGT	CAAGTGCATCATCGTTGTTCA
IL-10	GGCCTTGTAGACACCTTGGT	CTCCCCTGTGAAAATAAGAGCA
IL-17A	GCCAGGAGTATGAAGTGACTG	CACAGTCAGGCACAAAGATGA

Npy	GCCAGATACTACTCCGCTCT	GTGTCTCAGGGCTGGATCTC
P2rx5	CACTCTGCAGGGAAGTGTCA	CACTCTGCAGGGAAGTGTCA
Pat2	GTGCCAAGAAGCTGCAGAG	TGTTGCCTTTGACCAGATGA
Pepck	CTGCATAACGGTCTGGACTTC	CAGCAACTGCCCGTACTCC
Pgc1α	AGCCGTGACCACTGACAACGAG	GCTGCATGGTTCTGAGTGCTAAG
Pparγ	TCCTATTGACCCAGAAAGCGA	TGGCATCTCTGTGTCAACCA
Prdm16	CCCACCAGACTTCGAGCTAC	ATCTCCCATCCAAAGTCGGC
Srebp1c	GGAGCCATGGATTGCACATT	AGGAAGGCTTCCAGAGAGGA
Tbp	ACCCTTCACCAATGACTCCTATG	TGACTGCAGCAAATCGCTTGG
Tcf25	AGGAGTCCGTGTCAACAACC	GGCAGGGTACAGTCAGATCT
Tmem26	GAAACCAGTATTGCAGCACCC	CCCATTCCATTGGTGGCTCT
Tnfα	CCCACGTCGTAGCAAACCA	GTCTTTGAGATCCATGCCGTTG
Ucp1	CTGCCAGGACAGTACCCAAG	TCAGCTGTTCAAAGCACACA
Vegfa	CCACGACAGAAGGAGAGCAG	GTCCACCAGGGTCTCAATCG

2.1.4 Antibodies

Table 5: List of primary and secondary antibodies

Antibody	Company	Catalog #
Alexa Fluor 546 Phalloidin (F-actin)	Life Technologies	A22283
Alexa Fluor 647 Phalloidin (F-actin)	Life Technologies	A22287
α-tubulin	Santa Cruz Biotechnology	Sc-8035
β-actin	Santa Cruz Biotechnology	Sc-47778
Bin1	Abcam	Ab182562
Dapi	Sigma-Aldrich	D9542
Eif5	Abcam	Ab170915
HCS LipidTOX green (lipid)	Life Technologies	H34475
Gapdh (6C5)	CalbioChem	CB1001
Mouse IgG-HRP	Santa Cruz Biotechnology	Sc-2005
Rabbit Alexa Fluor 594	Dianova	111-585-144
Rabbit IgG-HRP	Cell Signaling	7074
Tcf25	ThermoFisher Scientific	PA5-21418
Ucp1 (for cells)	Abcam	Ab10983
Ucp1 (for tissues)	Cell Signaling	14670

Table 6: List of antibodies for FACS analysis

Antibody	Clone	Company
CD3	17A2	BioLegend
CD4	L3T4	BioLegend
CD45	30-F11	BD
CD8	53-6.7	eBioScience
CD11b	M1/70	BioLegend
CD11c	N418	BioLegend
CD206	C068C2	BioLegend
NK1.1	PG136	eBioScience
Ly-6G	1A8	BioLegend
Siglec-F	E50-2440	BD
FoxP3	FJK-16s	eBioScience
GATA3	TWAJ	eBioScience
RORc	AFKJS-9	eBioScience
Zombie Aqua™ Fixable Viability Kit		BioLegend

2.1.5 Mouse diets

Table 7: List of mouse diets

Name	Chow	LF	HF
Number	Altromin 1318	Research Diet D12329	Research Diet D12331
Protein (kcal%)	27	16.4	17
Carbohydrate (kcal%)	59	73.1	25
Fat (kcal%)	14	10.5	58
Total (kcal%)	100	100	100
Energy density (kcal/g)	3.47	4.07	5.56

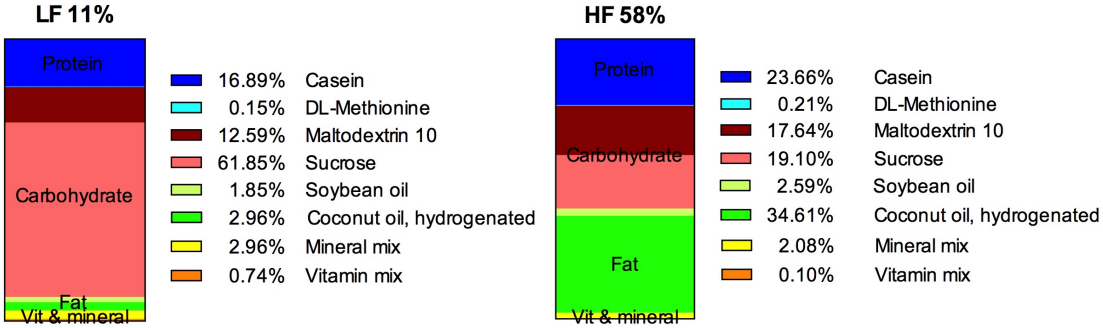

Figure 5: Composition of diet used in experiment

2.2 Methods

2.2.1 *In vivo* experiments

2.2.1.1 Mouse strain and housing condition

Wild type males and females BALB/c mice were purchased from Charles River (Germany) at the age of 7 weeks. Wild type males and females C57BL/6J mice were purchased from Charles River (Germany) at the age of 5 weeks. The Ucp1-KO mice originated from Jackson Laboratory, with C57BL/6J genetic background (strain name: B6.129-Ucp1tm1Kz/J). All animal studies were performed in a conventional animal facility at the Helmholtz Zentrum München (Neuherberg, Germany). Mice were kept in individually ventilated cages (IVC) and maintained at constant ambient temperature of 22 ± 2°C, 45-65% humidity, a 12h light-dark cycle, with *ad libitum* access to food and water. The colony of Ucp1-KO mice were bred, born and weaned at 30°C. Animal experiments were conducted under permission according to the German animal welfare law, relevant guidelines and regulations of the government of Upper Bavaria (Bavaria, Germany): ROB-55.2-2532.Vet_02-18-94.

2.2.1.2 House dust mite sensitization

Mice were sedated using isoflurane prior to bilateral intranasal (i.n.) installations with PBS (as control) or *Dermatophagoides farinae* extract (1µg in 20µl PBS). This occurred consecutively for 1 week. Afterwards,

mice were challenged intranasally with PBS or 10µg *Dermatophagoides farinae* extract for 3 consecutive days.

2.2.1.3 Diet studies

A preliminary study was performed in order to carefully decide on the right mouse model for studying the interaction between metabolic syndrome and allergy. Therefore, a number of 10 males and 10 females BALB/c mice were assigned for DIO study. Mice were matched by the body weight and fed either with standard chow (chow, Altromin 1318) or plant-based high fat diet (HF, D12331) for 23 weeks. The study was held as described in Figure 8A.

To observe the impact of house dust mites sensitization on metabolic impaired condition, a number of 64 C57BL/6J mice (32 males and 32 females) were matched by the body weight and fed either with low fat diet (LF, D12329) or HF for 10 weeks. After 8 weeks of diet, mice were assigned to the HDM sensitization protocol. Before read out, mice were subjected to a glucose tolerance test (GTT). This study was performed as depicted in Figure 12A.

To disentangle the interaction between metabolic syndrome and chronic allergic lung inflammation, a number of 32 male C57BL/6J mice were matched by the body weight and fed with LF or HF for 14 weeks. The first two weeks, mice were assigned to the HDM sensitization protocol and additionally challenged every 2 weeks for 3 consecutive days until the end of study. This study was performed as depicted in Figure 18A.

2.2.2 *In vivo* measurement

2.2.2.1 Body composition analysis

Body composition was assessed using nuclear magnetic resonance (EchoMRI™ Analyzer) at the time point according to the respective experimental setup.

2.2.2.2 *Glucose tolerance test*

Mice were fasted for 4 hours prior to glucose tolerance test (GTT). Glucose (2g/kg body weight, 20% glucose solution, B. Braun) was injected intraperitoneally (i.p.) to the mice. Glucose levels were measured from the blood collected from the tail before (0 minute), 15, 30, 60 and 120 minutes after injection, using a glucometer (Abbott).

2.2.2.3 *Insulin tolerance test*

Insulin (Actrapid, Novo Nordisk) was diluted in 0.9% saline with a dose of 0.75 IU insulin/kg body weight for the LF group and 1.25 IU insulin/kg body weight for the HF group. Mice were fasted for 4 hours prior to insulin tolerance test (ITT) and insulin was administered via i.p. injection. Glucose levels were measured from the blood collected from the tail before (0 minute), 15, 30, 60 and 120 minutes after injection, using a glucometer. In the case of hypoglycemia (blood glucose is too low to be detected), the mice were injected with 20% glucose solution (same volume) immediately via i.p. injection and the values are excluded from the analysis.

2.2.3 *Ex vivo* measurement

2.2.3.1 *Sacrifice and tissue collection*

Ad libitum blood glucose was measured via tail vein using a glucometer. Mice were weighed and anesthetized with Ketamine (100 mg/kg) and Xylazine (7 mg/kg) accordingly. Once anesthetized, blood was collected via retro-orbital bleeding. Blood serum was obtained by centrifugation at 10,000 G and temperature at 4°C for 5 minutes, which was then kept in -80°C until further analysis. After dissection, tissues were isolated, weighed, snap frozen on dry ice and stored at -80°C until further analysis. The Ucp1-KO mice and the mice for the BAT study were sacrificed by cervical dislocation.

2.2.3.2 Metabolic measurements

Fasted blood serum was collected 4 hours after food withdrawal and fasted serum insulin level was measured using Ultra Sensitive Mouse Insulin ELISA Kit (Crystal Chem). Liver triglyceride content was measured from liver extract using Triglyceride Quantification Colorimetric/Fluorometric Kit (BioVision).

2.2.3.3 Analysis of bronchoalveolar lavage (BAL) fluid

Euthanized mice were cut open at the neck, exposing salivary glands and the sternohyoid muscle. The mucle was incised to expose the trachea and place a thread under it. A small plastic tube (catheter) was inserted about 0.5 cm into the trachea. The catheter has to be fixed in place, thus the thread was knotted around the trachea. Airways were lavaged through the catheter 5 times with 0.8 mL PBS. Fluid was aspirated gently and collected in a tube on ice. To separate the cellular and noncellular components, the lavage fluid was centrifuged for 7 minutes at 400 G and 4°C. Aliquots of cell-free BAL fluid were used to measure cytokines using LEGENDplex^{TM} MU Th Cytokine Panel (Biolegend) according to manufacturer's instructions. Viability and yield of BAL cells were quantified using trypan blue (Sigma-Aldrich) exclusion in a hemocytometer. Differential BAL cell count (400 cells/sample) was performed on cytospins at 600 rpm for 10 minutes, fixed and stained with Diff-Quik (Dade Behring).

2.2.3.4 Analysis of leukocytes from lung and adipose tissue

Isolated lungs were excised, cut into small pieces and digested in RPMI medium supplemented with 100 µg/mL DNAse (Sigma-Aldrich) and 1 mg/mL Collagenase type 1A (Sigma-Aldrich) at 37°C for 20 minutes. Digested lungs were filtered through a 70 µm cell strainer and centrifuged at 400 G and 4°C for 5 minutes. Pellets were resuspended in a gradient of 40% Percoll® in RPMI (v/v) solution and 80% Percoll® solution (GE Healthcare-Life Sciences). Tubes were centrifuged at room

temperature and 1600 G for 15 minutes with brake set to 0. Lymphocytes were collected from the interphase and analyzed via fluorescence-activated cell sorting (FACS). The FACS analysis was performed by Dr. rer. nat. Stephanie Musiol from the Institute of Allergy Research (Helmholtz Zentrum München).

Adipose tissues were digested in PBS containing 100 µg/mL DNAse and 1 mg/mL Collagenase D (Roche Diagnostics GmbH) at 37°C for 20 minutes. Digested fat was filtered through a 70 µm cell strainer and centrifuged at 400 G and 4°C for 5 minutes. The lipid layer was then removed and erythrocytes were lysed using RBC lysis buffer (Invitrogen™). The cellular suspension was washed and analyzed via FACS.

Single cell suspension from lungs and adipose tissue were primarily stained with surface markers. Cells were stained for transcription factors using Foxp3 Staining Buffer Set (eBiosciences) according to the manufacturer's protocol and analyzed using BD LSRII Fortessa flow cytometer (BD Bioscience) and FlowJo Software (FlowJo, USA). Gating strategy to identify different lymphoid populations in lungs and adipose tissue are presented in the Figure 6 & 7. Antibodies that were used for flow cytometry purposes are listed in Table 6.

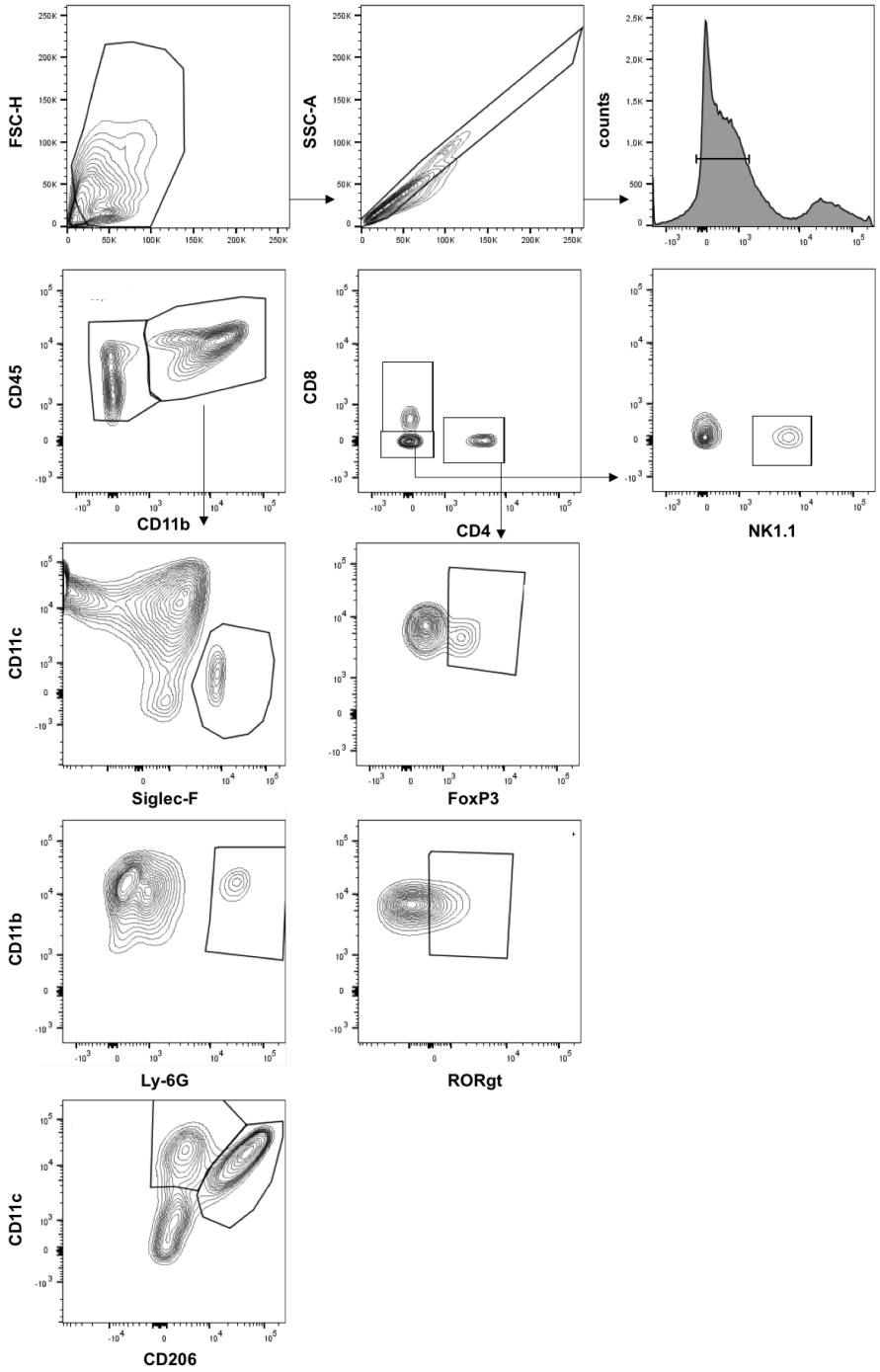

Figure 6: Gating strategy to analyze immune cell population in pgWAT.

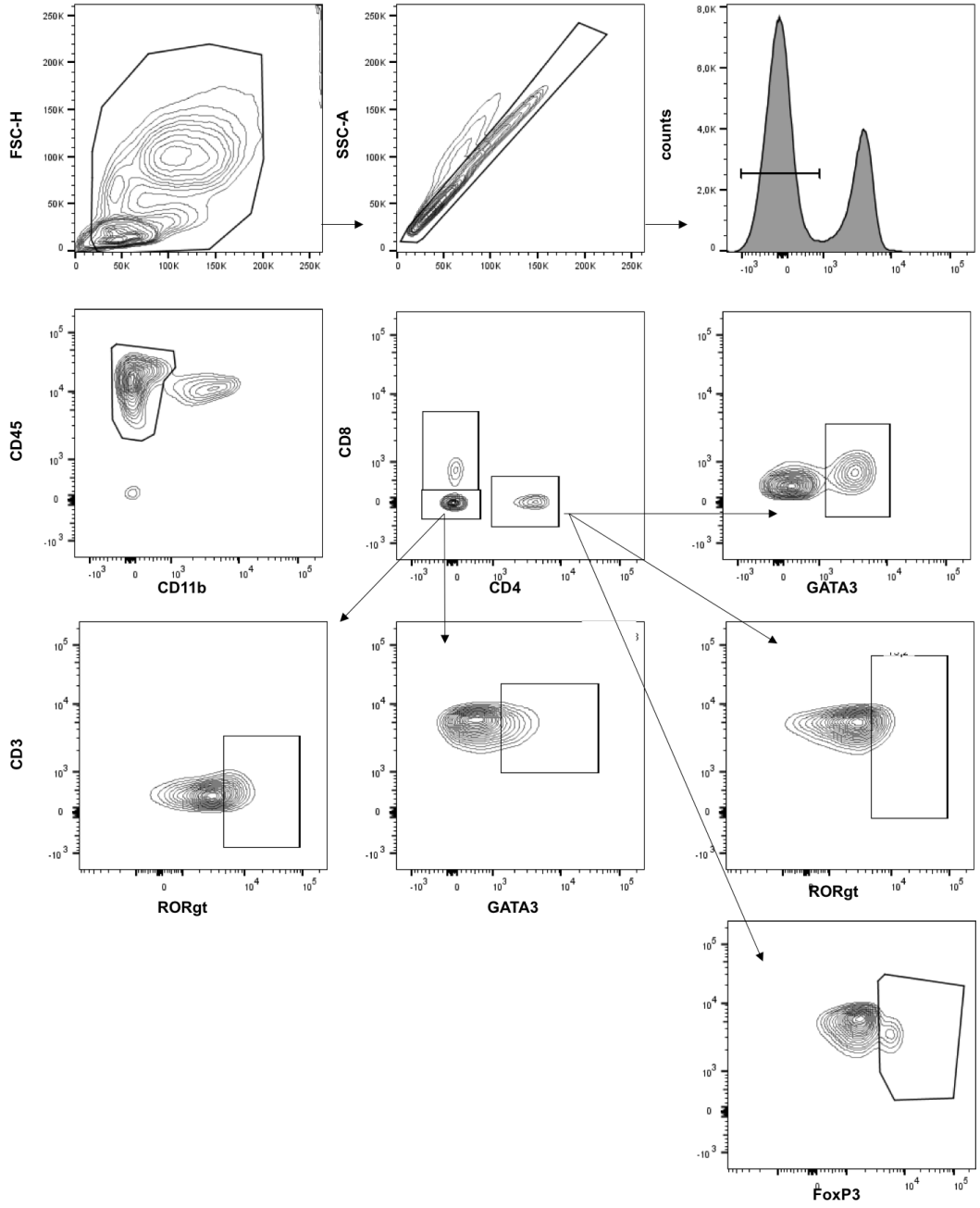

Figure 7: Gating strategy to analyze immune cell population in the lungs.

2.2.4 Histology

For histology, tissues were fixed in 4% PFA overnight at 4°C, transferred to 70% ethanol and stored in the 4°C fridge until further use. Prior to paraffin embedding, tissues were dehydrated in an increasing ethanol concentration series (80%, 90% and twice 100%), each for 1 hour. Subsequently, tissues were incubated in 3 times xylol for 10 minutes

each. Tissues were transferred into paraffin (Leica) twice, each for 1 hour and followed by one paraffin incubation overnight at 65°C. The next day, tissues were embedded in paraffin wax on a paraffin-embedding machine (Leica®, EG1150) and stored at room temperature. For microtome (Leica) sections, tissue blocks were chilled overnight at 4°C, then moved to -20°C a night before cutting. Tissues were cut at 2 µm thick sections and 4 µm thick sections for lungs. Sections were collected on SuperFrost Plus™ glass slides (Thermo Scientific) and were air dried at room temperature.

2.2.4.1 Hematoxylin & Eosin (H&E) staining

Tissue sections were deparaffinized twice in xylol for 2 minutes followed by a decreasing series of ethanol concentrations (twice 100%, 90%, 80%, 70%), each for 2 minutes. Slides were washed in deionized water for 2 minutes, prior to staining with Mayer solution (diluted in deionized water with a ratio of 1:5, then filtered) for 40 seconds. Sections were directly washed under running tap water for 2 minutes and dehydrated by incubation in 96% and 100% ethanol for 2 minutes each. Slides were then stained with chromotope II R solution (100 mg chromotrope II R diluted in 100 mL of 95% ethanol, combined with 100 µL of acetic acid and filtered) for 3 minutes. Subsequently, slides were dipped into 96% ethanol 3 times and transferred into 100% ethanol for 1 minute. Finally, slides were incubated twice with xylol, each for 5 minutes, and mounted with Roti®-Histokitt II (Carl Roth), covered with glass coverslip and air-dried.

2.2.4.2 Periodic acid Schiff (PAS) staining

The excised lungs were deparaffinized and hydrated with water the same way as mentioned above (see H&E staining protocol). Slides were oxidized in 0.5% periodic acid solution for 5 minutes and were rinsed in distilled water. Schiff reagent was then added for 15 minutes, which will turn the sections a light pink color. Slides were washed in lukewarm tap

water for 5 minutes and turned a dark pink color. Subsequently, the slides were counterstained with Mayer's solution for 40 seconds and were washed in running tap water for 5 minutes. The dehydration and mounting steps are the same as mentioned in H&E staining protocol. The mucus layer is stained as dark pink or red color and inflammatory cells are in dark purple.

2.2.4.3 Grading of mucus hypersecretion and inflammatory cell infiltration in the lung

Mucus hypersecretion and inflammatory cell infiltration were graded in a blinded fashion on a scale from 0 to 4 (0: none, 1: mild, 2: moderate, 3: marked and 4: severe), reflecting the degree of the pathological alteration [162].

2.2.4.4 Immunostaining on tissue

Interscapular BAT was excised from 3-4 month old, male C57BL/6J wild-type mice. BAT was fixed in 4% PFA for 30 minutes at room temperature on a shaker. BAT was embedded in 4% low melting temperature agarose (Sigma-Aldrich) in PBS and cut into 70 µm thick sections using Leica VT1000S Vibrating blade microtome (Leica). Sections were permeabilized with 1% Triton X-100/PBS on ice for 1 minute and blocked with filtered 3% BSA/PBS for 1 hour. Primary antibodies were added to detect Ucp1, Eif5, Tcf25 and Bin1 (antibody list: see Table 5) overnight in the 4°C fridge. The next day, sections were washed with PBS and incubated with secondary antibody (rabbit Alexa Fluor 594, Abcam), Alexa Fluor 647 Phalloidin (Invitrogen), HCS LipidTOX™ Green Neutral Lipid Stain (Invitrogen) and Dapi (Sigma-Aldrich) for 1 hour at room temperature. Sections were washed with PBS and mounted on microscope slides using DAKO fluorescence mounting medium. Images were captured using a Leica TCS SP5 Confocal (Leica).

2.2.4.5 Quantification of Ucp1 and Eif5 immunostainings

Quantification of the images was done by Dr. Annette Feuchtinger from the Research Unit Analytical Pathology of Helmholtz Zentrum München. Automated quantifications of Ucp1 and Eif5 were performed using the commercially available image analysis software Definiens Developer XD 2 (Definiens AG) following a previously published procedure [163]. A specific ruleset was developed in order to detect and quantify Ucp1 and Eif5 stained tissue. For the first step, the images were segmented based on color and shape features. The calculated parameter was the mean staining intensity of Ucp1 or Eif5 in the detected cells and they were divided into four classes using the fluorescent intensity of each marker.

2.2.5 *In vitro* experiments

2.2.5.1 Isolation and establishing brown preadipocyte lines

Brown preadipocytes were isolated from interscapular BAT of three 8 week old, male wild-type C57BL/6J mice. BAT was minced and digested in pure DMEM containing 1 mg/mL Collagenase type IV and 10 mg/mL BSA for 30 minutes at 37°C. Digested cells were filtered through a 100 µm sift and washed with PBS. The stromal vascular fraction (SVF) was separated by centrifugation at room temperature and 800 G for 5 minutes. The supernatant was removed and the pellet was washed with DMEM, and once more centrifuged. The SVF was resuspended in primary culture medium (DMEM + GlutaMAX^{TM,} 4.5 g/L D-glucose, pyruvate, 10% FBS, 1% Penicillin/Streptomycin and 0.1 mg/mL of Normocin) and plated on a 6-well plate. Subsequently, the cells were immortalized with ecotropic retrovirus encoding SV-40 large T antigen to generate stable cell lines. Once tested negative for mycoplasma, cell lines were maintained in normal growth medium (DMEM + GlutaMAX^{TM,} 4.5 g/L D-glucose, pyruvate, 10% FBS, 1% Penicillin/Streptomycin) at 37°C and 5% CO_2.

2.2.5.2 Picking single cell clones

Each cell line was sparsely seeded (1000 cells) in 15 cm plates to let them grow into colonies. Once the colonies were big, 96-well plates were prepared and filled with 20 µl of cold trypsin. Under the light microscope, a single colony was scraped, aspirated and transferred into the 96-well plate. Each colony was transferred, grown and expanded individually in separated wells or plates. When the cells were reaching a confluence of 70-80%, they were passaged. This is done by removing the medium, washed the cells with PBS, incubated in trypsin for 3 minutes at 37°C, resuspending and plating in normal growth medium. Cell culture medium was changed every 2 days.

2.2.5.3 Generating knockdown cell lines

Immortalized brown preadipocytes were infected using ecotropic lentiveral particles (Cell Biolabs, Inc.) with a random sequence or scrambled (Scr), anti-Eif5 shRNA (shEif5, SHCLNG-NM_173363, TRCN0000313045, Sigma), anti-Tcf25 shRNA (shTcf25, SHCLNG-NM_014972, TRCN0000241031, Sigma), or anti-Bin1 shRNA (shBin1, SHCLNG-NM_004305, TRCN0000238138, Sigma). After 24 hours, cells were selected with growth medium containing 2.5 µg/mL Puromycin (Biomol). Cells were maintained and cultured in growth medium with Puromycin.

2.2.5.4 Differentiation of preadipocytes

For differentiation, preadipocytes were seeded and grown to 90% confluency. Brown preadipocyte differentiation was induced with 0.5 mM 3-isobuthyl-1-methylxanthin (IBMX, Sigma), 5 µM dexamethasone (Sigma), 125 µM indomethacin (Santa Cruz), 1 nM Triiodothyronine (T3, Calbiochem) and 100 nM insulin (Sigma) in growth medium for 2 days. The differentiation was started when the induction medium was added to the cells (day 0, preadipocytes). Subsequently, medium was changed

every 2 days with growth medium containing 1 nM T3 and 100 nM insulin, and cells were harvested at day 8.

Subcutaneous preadipocytes were obtained in the same way as stated in section 2.2.5.1. They were differentiated into white and beige adipocytes. For white adipocytes, cells were induced with 0.5 mM IBMX, 5 µM dexamethasone and 100 nM insulin in growth medium for 2 days. In addition to that, 1 µM Rosiglitazone (Santa Cruz) was supplemented to the same induction mix in growth medium for beige adipocytes differentiation. Medium was changed every 2 days with growth medium containing 100 nM insulin. Beige and white adipocytes were harvested at day 8 of differentiation.

2.2.5.5 CL 316,243 (CL) treatment on brown adipocytes

CL treatment was performed at day 8 of differentiation. Medium was replaced with growth medium containing 1 nM T3, 100 nM insulin and 0.5 µM CL for 3 hours for acute treatment and 6 hours for chronic treatment.

2.2.5.6 MTT assay

Preadipocytes were seeded in four 96-well plates (2000 cells/well). MTT stock solution was prepared by diluting 50 mg MTT powder (Serva) in 10 mL sterile PBS. On the day of the measurement, 200 µL MTT stock solution was diluted in 1.6 mL DMEM and added to the wells. DMEM (200 µL) containing 0.003% Triton X-100 and 0.05% MTT was added to the wells and was perceived as the death control. After 2 hours, medium was removed and replaced by 100 µL solubilization buffer (10% Triton X-100 and 0.03% HCl in 100% isopropanol). The plate was incubated for 10 minutes at 24°C and 700 rpm. The lysate was then transferred to a new 96-well transparent plate to be measured at 570 nm using a microplate reader (PHERAstar FSX).

2.2.5.7 Oil Red O (ORO) staining

Mature brown adipocytes were fixed in 10% formalin (Roth) for at least 1 hour, at room temperature and washed in water. Cells were dehydrated in 60% isopropanol for 5 minutes and let dry. The filtered 60% (v/v) ORO working solution in water (stock: 0.35% (w/v) ORO, Alfa Aesar in 100% isopropanol) was added for 10 minutes and subsequently washed six times with ddH_2O. For normalization, cells were stained with Dapi and the fluorescence signal was measured at 460 nm using PHERAstar FSX. After cells were dried, ORO was eluted with 100% isopropanol and measured at 505 nm using PHERAstar FSX.

2.2.5.8 Measurement of cellular oxygen consumption rate (OCR)

Cells were plated on either 24-well or 96-well Seahorse plates and differentiated as described in 2.2.5.4. The OCR was measured with a XF24 or XF96 Extracellular Flux analyzer (Seahorse Bioscience) at day 8 of differentiation. One hour before the measurement, cells were equilibrated at 37°C in assay medium (DMEM D5030 supplemented with 0.2% fatty acid-free BSA, 25 mM glucose, 1 mM sodium pyruvate and 4 mM L-Glutamine (Sigma-Aldrich)). Compounds were diluted in assay medium and loaded to the equilibrated cartridge ports (A: 20 µM isoproterenol, B: 15 µM oligomycin, C: 250 µM dinitrophenol (DNP), D: 40 µM Antimycin A and 25 µM Rotenone). The cartridge was then calibrated for 20 minutes. Measurement was taken before and after each injection through 4 cycles. Each cycle was comprised of 3 minutes of mixing, 2 minutes of waiting and 2 minutes of measuring. Data was normalized with non-mitochondrial respiration. ATP-linked OCR value was calculated by subtracting basal OCR from proton leak OCR.

2.2.5.9 Immunostaining on cells

Cell clones were cultured on 96-well glass-bottomed plates and differentiated as stated before in section 2.2.5.4. Preadipocytes or differentiated brown adipocytes were fixed with 10% formalin for 10

minutes and blocked with filtered 3% BSA/PBS for 1 hour at room temperature. Cells were incubated with Alexa Fluor 546 Phalloidin, HCS LipidTOX™ and Dapi for 1 hour at room temperature, and washed with PBS. Cells were imaged by Dr. rer. nat Kenji Schorpp from the Institute for Molecular Toxicology and Pharmacology (Helmholtz Zentrum München) using the Operetta High-Content Imaging System (PerkinElmer, 20X magnification).

Knockdown cells were plated on 8-well chamber slides and differentiated as stated before in section 2.2.5.4. Cells were fixed with 10% formalin for 10 minutes and blocked with filtered 3% BSA/PBS for 1 hour at room temperature. Cells were incubated with Eif5 (Abcam), Tcf25 (Invitrogen), or Bin1 (Abcam) overnight at 4°C. The next day, sections were washed with PBS and incubated with secondary antibody rabbit Alexa Fluor 594, Alexa Fluor 647 Phalloidin, HCS LipidTOX™ and Dapi for 1 hour at room temperature. Sections were washed with PBS and mounted on microscope slides using DAKO fluorescence mounting medium. Images were captured using a Leica TCS SP5 Confocal (Leica).

2.2.6 Molecular biological methods

2.2.6.1 RNA isolation from cells and tissue

RNA from the brown adipocyte clones was isolated using the QuickExtract™ RNA extraction kit (Biozym), following the manufacturer's instructions. 5 µl lysate was used for cDNA synthesis.

RNA from knockdown cells was extracted the using RNeasy Mini Kit (Qiagen). Cells were lysed in RLT buffer containing 25 µM DTT, followed by adding the same volume of 70% ethanol. Lysates then were transferred into the RNeasy mini spin column and processed according to the manufacturer's procedure.

Tissue probes were homogenized in 1 mL Qiazol (Qiagen) and lysed using metal beads in the TissueLyzer II (Qiagen) at 30Hz/sec for 2 minutes. Homogenized tissue was centrifuged at 10,000 G at 4°C for 5 minutes. The fat layer was removed and chloroform was added.

Subsequently, probes were harshly shaken for 15 seconds and left to sit for 5 minutes. Samples were then centrifuged at 12,000 G at 4°C for 15 minutes. The upper aqueous phase was collected and mixed with the same volume of 70% ethanol. This lysate was then transferred into the RNeasy mini spin column and processed according to the manufacturer's procedure.

For human gene expression analysis, tissues from 6 autopsies conducted at the NIH Clinical Center were collected from superficial subcutaneous fat from the anterior abdomen, deep supraclavicular fat and periadrenal fat. Tissue was rinsed in PBS and immediately transferred into RNAlater (Qiagen). RNA was extracted by homogenizing 100µg tissue using RNeasy Mini Kit (Qiagen) according to the manufacturer's instructions. Total RNA concentration and purity were determined by spectrophotometer at 260 nm (NanoDrop 2000 UV-Vis Spectrophotometer, Thermo Scientific).

2.2.6.2 cDNA synthesis and qPCR

RNA of 500 ng or 1 µg was converted to cDNA using the High-Capacity cDNA Reverse Transcription Kit (Applied Biosystems) according to the manufacturer's protocol. Relative quantification of mRNA was performed using iTaq Universal SYBR® Green Supermix (BioRad), and 300 nM forward and reverse primers (primer sequences are listed in Table 4) in a C1000 Touch Thermal Cycler (BioRad). Real-time quantitative polymerase chain reaction (RT qPCR) assays were run in triplicates and quantified in CFX Maestro Software. All genes were normalized to the expression of TATA-binding protein (Tbp), unless indicated otherwise in the figure legend.

2.2.6.3 Preparation and analysis for RNAseq

For RNAseq samples, RNA was extracted with RNeasy kit (Qiagen), following the manufacturer's instructions. RNA Integrity Number (RIN) values were determined using an automated electrophoresis (Agilent

2100 Bioanalyzer) system and only RNA with a RIN value > 9 was used for further processing.

RNAseq analysis was performed by Dr. Elisabeth Graf from the Institute of Human Genetics (Helmholtz Zentrum München). Non-strand specific, polyA-enriched RNA sequencing was performed as previously described [164]. For library preparation, 1 µg of RNA was poly(A) selected, fragmented and revere transcribed with the Elute, Prime and Fragment Mix (Illumina). End repair, A-tailing, adaptor ligation and library enrichment were performed as described in the Low Throughput protocol of the TruSeq RNA Sample Prep Guide (Illumina). RNA libraries were assessed for quality and quantity with the Agilent 2100 BioAnalyzer and the Quant-iT PicoGreen dsDNA Assay Kit (Life Technologies). RNA libraries were sequenced as 100 bp paired-end runs on an Illumina HiSeq4000 platform. The STAR aligner [165] (v 2.4.2a) with modified parameter settings (--twopassMode=Basic) was used to split-read alignment against the human genome assembly mm9 (NCBI37) and UCSC knownGene annotation. HTseq-count [166] (v0.6.0) was used to quantify the number of reads mapping to annotated genes. Fragments Per Kilobase of transcript per Million fragments mapped (FPKM) values were calculated using custom scripts.

RNAseq results were evaluated by Dr. Dominik Lutter from the Institute of Diabetes and Obesity (Helmholtz Zentrum München). RNA count files were normalized using R package DESeq2 [167] and genes with expression values in the lowest 25% were removed from the data. Hierarchical clustering was performed using the ‘Euclidean’ distance measurement and nearest distance linkage method, if not indicated otherwise.

2.2.6.4 Single cell RNA sequencing (scRNAseq)

Interscapular BAT was taken from three 8-week-old C57BL/6J wild-type male mice. The SVF was isolated according to the protocol in section 2.2.5.1. Live cells were sorted using flow cytometry following dead cell exclusion using 7-AAD. Subsequently, cells were loaded onto a channel

of 10X chip to produce Gel Bead-in-Emulsions. This underwent reverse transcription to barcode RNA before cleanup and cDNA amplification followed by enzymatic fragmentation and 5'adaptor and sample index attachment. Library was sequenced on the HiSeq400 (Illumina) with 150 bp paired-end sequencing of read and 50,000 reads per cell.

2.2.6.5 Protein isolation from cells and tissue

Mature brown adipocytes were washed with PBS and lysed with protein lysis buffer (50 mM Tris pH 7.4, 150 mM NACl, 1 mM EDTA, 1% Triton X-100 containing 0.1% SDS, protease inhibitor and phosphatase inhibitor cocktail II an III). Cells were scraped with a cell scraper and homogenized with a 1 mm syringe. After incubation on ice for 10 minutes, tubes were centrifuged at 14,000 G at 4°C for 10 minutes. Clear lysates were then collected into new tubes and stored at -20°C.

Tissue probes were lysed in protein lysis buffer (without SDS) with magnetic beads in the TissueLyzer II at 30 Hz/sec for 2 times 2 minutes. Subsequently, 0.1% SDS was added to the lysate, mixed and incubated on ice for 10 minutes. Samples were then centrifuged at 14,000 G at 4°C for 15 minutes. The clear lysate was transferred into new tubes and stored at -20°C.

2.2.6.6 Sample preparation, SDS gel and Western blot

Protein concentrations were measured using a BCA Protein Assay Kit (ThermoFischer Scientifice), with a BSA serial dilution as the standard. Protein amounts of 15 to 30 µg were prepared from the samples, in addition to 25% Sample Buffer 4x (Life Technologies) and 2.5% beta-mercaptoethanol (Carl Roth). The mixture was then boiled at 95°C for 5 minutes and cooled down on ice.

Table 8: Recipe for SDS gel

Compound	10% resolving gel	4% stacking gel
Water	4.1 mL	3 mL
Rotiphorese® Gel 30 acrylamide	3.3 mL	750 µl
Tris-HCl 1.5 M pH 8.8	2.6 mL	-
Tris-HCl 0.5 M pH 6.8	-	1.3 mL
SDS 10%	100 µl	50 µl
APS 10%	50 µl	25 µl
Temed	15 µl	10 µl

An SDS gel was prepared (see Table 8) by stacking 10% resolving gel with 4% stacking gel. Samples were loaded and run in 1x running buffer (25 mM TRIS, 192 mM glycine and 0.1% SDS), along with Fisher BioReagents™ EZ-Run™ Prestained *Rec* Protein Ladder (ThermoFischer Scientific) as the molecular weight marker. Protein was transferred onto 0.45 µm PVDF membranes with blotting buffer (25 mM TRIS, 192 mM Glycine and 20% methanol). Unspecific binding sites were blocked with 5% BSA or skim milk in TBS-T (1x TBS with 0.1% Tween 20) at room temperature for 1 hour. Membranes were incubated with primary antibody solutions (see Table 5) overnight at 4°C on the shaker. The next day, membranes were washed with TBS-T and incubated with secondary HRP-conjugated antibody for 1 hour at room temperature on a shaker. Prior to imaging, membranes were washed with TBS-T and developed with ChemiDoc™ (BioRad). Quantification of band intensities was analyzed in Image Lab Software (BioRad).

2.2.6.7 NP40 liver extract for triglyceride assay

Liver was homogenized and powdered using a pestle and mortar in liquid nitrogen. 50 mg of liver powder was dissolved in 500 µl of 5% NP40 (v/v) in deionized water on ice. Using magnet beads, liver was once again homogenized in a TissueLyzer II at 30 Hz/sec for 1.5 minute twice. Samples were then centrifuged at full speed at 4°C for 30 seconds. The supernatant was transferred into a new cold tube and boiled at 90°C for 2 minutes until becoming cloudy. Samples were

cooled down to room temperature and boiled at 90°C for 2 minutes to solute the triglycerides. Subsequently, tubes were centrifuged at full speed at room temperature for 2 minutes. Clear lysate was transferred into fresh tubes and stored at -20°C until further use.

2.2.7 Computational analysis of the scRNAseq data

scRNAseq data was analyzed by Dr. Viktorian Miok from the Institute of Diabetes and Obesity and David Fischer from the Institute of Computational Biology (Helmholtz Zentrum München). Single cell libraries were generated using the Chromium™ Single cell 3'library and gel bead kit v2 (10X Genomics). For the analysis, an indexed mm10 reference genome was built based on the GRCm38 assembly and genome annotation release 94 from Ensembl. The alignment, QC, estimation of valid barcodes and creation of the count matrices ran by Cell Ranger pipeline (v 2.1.1, 10X Genomics) with the command "cellranger count" and standard parameters (except the number of expected cells was set to 10,000 and the chemistry was set to "SC3Pv2"). An anndata object was created using the phyton package Scanpy [168] (v 1.0.4). The full analysis of the scRNAseq is shown in the Appendix.

2.2.7.1 Cell type assignment

The workflow was performed in Scanpy [168] (v 1.4.3). Cells were filtered based on a UMI counts and the fraction of mitochondrial RNA. The remaining cell vectors were normalized to sum a total count of 1e4 by linear scaling, log(x+1) transformed and highly variable genes were selected. We then performed PCA with 50 PCs and used the PC space to compute a k-nearest neighbor (kNN) graph (k=100, method=umap). We computed UMAP and a louvain clustering (resolution=1, flavor=vtraag) based on the kNN graph (louvain_1). We assigned cell types to clusters based on marker gene expression by cluster.

2.2.7.2 Heterogeneity analysis of preadipocytes

We selected the Louvain clusters that correspond to preadipocytes and putative mature adipocytes from the overall clustering (louvain_1) and separately processed these cells: normalizing to 1e4 counts, then log(x+1) transforming the data and selecting highly variable genes followed by PCA with 50 PCs. Again, we computed a kNN graph (k=100, method=umap) based on the PC space. We computed UMAP and a Louvain clustering (resolution=1, flavor=vtraag) based on the kNN graph, which was called clustering louvain_2.

2.2.8 Statistical analysis

Nonlinear dimensionality reduction was performed using Laplacian eigenmaps [169] with Mahalanobis distance as similarity measure and k = 23 for nearest neighbor graph generation. The first eight eigenvectors of the graph Laplacian matrix were used as a low dimensional representation of preadipocyte expression matrix. For each gene in eigenvector-space we calculated the standardized Euclidean distance to geometrical median. K means with k = 2 was used to remove 'uninformative' proximal genes from the data. Silhouette was used to estimate an optimal k = 7 for k-means clustering of the remaining distal genes. KEGG pathway enrichments were calculated using hypergeometrical distribution tests. Network plots were created using Cytoscape v3.6. Calculations were done using R 3.4 and MATLAB 2017b.

Data are shown as mean ± standard error mean (SEM), if not indicated otherwise. Statistical significance for multiple comparisons was determined by One- or Two-Way ANOVA, with Tukey's multiple comparisons test, or unpaired t-test (two-tailed P value). Correlation graphs were analyzed with linear regression (two-tailed P value, 95% CI). GraphPad Prism 6 was used for statistical analysis. P values <0.05 were considered as statistically significant. Differences reached

statistical significance with * p< 0.05, ** p< 0.01, *** p< 0.001 and **** p< 0.0001.

3. Results

3.1 BALB/c mice are protected against DIO, regardless the gender

To dissect the interconnection of metabolic disorder and allergic lung inflammation, it is crucial to choose a robust and suitable mouse model for both conditions. Most of acute and chronic pulmonary allergy studies were performed using female BALB/c strain as the mouse model, since they are able to develop a Th2-mediated immunological response upon antigen challenge [170-173]. However, the propensities of BALB/c mice to develop metabolic disease upon DIO are controversially discussed. Some studies showed that male BALB/c mice have comparable responses with DIO in the rates of body weight gain, insulin resistance, and even possess more hepatosteatosis in comparison to C57BL/6J mice [174, 175]. Meanwhile, other studies showed a protection of BALB/c mice upon DIO, due to a lack of high fat diet-induced hyperphagia and the absence of hepatosteatosis [176]. Therefore, we ran a preliminary study using BALB/c male and female mice to identify a suitable mouse model to study the interaction between metabolic disease and allergic lung inflammation.

3.1.1 BALB/c mice are protected from high fat diet-induced weight gain and glucose intolerance

An experimental setup as shown in Figure 8A was performed on BALB/c mice in order to observe the physiological impact of DIO. A number of 20 mice were fed with chow (control diet, Altromin 1318) or HF for 23 weeks. There were 2 dropouts in the female HF group, due to health reason (mice were running in circle) and they had to be terminated. In addition, to compare with the commonly used strain in a DIO study, we inserted the weight curves from male C57BL/6J mice on chow as control diet (Altromin 1318) and HF for 23 weeks [177]. Body weight was

measured weekly to get a progression overview of the high fat diet (HFD) effect. After 23 weeks of experimental feeding, C57BL/6J mice showed a significant increase in body weight, more than double their initial weight (24.9 ± 0.3 g to 50.8 ± 2.1 g). On the other hand, BALB/c mice slightly gained body weight upon HF (male: 24.5 ± 0.3 g to 34.7 ± 1.3 g; female: 20.5 ± 0.8 g to 30.6 ± 1.4 g), but to a lesser extent than C57BL/6J mice (Figure 8B). The weight gain was reflected in the increase of fat mass in male HF (BALB/c) and even higher in C57BL/6J HF, while female HF did not show a significant increase of fat mass (Figure 8C).

Prolonged HFD feeding has been clearly shown to cause impairment in regulation of glucose homeostasis [178-180], which can be detected by fasting blood glucose levels and a glucose tolerance test. After 17 weeks of experimental diet, male and female BALB/c mice showed no glucose intolerance (Figure 8D and E), no hyperglycemia (Figure 8F) and no hyperinsulinemia (Figure 8G) upon HF feeding. In contrast, HFD feeding in C57BL/6J mice increased circulating glucose and insulin levels, and severely compromised glucose homeostasis upon high glucose challenge [181].

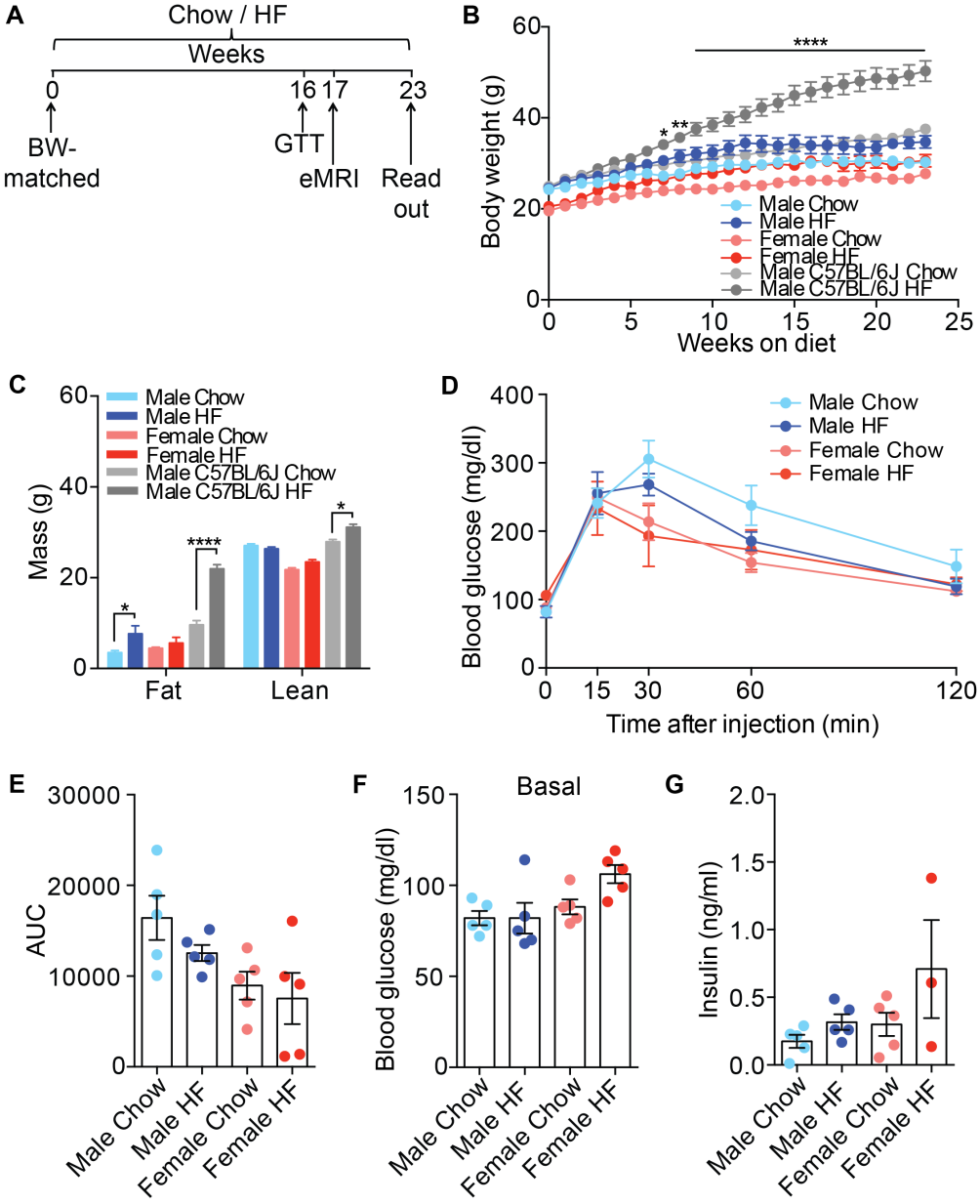

Figure 8: HFD was unable to trigger metabolic impairment in BALB/c mice, unlike in C57BL/6J mice.
(A) Experimental setup for DIO study on BALB/c mice. (B) Body weight curves of male and female BALB/c mice (n= 3-5), and male C57BL/6J mice fed with chow or HF (n= 11-12) for 23 weeks. (C) Body composition of male and female BALB/c mice 17 weeks after experimental diets (n= 3-5), and male C57BL/6J mice 16 weeks after experimental diets (n= 9-10). (D) Glucose tolerance test on male and female BALB/c mice 16 weeks after experimental diets (n= 5). (E) Basal glucose subtracted area under the curve (AUC) calculated from GTT in (D) (n= 5). (F) Basal blood glucose levels of 4 hours fasted male and female BALB/c mice on the day of GTT (n= 5). (G) Serum insulin levels of male and female BALB/c mice 23 weeks after feeding experiment (n= 3-5).

3.1.2 BALB/c mice are protected from HFD-induced inflammation in the adipose tissue

Obesity caused the adipose tissue to expand, which is a result of both hypertrophy and hyperplasia of adipocytes [182]. Therefore, at the end of the study, the weight of fat tissues was measured. HFD-fed mice showed a tendency to have higher scWAT and pgWAT weight compared to the chow-fed mice (Figure 9A and B). There were no striking differences on the adipocyte size of scWAT and pgWAT between HF and chow groups (Figure 10). In accordance with the fat mass (Figure 8C), male BALB/c mice possessed significantly heavier pgWAT upon HF feeding (Figure 9B).

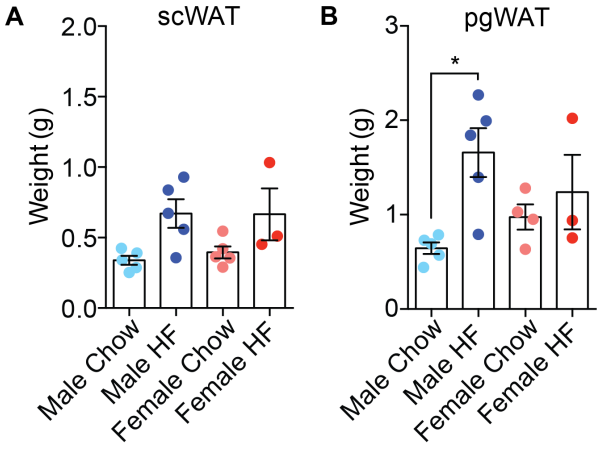

Figure 9: A tendency of heavier fat pad weights in BALB/c mice upon HFD feeding.
The weight of (A) scWAT and (B) pgWAT from male and female BALB/c mice after 23 weeks of feeding (n= 3-5).

As a part of chronic inflammatory process in the adipose tissue upon prolonged HFD feeding, hypertrophy in adipocytes increase the release of inflammatory cytokines, such as Tnfa, IL-6 and IL-1b [183]. These cytokines act as a chemo-attractant for macrophages, which then form crown-like structures surrounding the dead adipocytes, causing more release of inflammatory cytokines [184, 185]. In order to test this, histology sections and mRNA levels of pro-inflammatory cytokines from scWAT and pgWAT were analyzed. Adipocyte size was slightly bigger in male scWAT and female pgWAT with HF diet (Figure 10A). Crown-like structures were found prominently in males, regardless of the diet

(Figure 10A, lower panel). Expression of pro-inflammatory cytokines in scWAT was generally higher in females than males, but no significant changes between diets in all gene expressions (Figure 10B, left panel). There was an up-regulation of Tnfa in pgWAT from male BALB/c mice fed with HF, with no change in IL-6 and IL-1b (Figure 10B, right panel). Meanwhile, C57BL/6J mice showed adipose tissue inflammation upon chronic HFD feeding, as indicated by the increased in crown-like structures and the expression of pro-inflammatory markers [186].

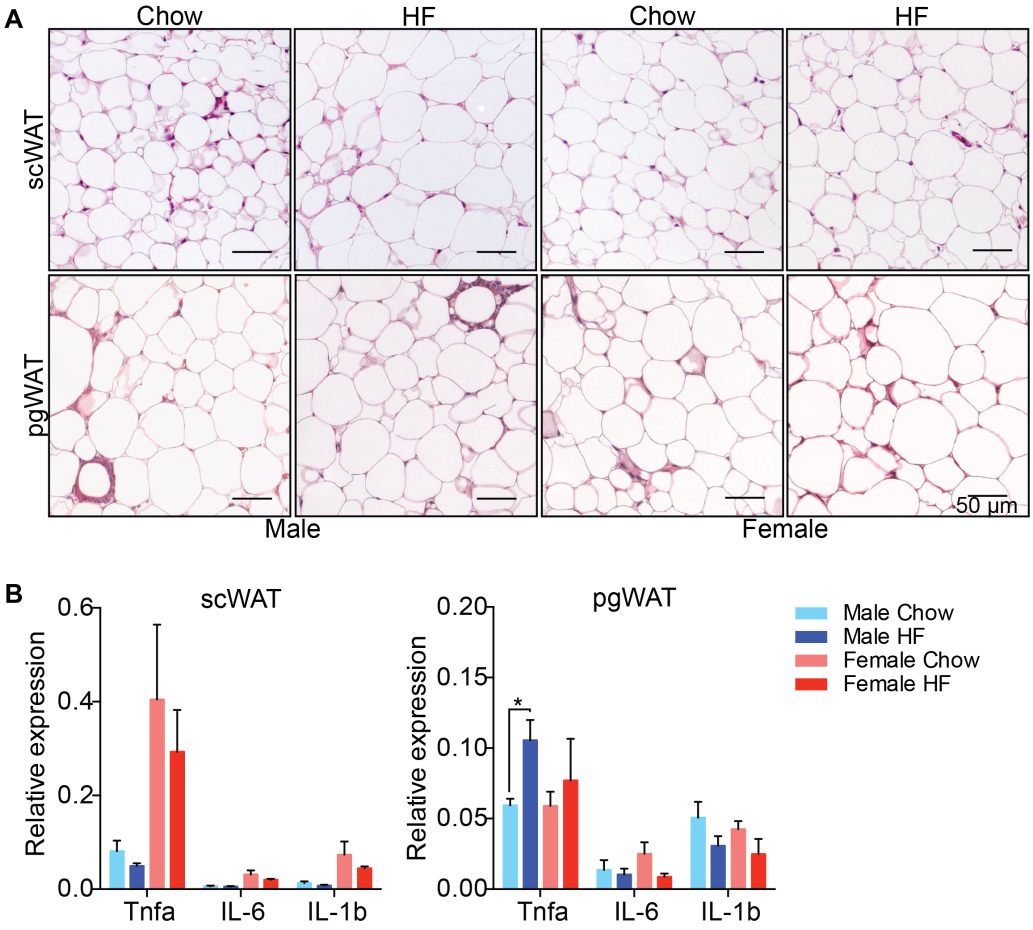

Figure 10: HFD was unable to induce inflammatory cytokines in the adipose tissue of BALB/c mice.
(A) Representative images of H&E staining on scWAT (upper panel) and pgWAT (lower panel) from male and female BALB/c mice after 23 weeks of feeding (scale bar= 50 µm). (B) Relative mRNA level of Tnfa, IL-6 and IL-1b from scWAT (left panel) and pgWAT (right panel) of male and female BALB/c mice after 23 weeks of experimental diet (n= 3-5).

3.1.3 BALB/c mice are protected from HFD-induced hepatosteatosis

Beside adipose tissue expansion, chronic excessive lipid intake is stored in liver, mainly in the form of triglycerides. Therefore, we measured the weight of the liver and the triglyceride content. BALB/c mice had similar liver weight in all groups (Figure 11A). H&E staining showed a slight increase in lipid accumulation in the HF groups, both male and female, compared to the chow diet groups (Figure 11B). According to liver triglyceride content, chow and HF groups showed no significant difference, though tend to increase with the HFD feeding (Figure 11C). On the other hand, C57BL/6J mice increased the liver triglyceride levels by two-fold over 24 weeks of HFD challenge [186].

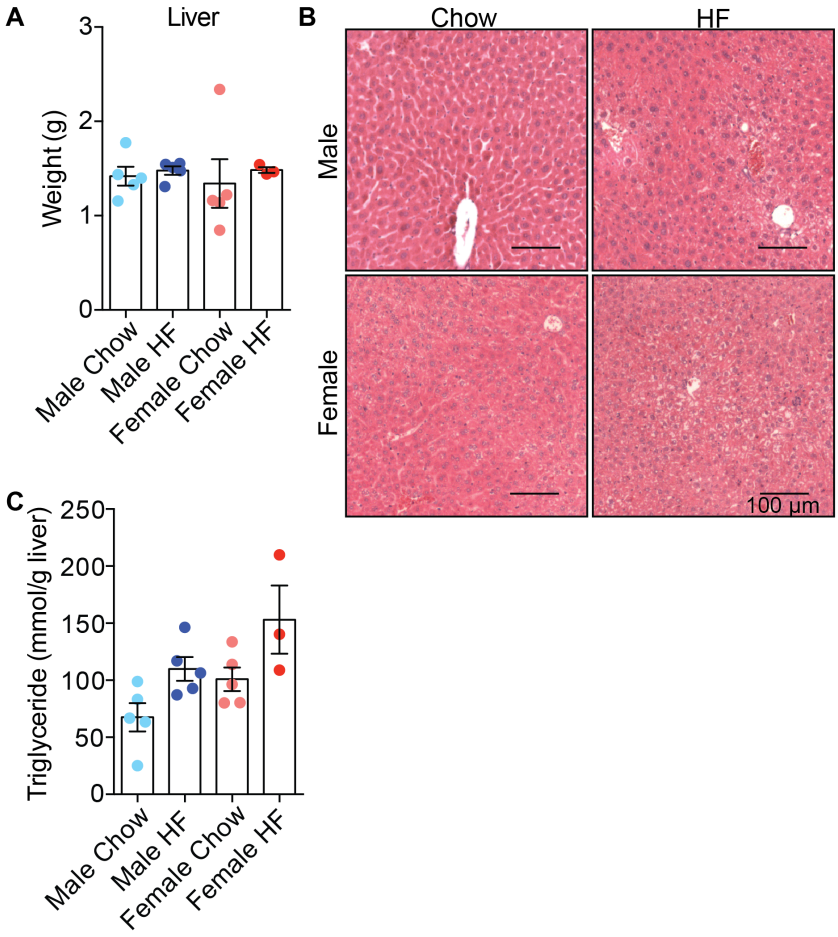

Figure 11: No significant difference in the liver of BALB/c mice upon HFD challenge in the context of lipid accumulation.
(A) Liver weight of male and female BALB/c mice after 23 weeks of diet challenge (n= 3-5). (B) Representative images of H&E staining on liver from male and female BALB/c mice after 23 weeks of feeding (scale bar= 100 µm). (C) Triglyceride content of liver from male and female BALB/c mice after 23 weeks of diet challenge (n= 3-5).

In comparison to C57BL/6J mice, BALB/c mice showed none to minor changes in the phenotype upon DIO. BALB/c mice were protected from HFD-induced weight gain, glucose intolerance and inflammation in the adipose tissue and lipid accumulation in the liver. Taken together, the studies suggested that C57BL/6J mice should be used as the mouse model to study the interaction between metabolic disease and allergic lung inflammation.

3.2 HFD feeding does not aggravate the prognosis of allergic lung inflammation, even show a slight improvement

In response to inflammation, pro-inflammatory cytokines, such as Tnfa, IL-6 and IL-1b, have been implicated in the development of insulin resistance [183]. Increased levels of Tnfa contributed to the redirection of the immune system towards a T-helper type 2 (Th2) cytokine profile, which is associated with a higher risk to develop allergies [187]. Obesity has been known to be a major risk factor for asthma. Thus, it is appealing to study if the development of obesity into metabolic disease would affect the prognosis of allergic lung inflammation.

3.2.1 No difference in body weight gain, but slight improvement in glucose tolerance test of sensitized mice fed with HFD

Male and female C57BL/6J mice were used in this study to identify potential gender differences. To study the effect of HFD on asthma development, mice were assigned to a diet challenged for 8 weeks and subjected to allergic airway inflammation using house dust mites (HDM) sensitization (Figure 12A). We analyzed serum IgE levels as an indicator of successful HDM sensitization. Serum IgE levels on the last day of the

study (week 10) were calculated as fold-change normalized to serum IgE levels before the HDM challenge took place. To avoid data misinterpretation, the non-responders towards allergen with the fold change below 1 (Figure 12B, red circles), were excluded from all the analyses.

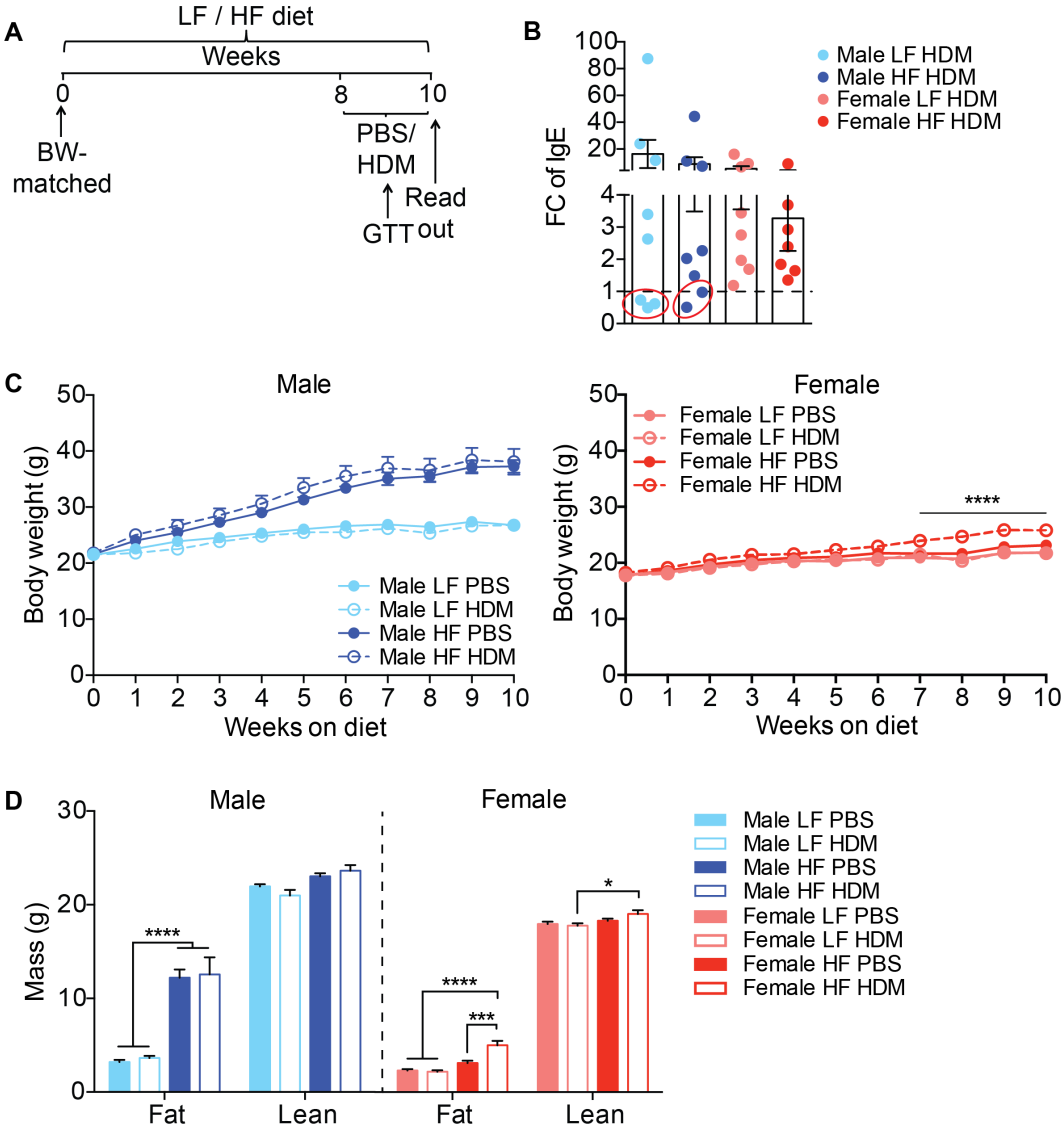

Figure 12: HFD feeding induced body weight gain, with no differences between sensitized and non-sensitized group.
(A) Experimental set up for diet challenge followed by HDM sensitization on male and female C57BL/6J mice. (B) Fold change of serum IgE level collected on the last day of the study was normalized to serum IgE level collected at week 8 after diet challenge from sensitized male and female C57BL/6J mice (n= 7-8). (C) Body weight curves of male (left panel) and female (right panel) C57BL/6J mice over 10 weeks on diet and PBS/HDM challenge without non-responders (n= 5-8). (D) Body composition of male and female C57BL/6J mice 10 weeks after experimental diets and PBS/HDM challenge without non-responders (n= 5-8).

Male C57BL/6J mice were responsive to DIO in the context of body weight gain (Figure 12C), due to the increase in fat mass (Figure 12D). Meanwhile, females were resistant to HFD-induced weight gain (Figure 12C, right panel), as studied before [188], or at least required a longer exposure to HFD to exhibit weight difference from the LF group. Sensitized females showed higher body weight compared to the non-sensitized females in the HF group (Figure 12C, right panel), which was supported by higher fat mass (Figure 12D). Nonetheless, this difference occurred before PBS/HDM challenge took place. Therefore, it was uncertain whether the difference in the body weight was due to HDM challenge or a heterogeneous response to HFD feeding in female C57BL/6J mice, as reported before [189].

Upon HFD challenge, both male and female mice showed a lower tolerance to glucose, but to a lesser extent in HDM-sensitized groups (Figure 13A). Looking at the fasted blood glucose, insulin levels and liver triglyceride values, only male C57BL/6J mice responded to HFD and developed insulin resistance, with no significant difference in between the sensitized (HDM) and non- sensitized (PBS) groups (Figure 13B-D). Meanwhile, female mice were able to maintain blood glucose (Figure 13B) with comparable serum insulin level and triglyceride content in the liver between LF and HF groups (Figure 13C and D). The effect of HFD on metabolic changes was more prominent in male mice as they were more sensitive to DIO [190].

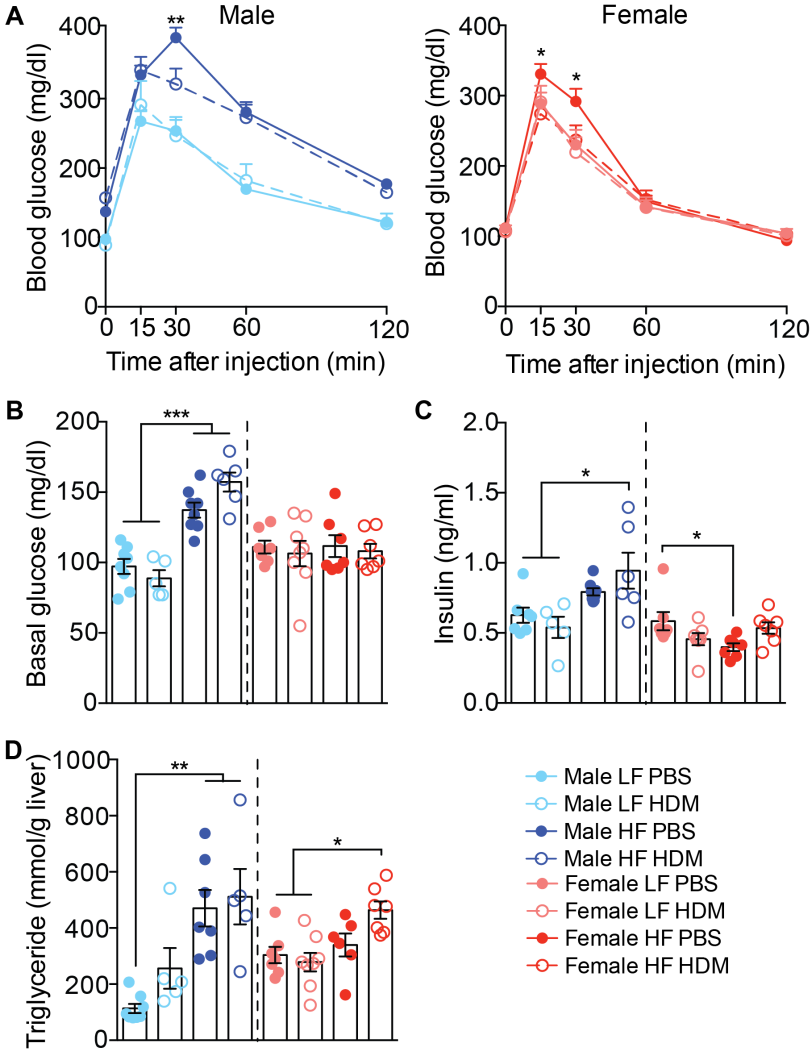

Figure 13: HFD impaired glucose tolerance in male C57BL/6J mice, to a lesser extent in sensitized groups.
(A) Glucose tolerance test and (B) fasted blood glucose on male (left panel) and female (right panel) C57BL/6J mice at week 9 after HDM protocol (n= 5-8). (C) Serum insulin level and (D) Liver triglyceride content of male and female C57BL/6J mice challenged by diet and allergen collected on the read out day (n= 5-8).

3.2.2 HFD-induced pro-inflammatory cell recruitment into pgWAT of male C57BL/6J mice, is reduced upon HDM allergen exposure

The weight of pgWAT was significantly higher in male C57BL/6J mice upon HF feeding, with no difference between sensitized and non-sensitized groups. In accordance with the body composition measurement (Figure 12D), female mice were protected from DIO,

except in the presence of HDM (Figure 14A). Visceral or perigonadal WAT has been linked to the development of metabolic diseases [191], such as insulin resistance, which causes an alteration in the immune cell population [192]. In order to distinguish the difference in immune cell population, FACS analysis was performed on the pgWAT. In response to HF diet, $CD4^+$ and $CD8^+$ cells were unaltered in male mice (Figure 14B). Only females with HDM sensitization showed a reduction in $CD4^+$ cells in the LF group and an induction of $CD8^+$ cells in the HF group (Figure 14B). Only eosinophils and neutrophils were infiltrating into the pgWAT of sensitized mice (Figure 14C, left and middle panel). However, there was a slight reduction in Th17 and M1 macrophages in the male and female HF HDM groups (Figure 14C, right panel and Figure 14D, left panel), indicating HDM sensitization did not exacerbate inflammation processes in pgWAT. M2 macrophage count was unaltered in all groups (Figure 14D, right panel).

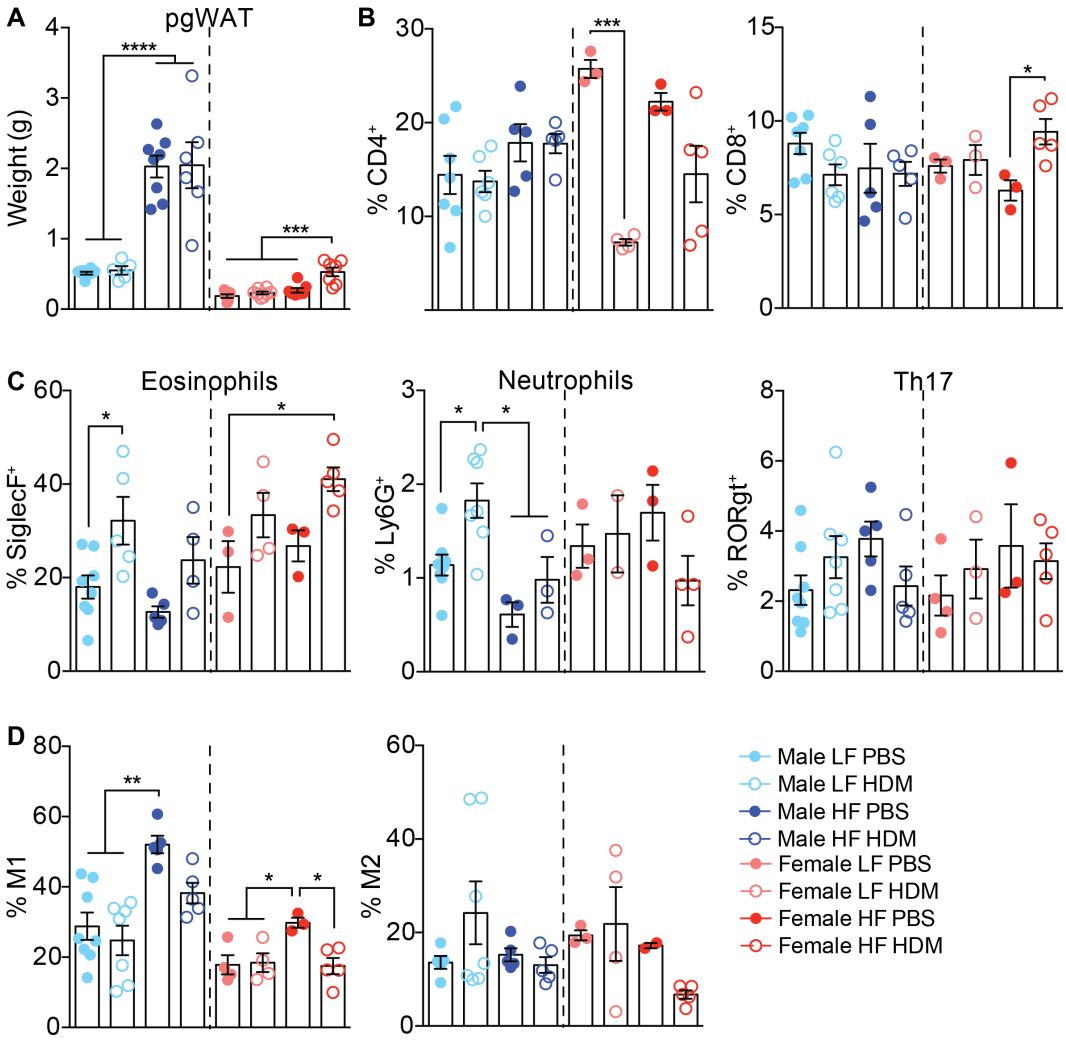

Figure 14: Altered immune cell population in pgWAT of C57BL/6J mice upon HFD and sensitization challenges.
(A) The weight of pgWAT of male and female mice upon diet and HDM challenge, measured on the read out day (n= 5-8). FACS analysis of pgWAT measuring the percentage of (B) $CD4^+$ (left panel) and $CD8^+$ (right panel) of $CD45^+CD11b^-$ cells, (C) $SiglecF^+$ (left panel) and $Ly6G^+$ (middle panel) of $CD11b^+$ cells, $RORgt^+$ (right panel) of $CD3^+$ / $CD4^+$ cells, (D) M1 (left panel) and M2 (right panel) of $CD11b^+$ cells from male and female mice after diet and HDM challenge (n= 2-8).

3.2.3 DIO does not aggravate and even reduce progression of allergic lung inflammation compared to the LF groups

To characterize the effect of DIO on lung inflammation, lung histology and infiltration of inflammatory cells into BAL and lung were evaluated. HDM-sensitized mice revealed increased perivascular and peribronchiolar inflammatory cell infiltration and mucus production, with

more profound effects in the LF groups in both sexes (Figure 15A and B).

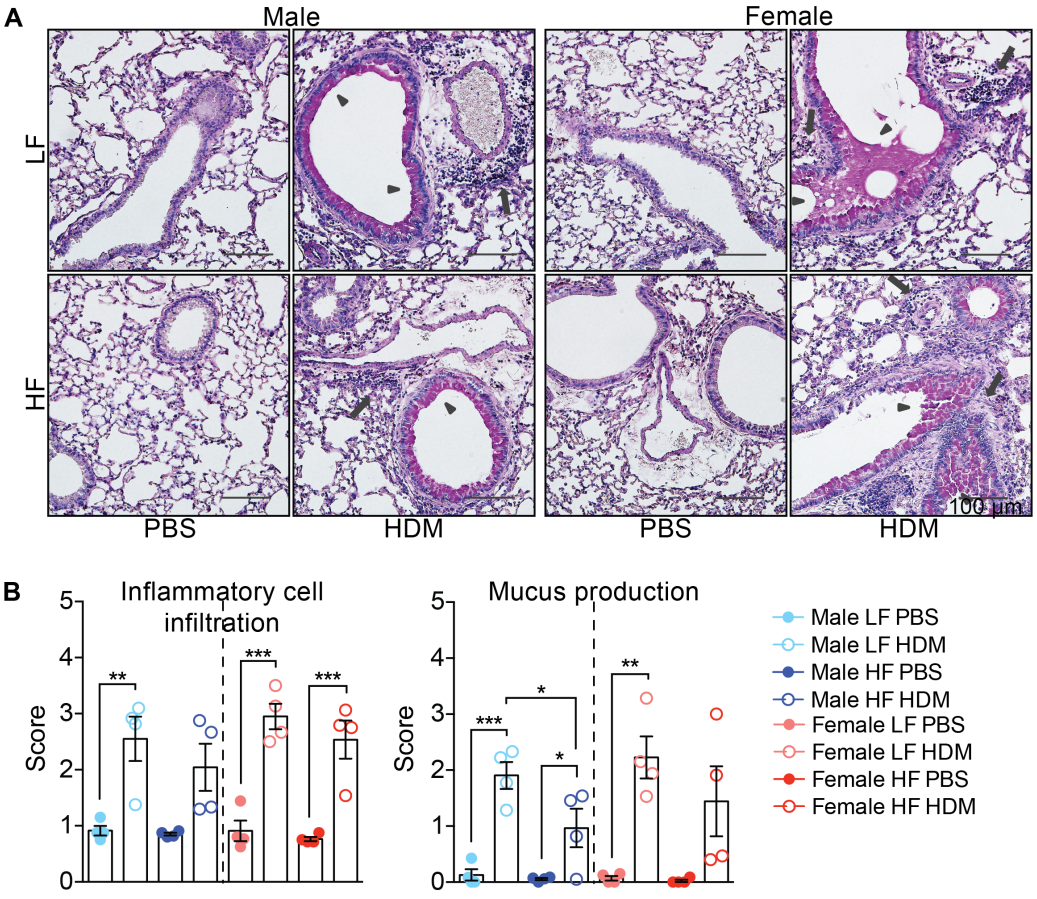

Figure 15: HDM challenge induced inflammatory cells infiltration and mucus secretion in the lungs, more prominent in the LF groups.
(A) Representative PAS staining on lung sections of male and female C57BL/6J mice upon diet and HDM challenge (arrows: inflammatory cells, arrowheads: mucus hypersecretion, scale bar: 100 µm). (B) Scoring of inflammatory cell infiltration (left panel) and mucus production (right panel) in the lungs of male and female C57BL/6J mice upon diet and HDM challenge (n= 4).

The induction of an immune response upon HDM allergen challenge significantly increased the number of inflammatory cells in the BAL fluid in both diet and sex groups. Cells were dominated by eosinophils and to a lower extent by neutrophils and lymphocytes in both sexes (Figure 16A). Total BAL cell count, total eosinophils and relative percentage of eosinophils were higher in the LF groups than in the HF groups in both sexes of sensitized mice, but more noticeable in males (Figure 16A and B).

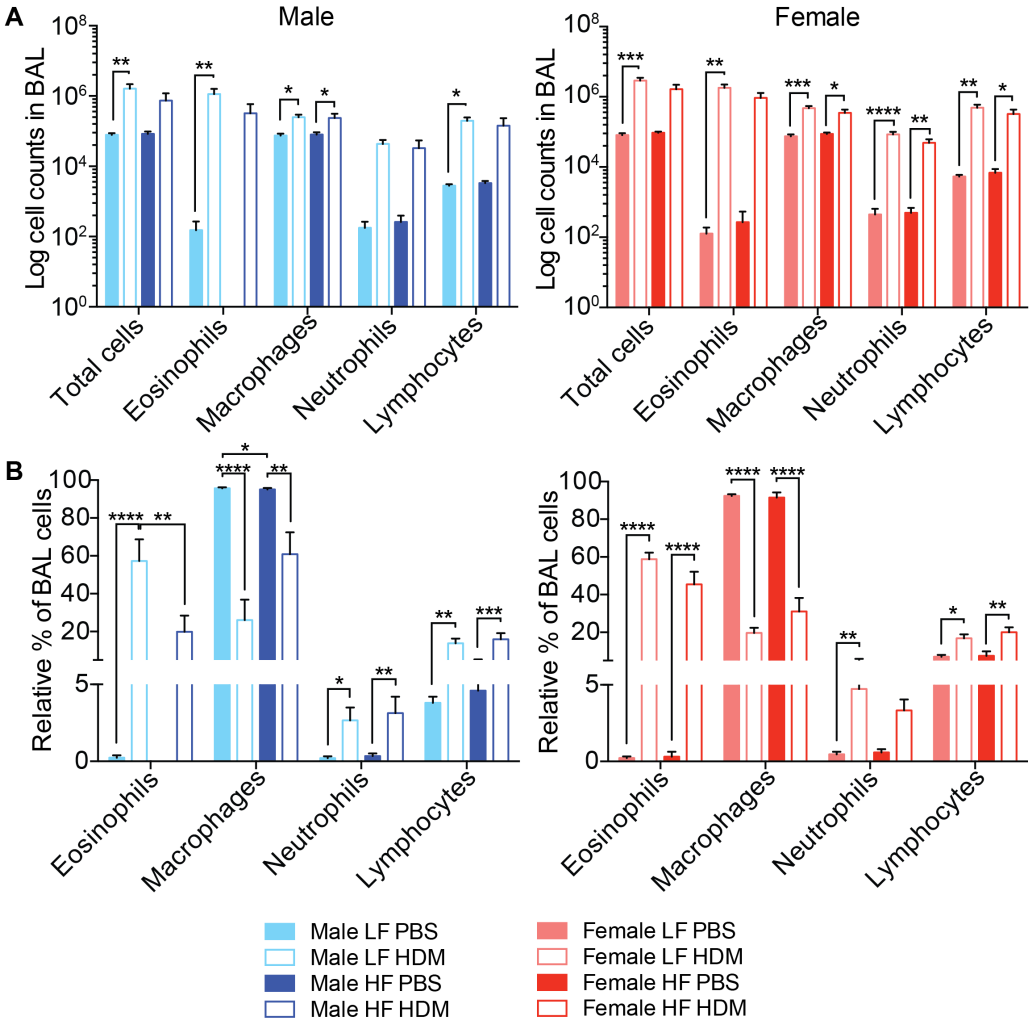

Figure 16: HDM-induced BAL cell counts was more prominent in the LF group in both sexes.
(A) Total and (B) percentages of BAL cell counts of male (left panel) and female (right female) C57BL/6J mice after diet and HDM challenge (n= 5-8).

HDM allergen triggered type 2 inflammatory responses in the lungs. Thus, FACS analysis was performed on immune cell populations recruited to the lungs in the presence of HDM. Sensitization promoted lung inflammation by the increase of $CD4^+$, but not $CD8^+$ cells, in both sexes, and the more profound results were found in LF groups (Figure 17A). As expected, the percentage of Th2 cells was highly up regulated upon HDM challenge in all groups, while being higher upon LF in males and HF in females (Figure 17B, left panel). No difference was observed concerning Treg (Figure 17B, middle panel), with a gradual increase in Th17 from LF PBS to HF HDM in both sexes (Figure 17B, right panel). In addition, the percentage of ILC2s, another inflammatory type 2 in lungs,

was increased in the males with HF HDM group, while no changes in ILC3s were observed (Figure 17C).

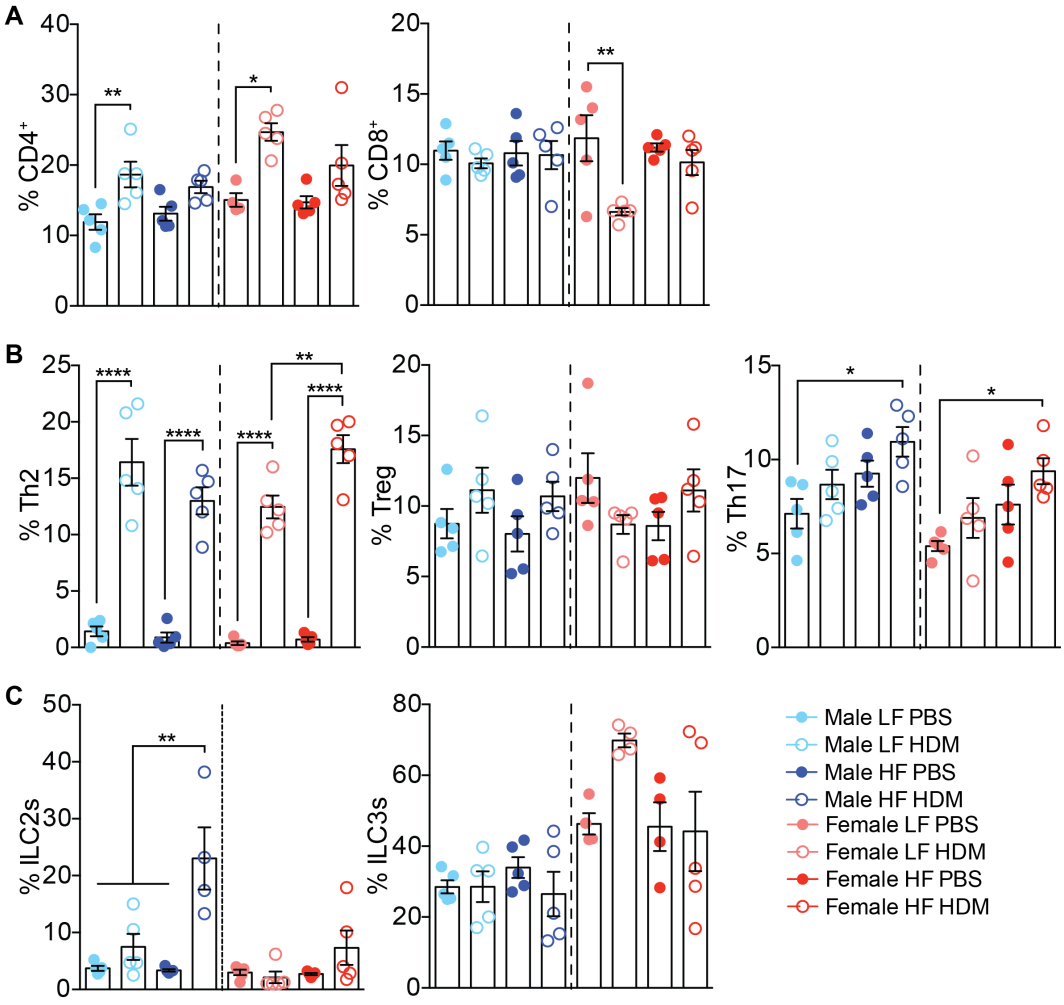

Figure 17: Lung inflammation was induced by HDM inhalation, with slightly higher immune response in the LF groups.
FACS analysis of lungs measuring the percentage of (A) $CD4^+$ (left panel) and $CD8^+$ (right panel) of $CD45^+CD11b^-$ cells, (B) Th2 (left panel), Treg (middle panel), Th17 (right panel) of $CD3^+$ / $CD4^+$cells, (C) ILC2s (left panel) and ILC3s (right panel) of $CD3^-$ $ST2^+$ cells from male and female C47BL/6J mice upon diet and allergen challenge (n= 4-5).

Taken together, male C57BL/6J mice exhibited a more severe response upon DIO compared to the female mice, such as higher fat mass, glucose intolerance, hyperglycemia, hyperinsulinemia and more hepatosteatosis. Regarding the response to HDM allergen, regardless of gender, mice showed a slight improvement in glucose tolerance and less immune responses in the pgWAT and lungs in the HFD groups. Thus, HFD feeding did not have an exacerbation effect on allergic lung

inflammation. In contrast, we observed even less immune response in the lungs compared to the LF group.

3.3 Studying the simultaneous development of metabolic disease and airway allergy reveal improvement in metabolic phenotype and lung inflammation

As mentioned in the introduction, sedentary lifestyle often results from staying indoors and little physical activity. An inactive person therefore is also continuously exposed to HDM. Thus, it is not surprising that most of sedentary obese subjects develop metabolic disease and lung allergy simultaneously. However, if there is an interaction between both diseases remains elusive.

3.3.1 Sensitized mice reveal less fat mass upon HFD feeding

To dissect the interconnection between metabolic disease and lung allergy, an experimental setup closer to the human condition was designed. We performed a study focusing on the simultaneous occurrence of these conditions as putlined in Figure 18A. This study was performed in male C57BL/6J mice only, because they are more susceptible to DIO and exhibit a similar immune response in the lung in comparison to female mice. After chronic exposure to HDM, total IgE serum levels were increased regardless of the type of diets. Serum was collected before and after HDM exposure took place. To avoid any misinterpretation and bias, three mice in LF CPBS group (Figure 18B, red circle) had to be excluded from data analyses due to high IgE level at day 0 (before the experiment started). Weight gain was induced by HF diet feeding, although to a lesser extent in sensitized mice, due to a slight reduction in the fat mass (Figure 18C and D).

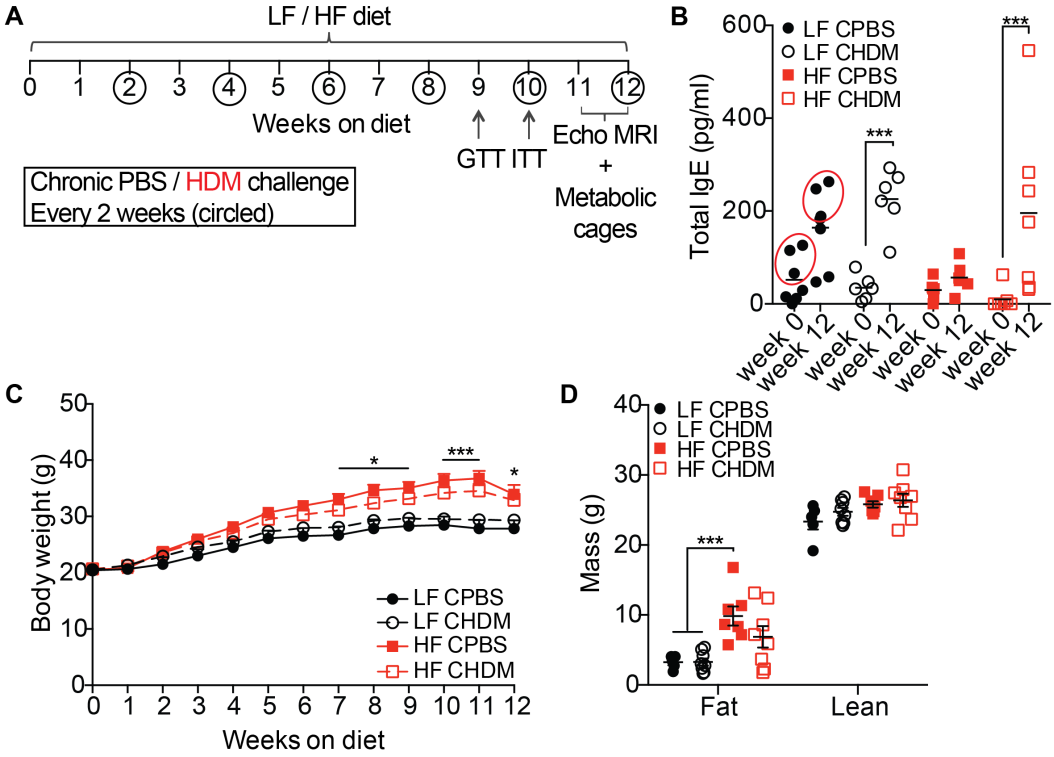

Figure 18: Reduction of fat mass in sensitized mice fed with HF diet.
(A) Experimental setup of chronic PBS or HDM exposure along with constant LF or HF diets feeding. (B) Total serum IgE measured before and after PBS/HDM installation (n= 7-8). (C) Body weight curves and (C) Body composition of mice upon chronic exposure to PBS or HDM and LF or HF diet food (n= 5-8).

3.3.2 Less inflamed lungs are found in obese sensitized mice

Upon constant HDM challenge, lungs were expected to show increased inflammation and to develop immune responses. Both diet groups exhibited more infiltration of inflammatory cells and mucus hypersecretion in the perivascular and peribronchiolar region upon HDM allergen exposure (Figure 19A and B). In addition, the number of total cells in BAL fluid was increased, to a lesser degree in the HF group (Figure 19C). BAL cells were mostly eosinophils, neutrophils and lymphocytes (Figure 19C and D).

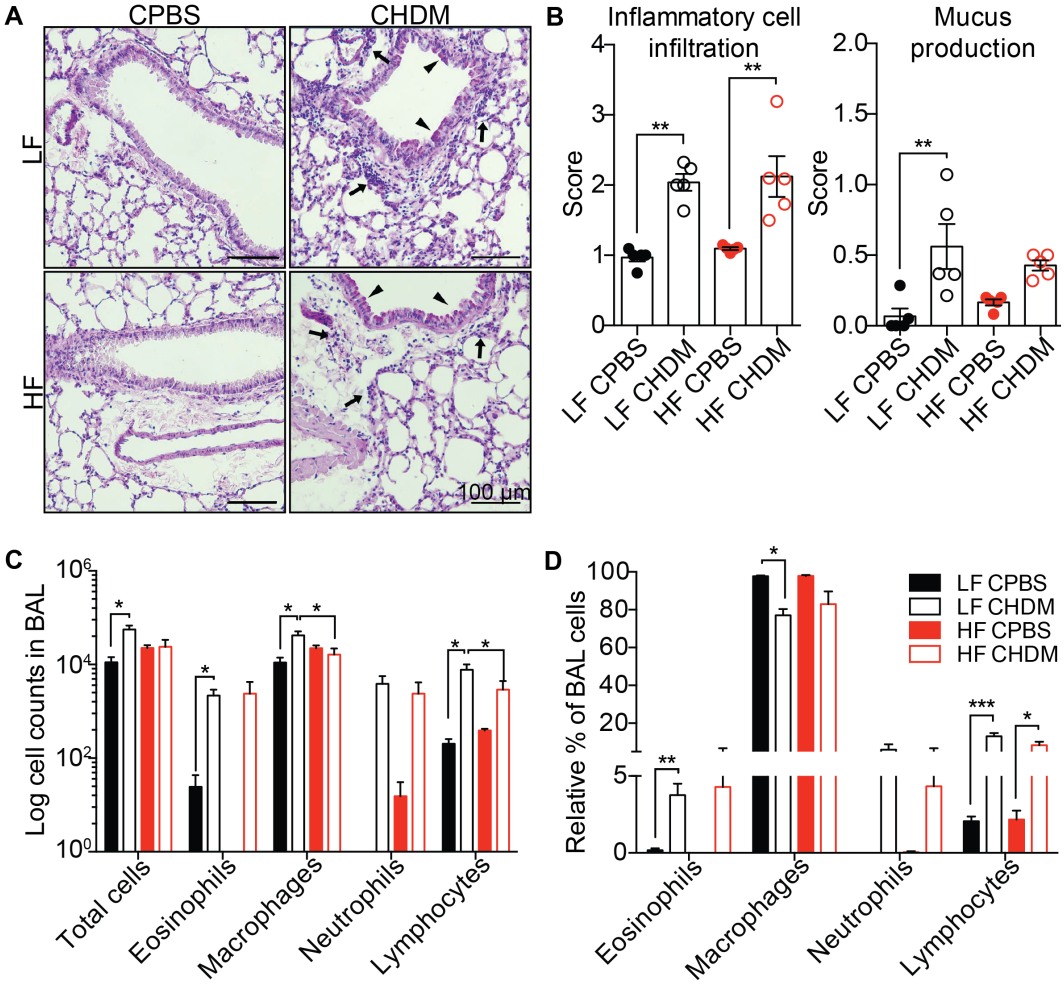

Figure 19: Inflammatory cells in lungs were induced by HDM allergen, to a smaller degree in the HF group.
(A) Representative PAS staining on lung sections from mice chronically exposed to PBS or HDM and LF or HF diet (arrows: inflammatory cells, arrowheads: mucus hypersecretion, scale bar: 100 µm). (B) Scoring of inflammatory cell infiltration (left panel) and mucus production (right panel) from (A) (n= 5). (C) Total and (D) percentages of BAL cell counts of chronically sensitized mice (n= 5-8).

To define immune responses in the lung upon constant HDM challenge, FACS analysis was performed. As expected, the immune response was boosted in the HDM groups, evidenced by the increase percentage of RORgt$^+$, FoxP3$^+$, GATA3$^+$ and ST2$^+$ cells. There were no significant changes in CD4$^+$ and CD8$^+$ cell residents. RORgt, a transcription factor for Th17 [193], was less recruited in the HF CHDM compared to the LF CHDM mice. In addition, FoxP3 and GATA3, differentiation markers for Th2 cells [194, 195], were markedly reduced in HF CHDM in comparison to LF CHDM. ST2$^+$ cells were dominated by ILC3s rather than ILC2s in sensitized mice (Figure 20).

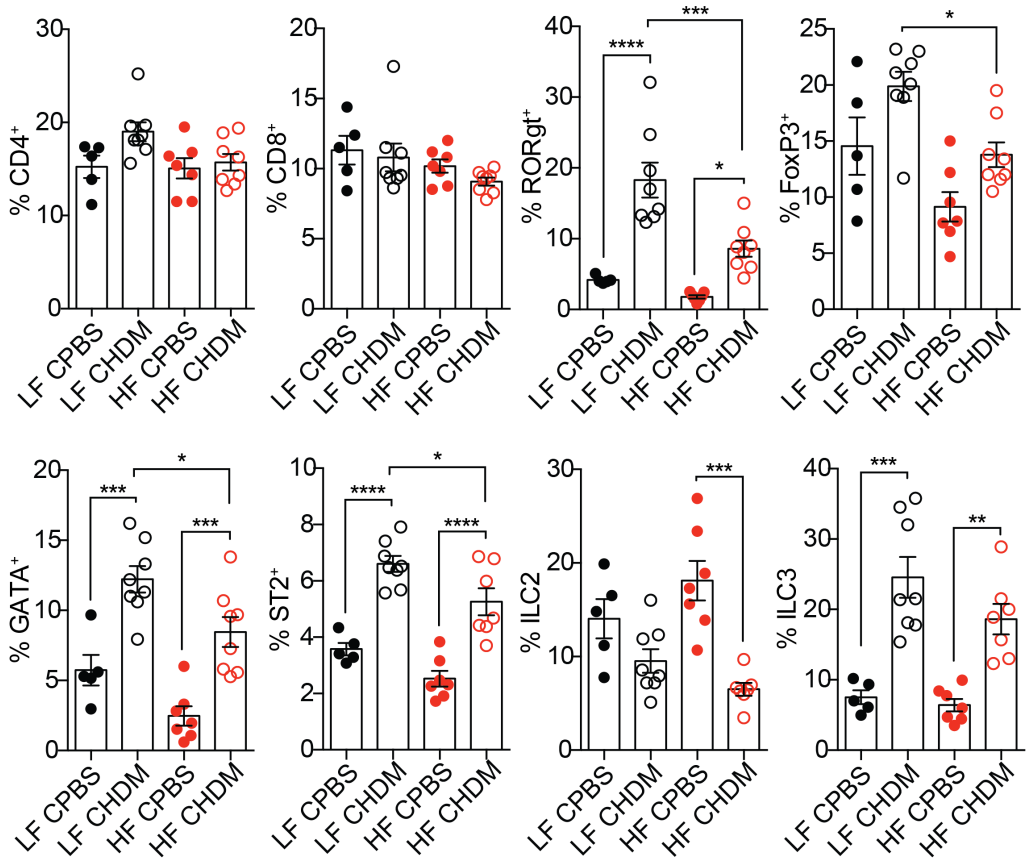

Figure 20: HFD-fed mice revealed less immune response in the lungs.
FACS analysis of lungs measuring the percentage of $CD4^+$ and $CD8^+$ of $CD45^+CD11b^-$ cells, $RORgt^+$, $FoxP3^+$ and $GATA3^+$ of $CD4^+$ cells, $ST2^+$ of $CD3^-$ cells, ILC2s and ILC3s of $CD3^-ST2^+$ cells from mice upon chronic diet and allergen challenge (n= 5-8).

3.3.3 pgWAT inflammation is reduced in obese sensitized mice

Adipose tissue inflammation was mainly characterized by a shift in immune cell populations from anti-inflammatory M2-like to pro-inflammatory M1-like macrophages, which also correlated with insulin resistance [196]. In accordance with a slight decrease in the fat mass of sensitized mice fed with HF diet (Figure 18D), the weight of pgWAT was reduced in HF CHDM mice (Figure 21A). Histology did not show a striking difference, besides slightly bigger adipocytes upon HF diet feeding (Figure 21B). To observe if there was a shift to M1-like macrophages, pro-inflammatory cytokines that are highly secreted by M1-like macrophages, such as Tnfa, IL-6 and IL1b were measured. Cd68, a total macrophages marker, was increased only in the HF CPBS

group, while HF CHDM exhibited a comparable level with LF CHDM. A similar trend was observed in the expression levels of IL-6 and IL-1b, which were reduced in the HF CHDM group (Figure 21C).

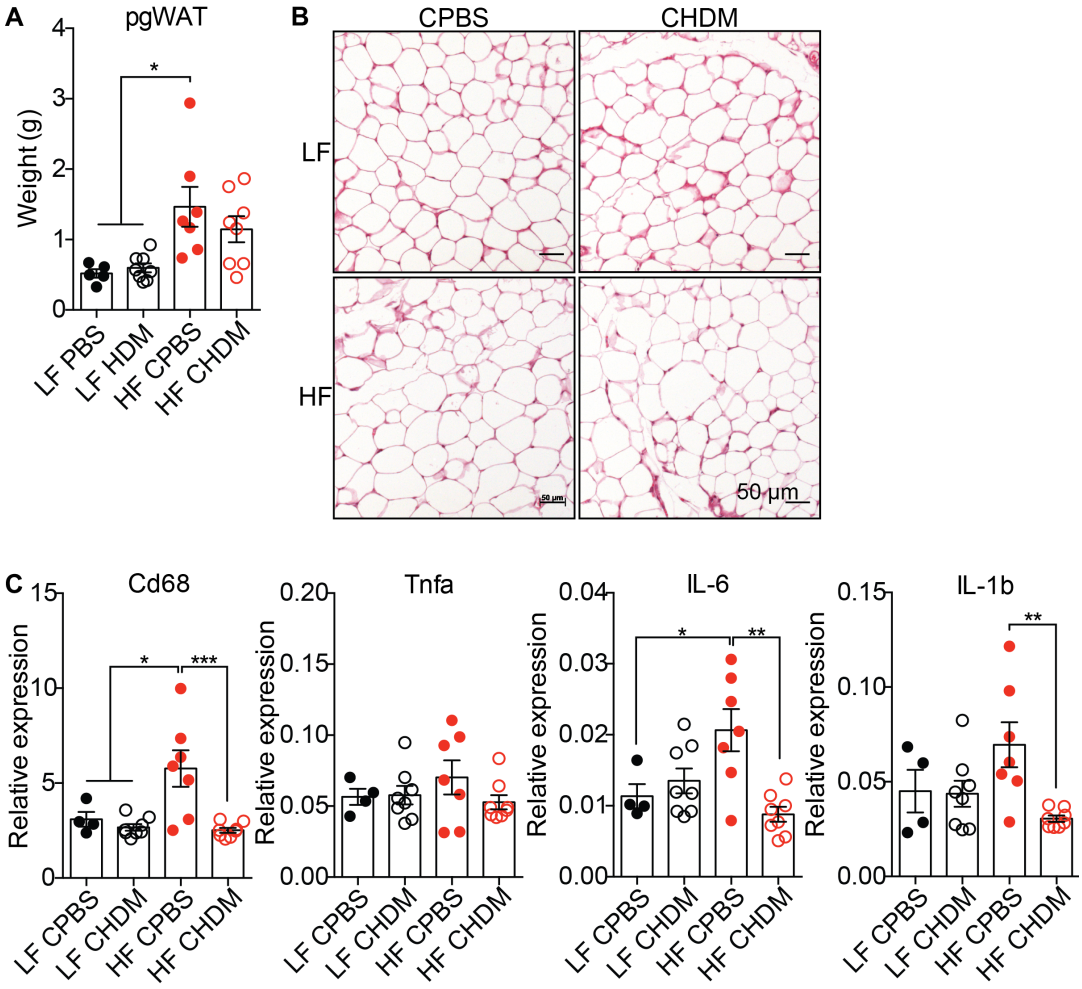

Figure 21: Polarization to M1-like macrophage occurred in HF diet group, but not in the sensitized mice.
(A) Weight of pgWAT, (B) Representative image of H&E staining and (C) Relative mRNA levels of Cd68, Tnfa, IL-6 and IL1b of pgWAT from sensitized and non-sensitized mice fed with LF or HF diet (n= 4-8).

To further investigate the immune cell population in pgWAT, FACS was performed on the same pgWAT samples. The number of $CD11b^+$ cells was increased in sensitized and HF diet groups. The increase of these cells was not correlated with the percentage of M1- and M2-like macrophage populations. However, there was a significant reduction in the percentage of eosinophils upon HFD feeding, and further reduction in neutrophils in HF CHDM group (Figure 22A). The population of $CD4^+$ and $CD8^+$ cells remained unchanged throughout all groups, while the

percentage of RORgt$^+$ cells that was gated from CD4$^+$ cells showed a reduction upon HDM sensitization especially in the HF-fed mice. As mentioned before, RORgt is a transcription factor for Th17, which produces IL-17. The mRNA expression of IL-17a supported the decrease of RORgt expressing cells in HF CHDM group (Figure 22B).

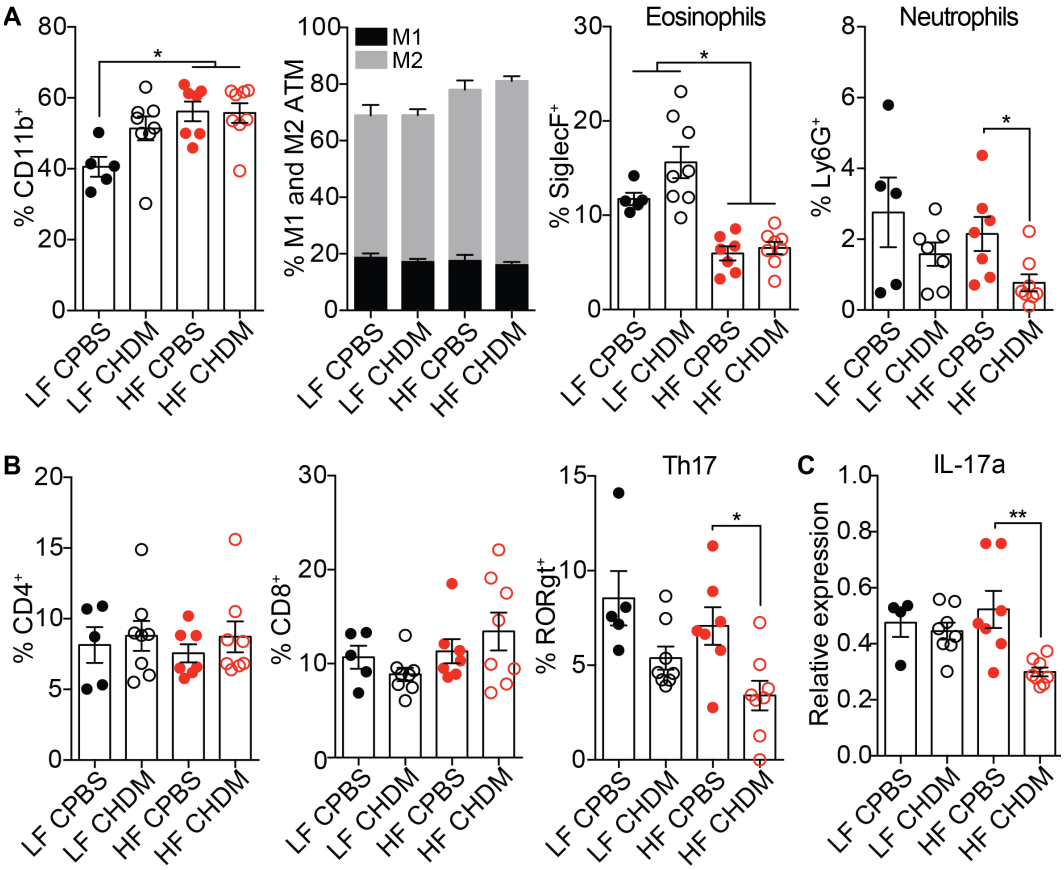

Figure 22: HDM-induced inflammatory cells were found less in the pgWAT of obese mice
FACS analysis of pgWAT measuring the percentage of (A) CD11b$^+$ of CD45$^+$CD11b$^+$ cells, M1 and M2 of CD11b$^+$ cells, SiglecF$^+$ and Ly6G$^+$ of CD11b$^+$ cells, (B) CD4$^+$ and CD8$^+$ of CD45$^+$CD11b$^-$ cells and RORgt$^+$ of CD4$^+$ cells from mice undergo chronic PBS or HDM exposure fed with LF or HF diet (n= 5-8). (D) Relative mRNA level of IL-17a coming from pgWAT of mice chronically exposed to PBS or HDM and under LF or HF diet (n= 5-8).

3.3.4 DIO-induced hepatosteatosis is attenuated in sensitized mice, along with improved glucose tolerance and insulinemia

The liver plays an important role in glucose homeostasis, and in most metabolic diseased people this function is dysregulated and causes hyperglycemia in fasted states [197]. Furthermore, HFD feeding induces

lipid accumulation in the liver, so-called hepatosteatosis. Chronic HDM exposure increased the weight of the liver, with apparent induction in the LF group (Figure 23A). H&E staining of the liver showed healthy-looking hepatocytes in the LF groups, with more lipid droplets accumulated in HF CPBS group (Figure 23B). In accordance with that, less DIO-induced hepatosteatosis was found, supported by a smaller amount of triglyceride content, in the HDM groups (Figure 23C). However, there were no striking changes in the expressions of phosphoenolpyruvate carboxykinase (Pepck), a key enzyme involved in gluconeogenesis, Tnfa or IL-6 in the liver (Figure 23D). The expression of the Kupffer cell marker, Cd68, was reduced in all groups compared to LF CPBS (Figure 23D).

To further investigate the metabolic changes, a GTT and ITT were performed on week 9 and 10, respectively of the experiment. The blood glucose curve after glucose injection revealed glucose intolerance in the HF groups (Figure 24A), which was mildly reduced upon HDM challenge (Figure 24B). Constant HDM exposure in LFD-fed mice increased fasting blood glucose levels, which was not observed in the HFD-fed mice (Figure 24C). In addition, ITT results showed no significant difference between control and HDM groups, regardless of diet (Figure 24D). Nevertheless, hyperinsulinemia occurred in HFD-fed groups, with attenuation in sensitized mice (Figure 24E). Altogether, obese sensitized mice exhibited less triglyceride accumulation in the liver, with improved glucose tolerance and less hyperinsulinemia.

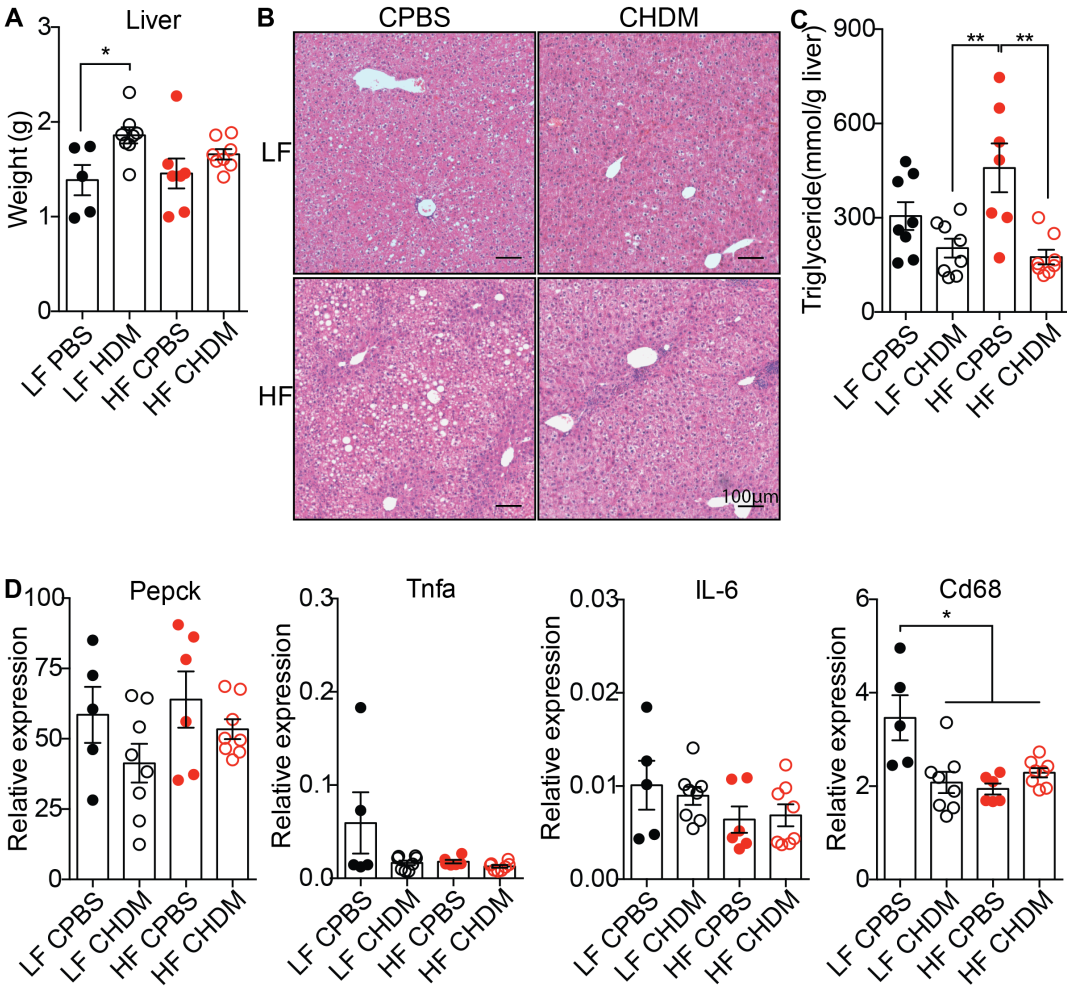

Figure 23: Reduced hepatosteatosis in obese sensitized mice with no changes in inflammatory marker expressions.
(A) Tissue weight, (B) representative image of H&E staining, (C) triglyceride content and (D) relative mRNA expression level measuring Pepck, Tnfa, IL-6 and Cd68 from liver samples of mice that were chronically exposed to HDM or PBS and HF or LF diet (n= 5-8).

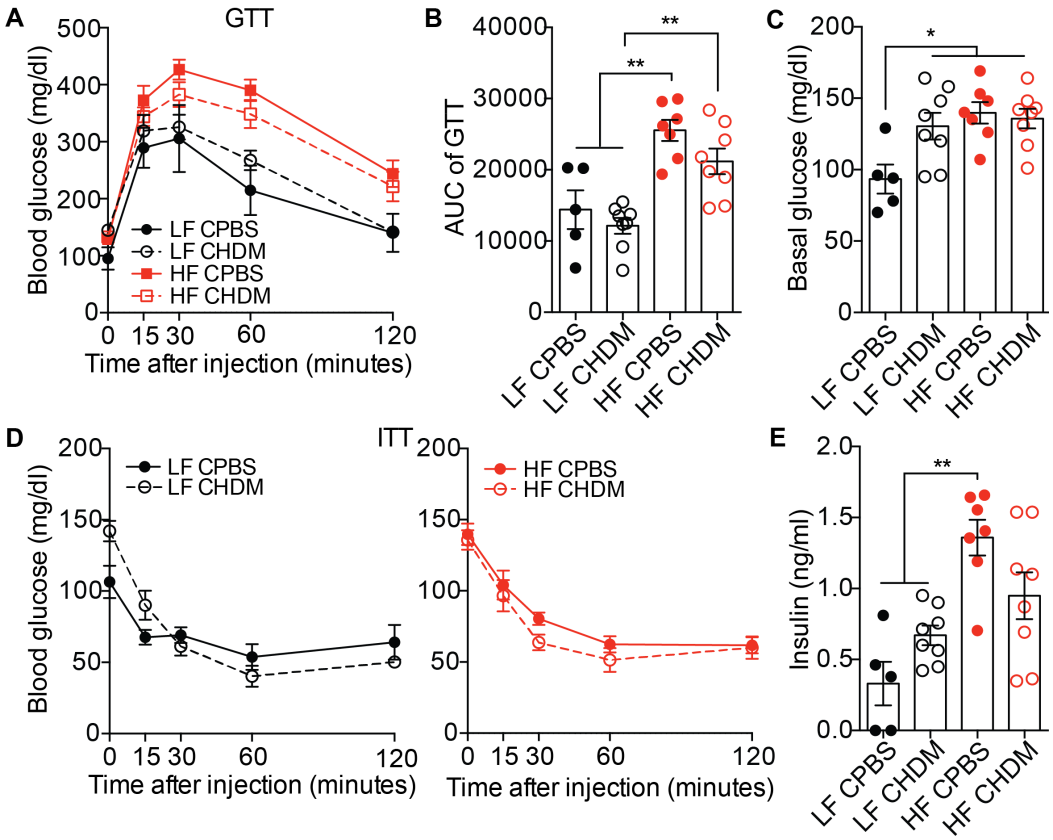

Figure 24: DIO-induced hyperglycemia and hyperinsulinemia were improved in the sensitized mice.
(A) Glucose tolerance test after 9 weeks of diet, (B) area under the curve of basal normalized GTT and (C) basal blood glucose level after 4 hours of fasting (n= 5-8). (D) Insulin tolerance test after 10 weeks of diet: LF groups (left panel, n= 3-6) and HF groups (right panel, n= 7-8). There were 2 dropout mice from each LF group due to hypoglycemia (blood glucose was not detected with glucometer) during insulin injection. (E) Fasted serum insulin level collected after 10 weeks of diet (n= 5-8). There were 2 samples from LF CPBS group that was not detected (ND, too low value).

3.3.5 Chronic HDM exposure slightly increases food intake and energy expenditure in obese mice

One possibility to explain the improvement in the metabolic parameters in obese sensitized mice was that HFD-induced hyperphagia was diminished in sensitized mice. Therefore, metabolic cages were utilized to assess food intake, respiratory quotient, energy expenditure and locomotor activity from all groups. Mice were individually housed for 6 days, with the same habitual settings (humidity, temperature and dark-light cycle). Food intake was displayed as the mean of daily food intake

and showed a slight increase in HF CHDM compared to HF CPBS, while no difference between PBS and HDM in LF groups (Figure 25A).

Food that is consumed is composed of different molecules (e.g. carbohydrates and fats), varying the amounts of oxygen that is needed to efficiently digest the food. Thus, it ends with water and carbon dioxide (CO_2) as the byproduct. The respiratory quotient (Rq) is a metabolic exchange ratio that is equal to CO_2 production over O_2 uptake (CO_2/O_2). Gas ratio fluctuates depending on the food substance that is metabolized. In the LF groups, the Rq value was close to 1 (Figure 25B, left panel), indicating that carbohydrates were the main fuel for energy substrate. This is simply because in order to oxidize one molecule of glucose, the same amount of O2 is needed and CO2 is produced. However, the sensitized and non- sensitized mice did not change the substrate utilization to acquire energy. Meanwhile, in the HF groups, the Rq value was approximately 0.7 – 0.8, indicating more fatty acids utilization, since it required more oxygen for the complete digestion (Figure 25B, right panel). There were no differences between control and HDM groups, although in general the values were higher during dark phase, since mice are nocturnal animals.

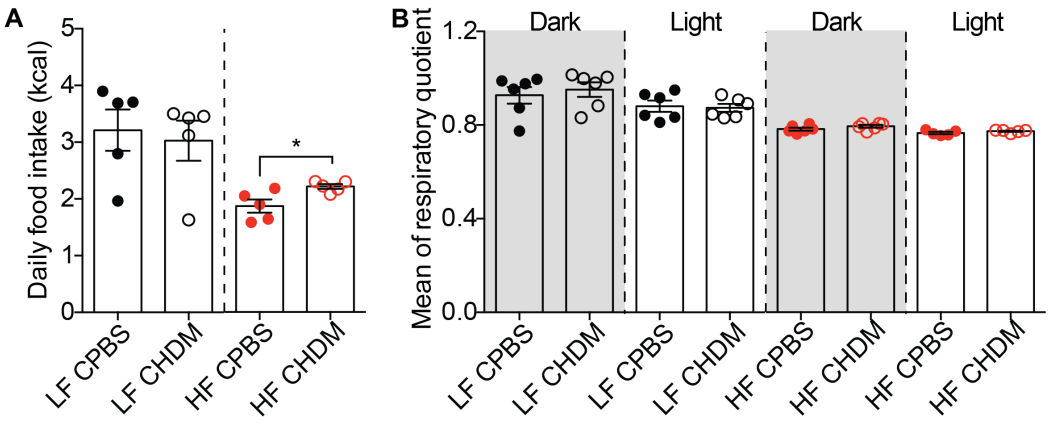

Figure 25: Increased mean of daily food intake in HF CHDM mice compared to HF CPBS with no changes in the mean of respiratory quotient.
Metabolic cages assessment of LF and HF diet-fed mice at week 11-12 for 137 hours (dark phase is shown in grey shade): (A) mean of daily food intake (n=4-5) and (B) respiratory quotient (n= 5-6).

Obese sensitized mice consumed a similar amount of food, yet had ameliorated glucose intolerance, less hepatosteatosis and a slight reduction in fat mass. In this context, either the excess energy was stored in another tissue or EE was increased. Mean of EE was calculated per day, and differed in dark and light phase in each group. The EE of LF CHDM mice was slightly lower than the control group, especially in the light phase. On the other hand, HF CHDM mice had higher EE in both dark and light phase compared to the HF CPBS (Figure 26A). Basal metabolic rate (BMR) was counted as the minimum EE in 24 hours (12 hours of dark and light phase). A similar trend as the EE was observed, with less BMR in the LF CHDM and higher BMR in HF CHDM compared to their PBS controls (Figure 26B). Motor activity did not contribute to changes in the EE, as shown in Figure 26C, except in the LF CHDM, which moved more in the dark phase.

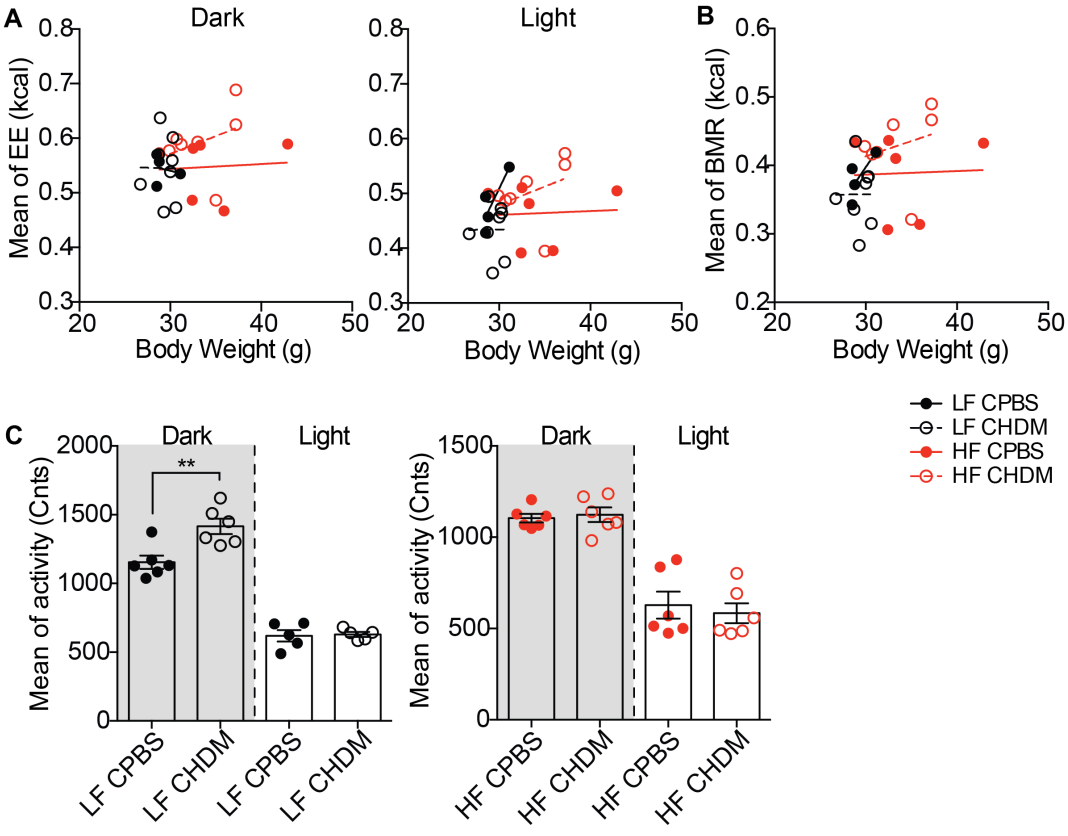

Figure 26: Constant HDM exposure tended to increase the energy expenditure in HFD-fed mice, while decrease in the LFD-fed mice.
Metabolic cages measurement of (A) mean of EE in correspond to individual body weight during dark phase (left panel) and light phase (right panel), (B) mean of basal metabolic rates correlated to individual body weight (n= 4-8) and (C) mean of locomotor

activity during dark and light phase on LF (left panel) and HF (right panel) diet-fed mice (n= 5-6).

3.3.6 Increased beiging in the scWAT of HF CHDM mice

In comparison to pgWAT, scWAT is not as susceptible to developing adipose tissue inflammation upon DIO [182]. Besides, scWAT is an important target for 'browning', where it can be induced to develop into a brown-like adipocyte resulting in an improvement in metabolism upon DIO [198]. The weight of scWAT was not affected as significantly as the pgWAT upon DIO (Figure 27A). Histological images showed no enlargement in adipocyte size between LF and HF groups (Figure 27B). In general, HFD reduced brown adipocyte specific marker expression in scWAT, like Ucp1 and Cidea, but to a smaller degree in the sensitized mice. Prdm16, a determinant factor for brown-like adipocytes, had increased mRNA expression upon chronic HDM sensitization along with HFD feeding. In accordance, HF CHDM mice had higher Tmem26 expression, a beige adipocytes specific marker gene [147] (Figure 27C) and higher Ppargc1a expression than control mice (Figure 27D). In addition, obese sensitized mice showed higher expression of IL-13 and IL-4 in the scWAT compared to the other groups (Figure 27D).

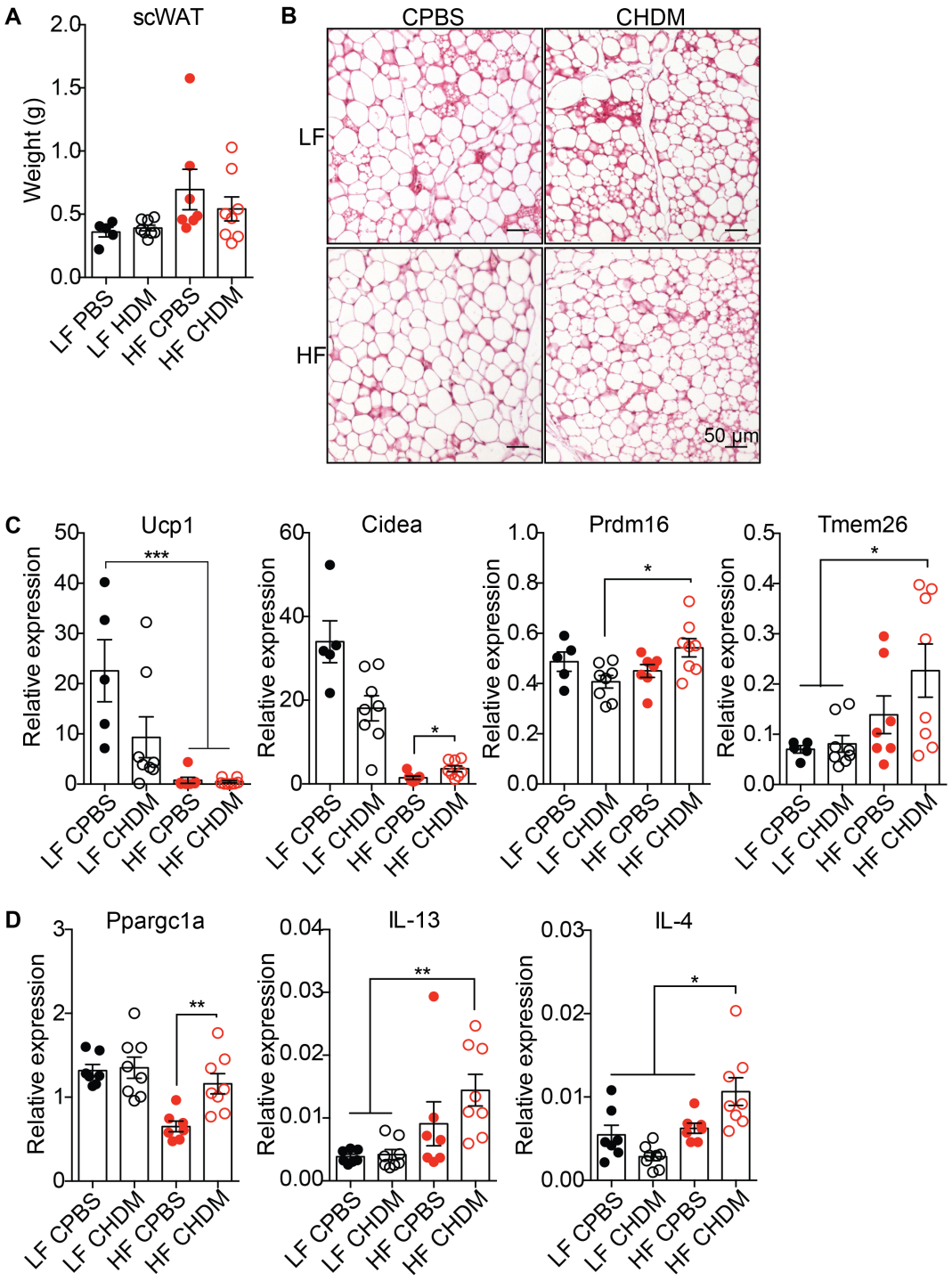

Figure 27: Increased beiging markers in the scWAT of obese sensitized mice.
(A) The weight, (B) representative image of H&E staining and (C) relative mRNA expression of Ucp1, Cidea, Prdm16, Tmem26, (D) Ppargc1a, IL-13 and IL-4 from scWAT of mice chronically exposed to PBS or HDM and fed with LF or HF diet (n= 5-8).

3.3.7 Increased expression of Vegfa and glucose transporter 1 (Glut1) in the BAT of obese sensitized mice

One of the possibilities contributing to an increase in EE is via activation of BAT. H&E staining of BAT sections showed bigger lipid droplets upon HFD feeding, with no difference between PBS and HDM groups (Figure 28A). Ucp1, the hallmark protein of human and murine BAT that plays a role in adaptive thermogenesis [199], was unaltered upon DIO and HDM sensitization at the mRNA and protein levels (Figure 28B-D). In addition, IL-6 is secreted by BAT upon β-adrenergic stimulation [200] and beneficial in the regulation of BAT metabolism. However, the expression of IL-6 was not changed upon HFD or HDM (Figure 28E).

Even though there were no changes in the Ucp1 levels, Vegfa, a proangiogenic factor that induces endothelial cell proliferation and vessel permeability [201], was up regulated upon chronic HDM exposure in the HFD group. The increase in Vegfa expression was exclusive in BAT and did not occur in scWAT or pgWAT (Figure 28E). Simultaneously, the expression of Glut1, but not Glut4 was elevated in the HF CHDM group (Figure 28F). Compared to its control, obese sensitized mice showed higher expressions in glycine amidinotransferase (Gatm) and guanidinoacetate N-methyltransferase (Gamt) in BAT (Figure 28F), which are two key enzymes in creatine synthesis pathway [202]. Unfortunately, BAT is a complex tissue and translation from murine BAT data to humans is limited due to putative differences in cellular composition between species. Therefore, a more comprehensive study regarding its cellular distinction is needed to gain an elaborative conclusion.

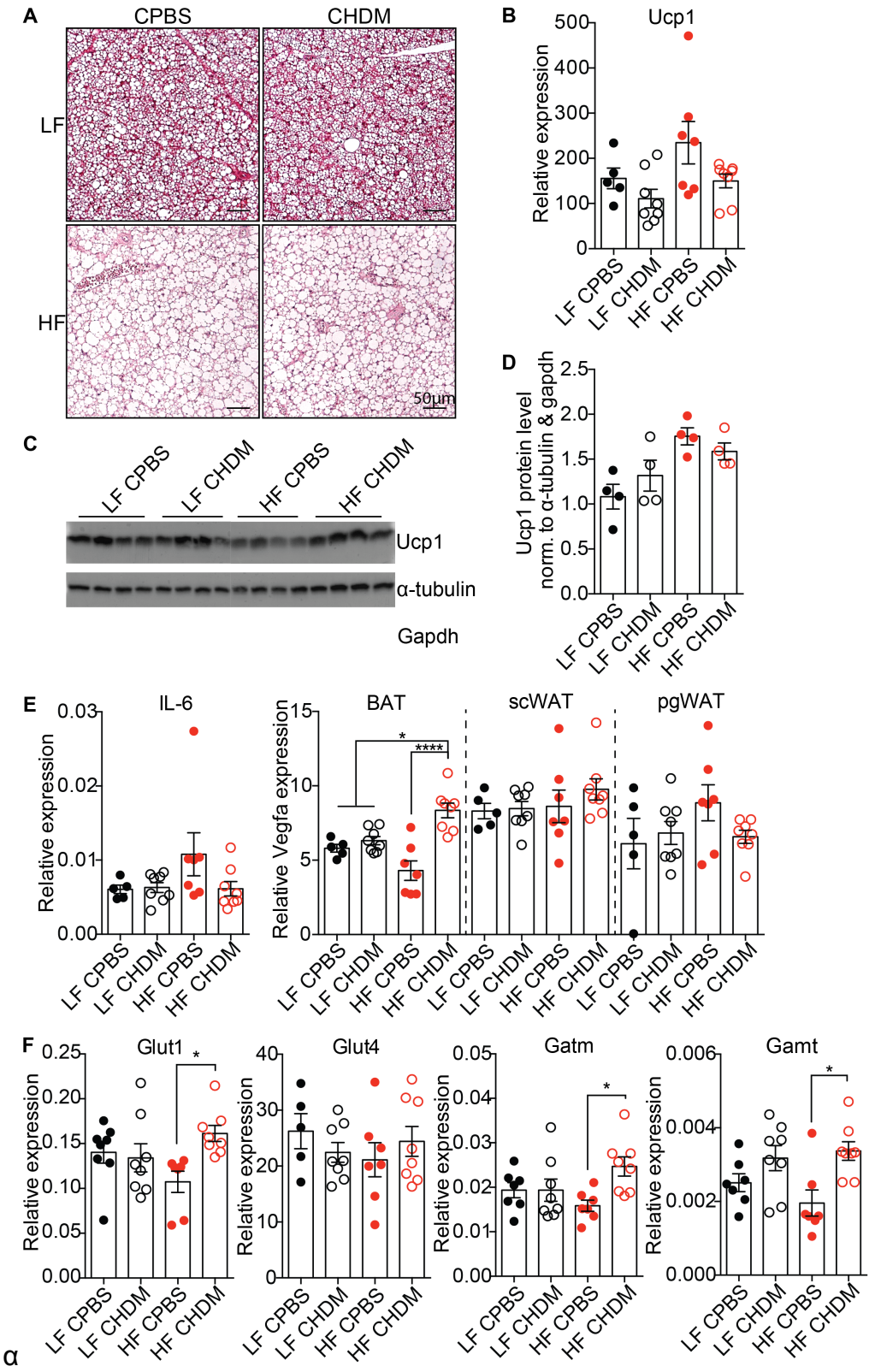

Figure 28: Chronic HDM exposure on obese mice resulted in the up regulation of Vegfa and Glut1 mRNA level in BAT.
(A) Representative images of H&E staining, (B) relative mRNA level of Ucp1 (n= 5-8), (C) Ucp1, α-tubulin and Gapdh western blot, (D) quantified Ucp1 western blot shown in (C, n= 4) normalized to mean α-tubulin and Gapdh, (E) relative mRNA level of IL-6, Vegfa, (F) Glut1, Glut4, Gatm and Gamt in BAT (Vegfa expression in BAT, scWAT and pgWAT) from mice sensitized to HDM or PBS and fed with HF or LF diet (n= 5-8).

3.4 Multiple brown adipocyte lineages hold distinct functional properties

BAT was thought to be absent in the adult human, but since several studies discovered the presence of a metabolically active BAT depot in human [203, 204], plenty of research has been conducted to explore its full potential to combat obesity. A detailed understanding on the developmental origin of brown adipocytes is important to mediate the translation of murine model research data to human physiology. In this part, we investigated brown adipocyte lineages with identified markers to distinguish different subpopulations of brown adipocytes.

3.4.1 Heterogeneous expression of Ucp1 in murine interscapular BAT

As mentioned above, Ucp1 is a specific marker for BAT and its expression is highest in interscapular (iBAT) and subscapular brown adipose tissue (sBAT) (Figure 1 and 29A). Nonetheless, this study was focused on iBAT, as it is abundantly used in many BAT-related studies. Immunofluorescence staining of BAT sections from adult male C57BL/6J mice showed a mosaic expression of Ucp1 (Figure 29B), as recently described [205]. Fluorescent intensity of Ucp1 was classified and quantified as described in section 2.2.4.5, and revealed even division of cells expressing high and low Ucp1 (Figure 29C). However, no clear anatomical pattern correlated to the various expression of Ucp1.

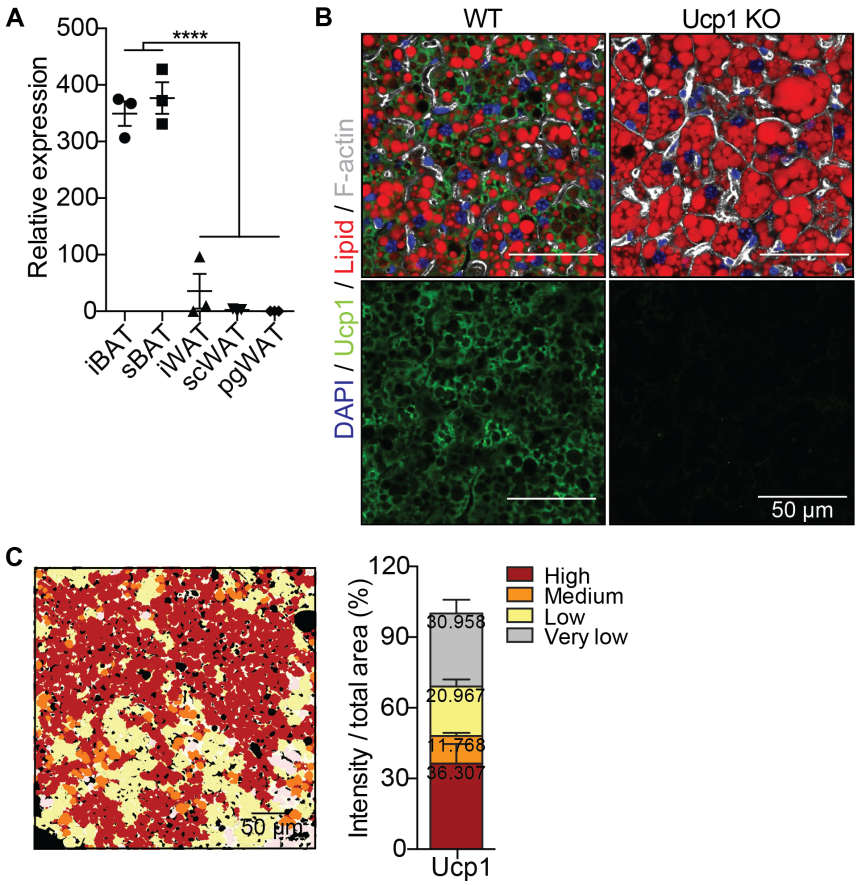

Figure 29: Specific brown fat marker was expressed in a mosaic pattern on the BAT section. (A) Relative mRNA level of Ucp1 measured from interscapular BAT (iBAT), subscapular BAT (sBAT), interscapular WAT (iWAT), scWAT and pgWAT of 6 week old C57BL/6J male mice (n= 3). (B) Immunofluorescence staining of Ucp1 (green), lipid droplets (red), F-actin (white) and nucleus (blue) from wild type and Ucp1-KO mice. (C) Quantification of Ucp1 content in individual brown adipocytes in BAT normalized to total area. Lipid droplets are included into area measured and F-actin was used to distinguish each cell (n= 11).

3.4.2 Single cell RNA sequencing (scRNAseq) from SVF of murine BAT reveals distinct differentiation stages

To gain better knowledge on whether the heterogeneity is occurring during preadipocyte state, scRNAseq analysis was performed on isolated SVF of iBAT from 8-week-old male C57BL/6J mice. Louvain clustering of the gene expression identified 12 different clusters, including immune cells, erythrocytes and 2 distinct brown preadipocyte clusters marked by preadipocyte marker, Pdgfra. In addition, a presumed cluster of mature brown adipocyte with high Pparg and Fabp4 expression in cluster 7 was identified (Figure 30A and B). Preadipocyte clusters were divided into 4 distinct groups (Figure 30C).

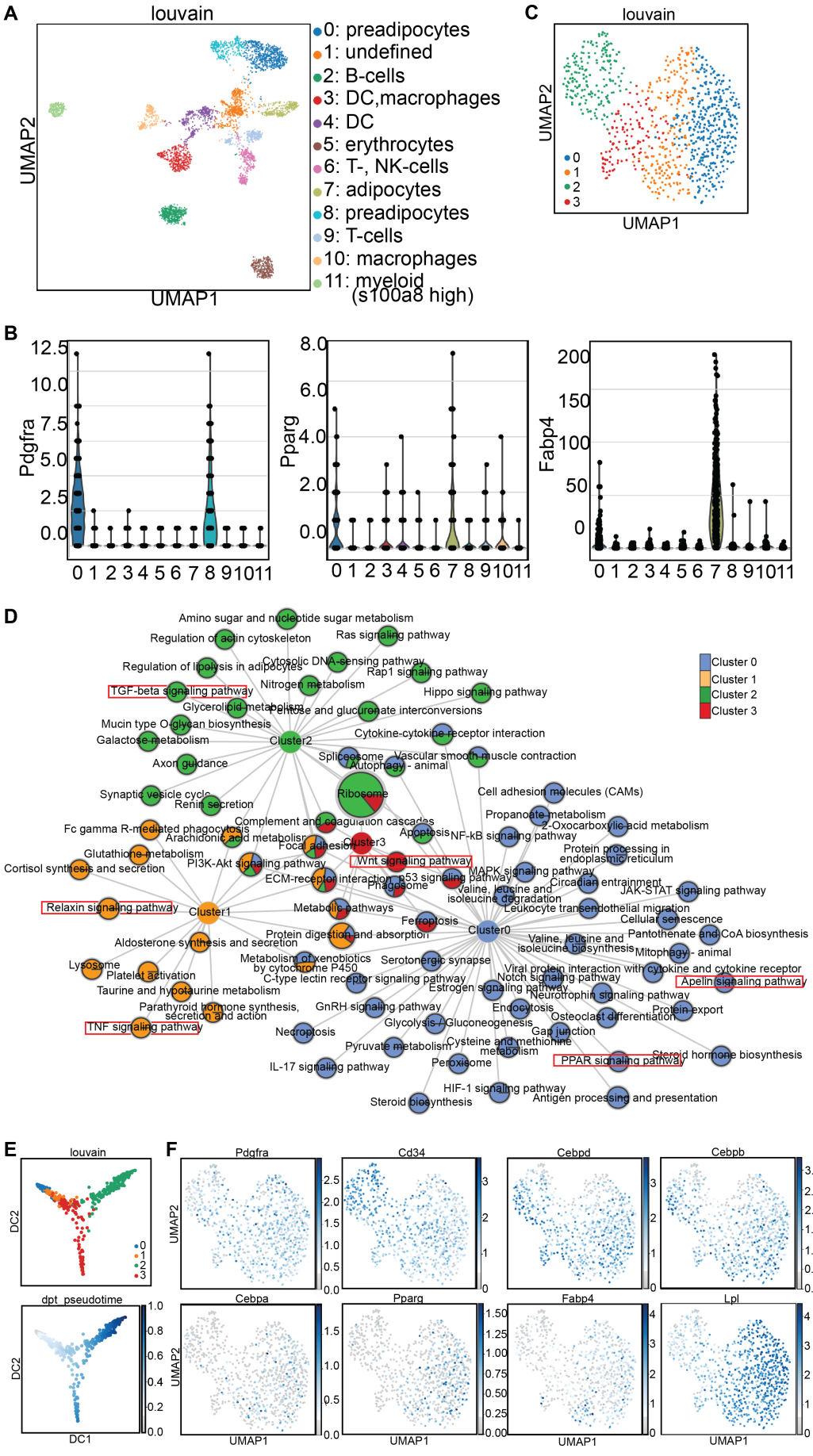
A
louvain
UMAP2
UMAP1
0: preadipocytes
1: undefined
2: B-cells
3: DC,macrophages
4: DC
5: erythrocytes
6: T-, NK-cells
7: adipocytes
8: preadipocytes
9: T-cells
10: macrophages
11: myeloid (s100a8 high)
C
louvain
UMAP2
UMAP1
0
1
2
3
B
Pdgfra
Pparg
Fabp4
0 1 2 3 4 5 6 7 8 9 10 11
D
Amino sugar and nucleotide sugar metabolism
Regulation of actin cytoskeleton
Ras signaling pathway
Regulation of lipolysis in adipocytes
Cytosolic DNA-sensing pathway
Rap1 signaling pathway
TGF-beta signaling pathway
Nitrogen metabolism
Hippo signaling pathway
Glycerolipid metabolism
Pentose and glucuronate interconversions
Mucin type O-glycan biosynthesis
Galactose metabolism
Cluster2
Cytokine-cytokine receptor interaction
Axon guidance
Spliceosome
Vascular smooth muscle contraction
Autophagy - animal
Synaptic vesicle cycle
Renin secretion
Ribosome
Cell adhesion molecules (CAMs)
Propanoate metabolism
Fc gamma R-mediated phagocytosis
Complement and coagulation cascades
2-Oxocarboxylic acid metabolism
Arachidonic acid metabolism
Apoptosis
NF-kB signaling pathway
Focal adhesion
Cluster3
Protein processing in endoplasmic reticulum
Glutathione metabolism
Wnt signaling pathway
Cortisol synthesis and secretion
PI3K-Akt signaling pathway
MAPK signaling pathway
ECM-receptor interaction
p53 signaling pathway
Circadian entrainment
Phagosome
Valine, leucine and isoleucine degradation
JAK-STAT signaling pathway
Relaxin signaling pathway
Cluster1
Leukocyte transendothelial migration
Metabolic pathways
Ferroptosis
Cellular senescence
Protein digestion and absorption
Cluster0
Pantothenate and CoA biosynthesis
Aldosterone synthesis and secretion
Valine, leucine and isoleucine biosynthesis
Mitophagy - animal
Lysosome
Metabolism of xenobiotics by cytochrome P450
Serotonergic synapse
Viral protein interaction with cytokine and cytokine receptor
Platelet activation
C-type lectin receptor signaling pathway
Notch signaling pathway
Apelin signaling pathway
Taurine and hypotaurine metabolism
Estrogen signaling pathway
Neurotrophin signaling pathway
Parathyroid hormone synthesis, secretion and action
GnRH signaling pathway
Endocytosis
Protein export
TNF signaling pathway
Glycolysis / Gluconeogenesis
Osteoclast differentiation
Necroptosis
Gap junction
Pyruvate metabolism
Cysteine and methionine metabolism
Steroid hormone biosynthesis
IL-17 signaling pathway
Peroxisome
PPAR signaling pathway
HIF-1 signaling pathway
Steroid biosynthesis
Antigen processing and presentation
Cluster 0
Cluster 1
Cluster 2
Cluster 3
E
louvain
DC2
DC1
dpt_pseudotime
F
Pdgfra
Cd34
Cebpd
Cebpb
Cebpa
Pparg
Fabp4
Lpl
UMAP2
UMAP1

Figure 30: Distinct differentiation stages identified by scRNAseq.
(A) UMAP computed on full processed scRNAseq dataset with annotated Louvain clusters superimposed. (B) Violin plots showing the distribution of Pdgfra, Pparg and Fabp4. (C) UMAP computed on set of preadipocyte clusters. (D) Network of KEGG enriched pathways of preadipocyte clusters. Significantly enriched pathways were connected to the respective cluster nodes. Size of the pathway nodes and proportion of the node-pie-chart referred to –log10 of enrichment p-value. Node colors referred to single cell cluster identified in (C). (E) Diffusion map dimensionality reduction of preadipocytes colored by Louvain clusters (top panel) and pseudotime (lower panel). (F) Expression of Pdgfra, Cd34, Cebpd, Cebpb, Cebpa, Pparg, Fabp4 and Lpl in preadipocyte clusters shown in (C). The expression values were size factor normalized and log transformed.

KEGG enrichment analysis showed a number of differentially expressed genes and related pathways. Clusters 0, 1 and 2 composed of distinct pathways, and only cluster 3 shared most of its enriched pathways, except the 'Wnt signaling pathway'. Cluster 0 was related to PPAR and Apelin signaling pathways, which are important for brown adipocyte differentiation [206, 207]. Meanwhile, clusters 1-3 revealed enrichment in pathways that were associated with the inhibition of adipogenesis, such as TGF-beta, Wnt, relaxin and TNF signaling (Figure 30D) [208-210].
Pseudotime mapping of the preadipocytes showed two distinct developmental branches that came from one common precursor (Figure 30E). Gene expression of known markers in adipogenesis identified cluster 2 as the most undifferentiated phase (high in Cd34), cluster 1 and 3 as the transition phase (high in Cebpd and Cebpb) and cluster 0 as the most differentiated phase (high in Cebpa, Pparg, Fabp4 and Lpl) (Figure 30F). Therefore, scRNAseq disclosed four distinct differentiation stages of preadipocytes. However, scRNAseq results describe a static screenshot of a tissue, thus it is impossible to infer the future development of individual cells from these experiments.

3.4.3 Brown adipocytes clones derived from mice show gene expression patterns of brown, beige and white fat

To overcome the limitation of scRNAseq, 67 cell clones derived from immortalized SVF of three 8-week-old male C57BL/6J mice were established. Cell clones were differentiated for 8 days into mature, lipid-laden brown adipocytes (Figure 31), although to different extents. Lipid

accumulation was quantified from oil red o (Figure 32A) and LipidTox staining (Figure 31 and 32B). There was no striking difference in shape and lipid droplet size between clones, except 1A6 and 1D5, which had smaller lipid droplets in association to overall lipid content (Figure 32B). In addition, there was a strong positive correlation between lipid accumulation and Pparg mRNA levels. However, clones 1B1, 1B3, 2C12, 3C7 and 3D6 showed higher Pparg expression than expected compared to the lipid content (Figure 32C).

In accordance with the function of Pparg in brown adipocyte differentiation, clones mentioned above showed the highest Ucp1 expression compared to other cell clones (Figure 33A). Specific markers for brown (Prdm16 and Ppargc1a) and beige (Cd137 and Tmem26) fat were measured from differentiated clones. In order to see if the clones were grouped using these markers, the expressions were plotted according to unsupervised hierarchical clustering (Euklidean distance and Ward's linkage method). *In vitro* differentiation of brown, beige and subcutaneous white adipocytes were included into the analysis. There were 19 cell clones clustered with brown adipocytes, 18 clones with beige adipocytes and 15 with white adipocytes. In addition, two clusters containing 6 and 9 clones with either high or low thermogenic gene expression, respectively, were largely determined as Cd137-high and –low (Figure 33B).

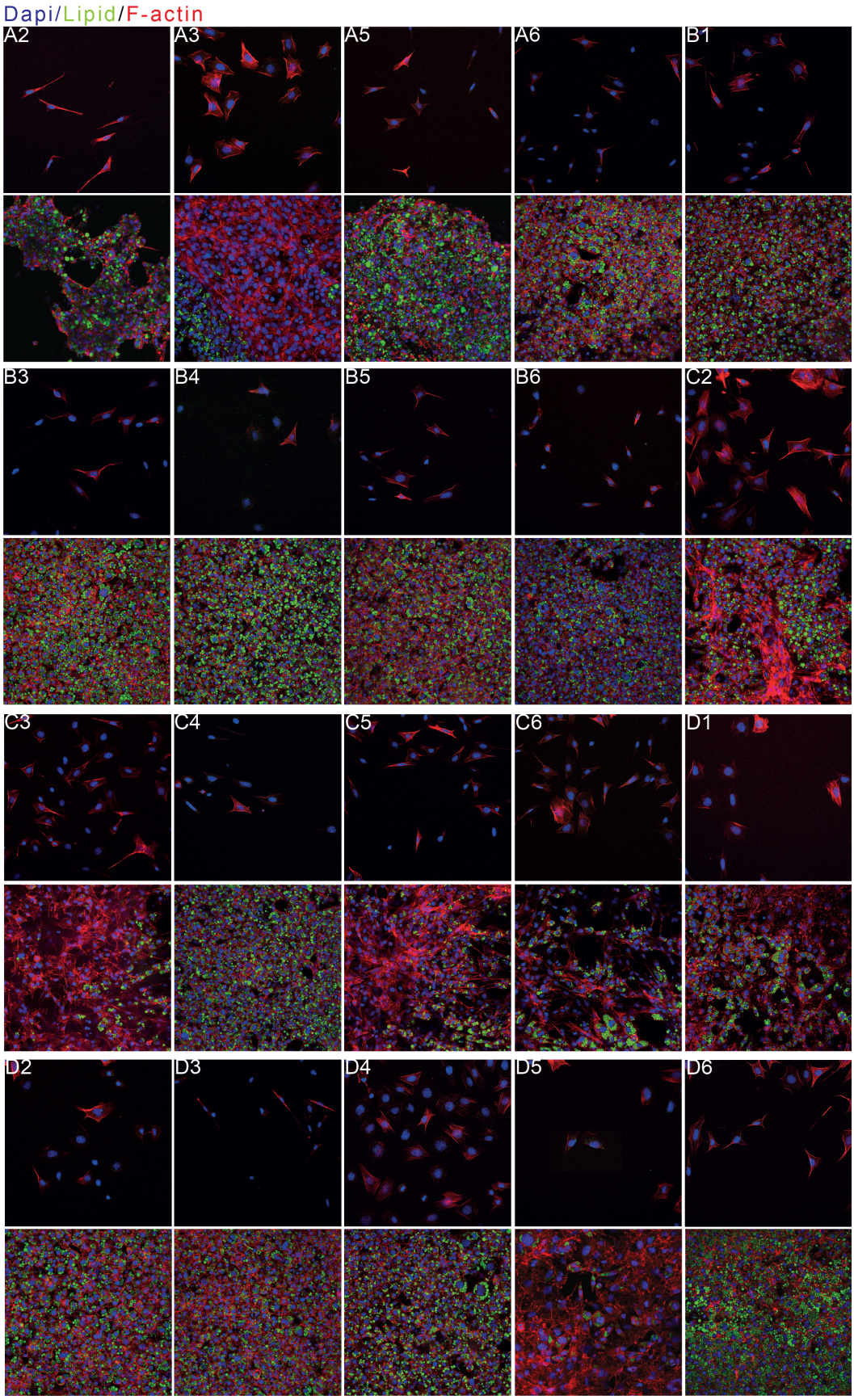

Figure 31: Representative immunofluorescence images of preadipocyte (upper panel) and mature adipocyte (lower panel) clones from BAT 1 (blue= Dapi, green= lipid and red= F-actin).

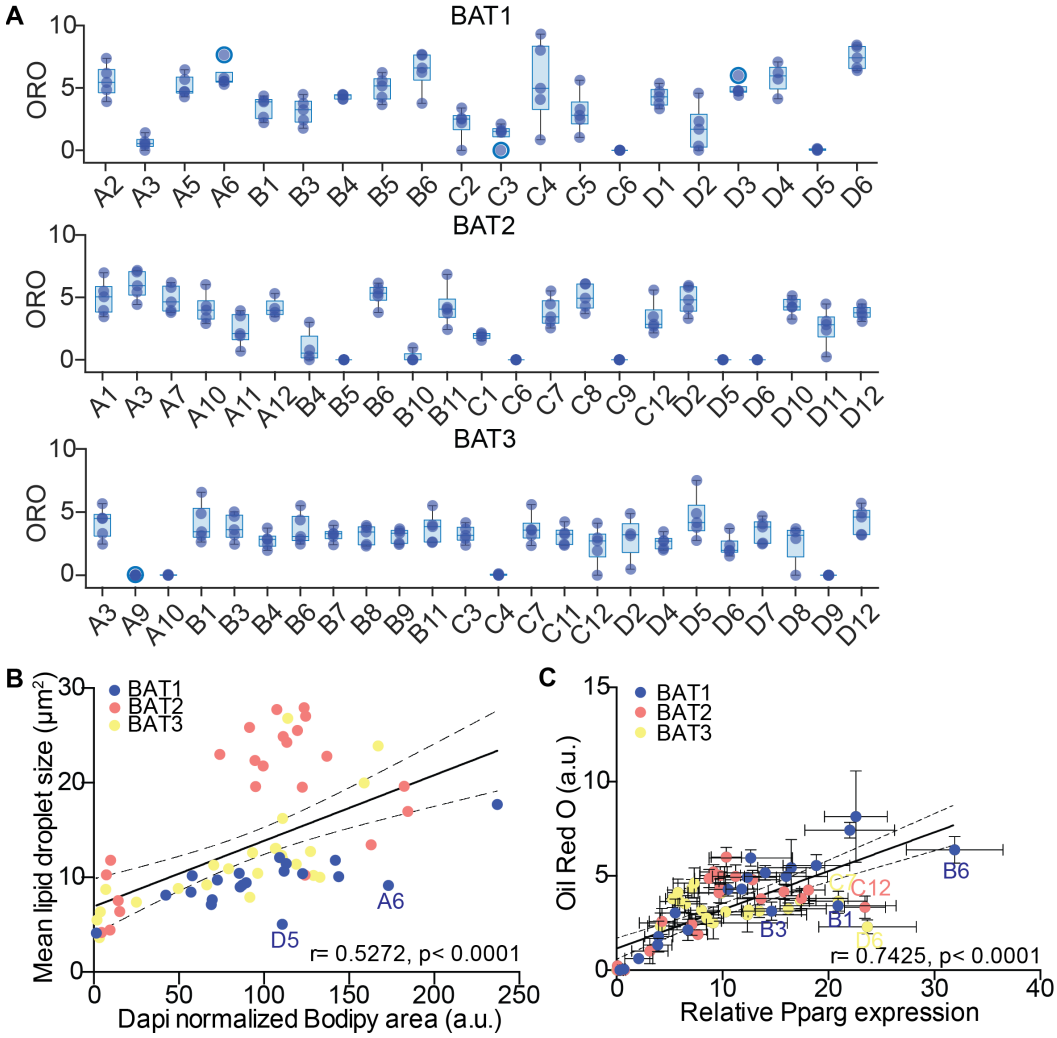

Figure 32: Heterogeneity in differentiation and lipid accumulation between brown adipocyte clones.
(A) Quantification of relative lipid accumulation measured by ORO staining at day 8 of differentiation from 67 immortalized brown preadipocyte clones (n= 5, mean OD normalized to Dapi ± SEM). (B) Correlation graph between mean lipid droplet size and lipid area normalized by the number of nuclei per clone (n> 200), calculated from pictures shown in Figure 26. Values are mean of different area scanned per clones (n= 9). (C) Correlation analysis of Pparg expression and lipid accumulation (n= 5).

Additionally, we treated differentiated clones with β3-adrenergic receptor agonist CL-316,243 (CL) for 3 hours to observe their cellular response upon 0.5 µM CL. Most of the Ucp1 expression from the clones was induced by acute CL treatment, except 1A3, 1C6, 2B4, 2B5, 2B10, 2C6, 2D5, 3A10, 3C4 and 3D9, which were the least differentiating clones (Figure 33C and 32A). Thus, the data derived from the 67 different brown adipocyte clones suggested functional and developmental heterogeneity.

3.4.4 RNAseq expression profiling shows differences in brown preadipocytes and adipocytes

RNAseq was performed in order to gain insight on the transcriptional differences between undifferentiated (preadipocytes) and differentiated (adipocytes) brown adipocytes. The cells were collected from 20 clones of mouse 1 (BAT1), since all showed comparable proliferation rates (Figure 33A), indicating no variability in the effect of SV40 immortalization. Data processing performed as described in section 2.2.6.3, resulted in 9483 and 10363 genes for preadipocytes and adipocytes, respectively, for further analysis. PCA plots on preadipocytes and adipocytes did not show any clustering or pattern for identification of distinct brown adipocyte lineages (Figure 33B).

To get a better understanding on how the gene profiles of the clones correlated with the whole white or brown adipose tissue, we analyzed our data sets using the ProFAT database [211]. This web tool allowed us to get a relative estimation of the 'BATness', similarity to brown fat profile, using a scale of 0 for low and 1 for high relation to the BAT. We performed pairwise comparison for each preadipocytes and adipocytes of each clones. There were three different clusters identified by k-means clustering: 1) cluster with the least similarity to BAT in both, preadipocytes and adipocytes (symbolized in dots); 2) cluster with BAT characteristic only by differentiation (adipocytes, symbolized in triangles); 3) cluster with highest similarity to BAT in both preadipocytes and adipocytes (symbolized in squares) (Figure 33C).

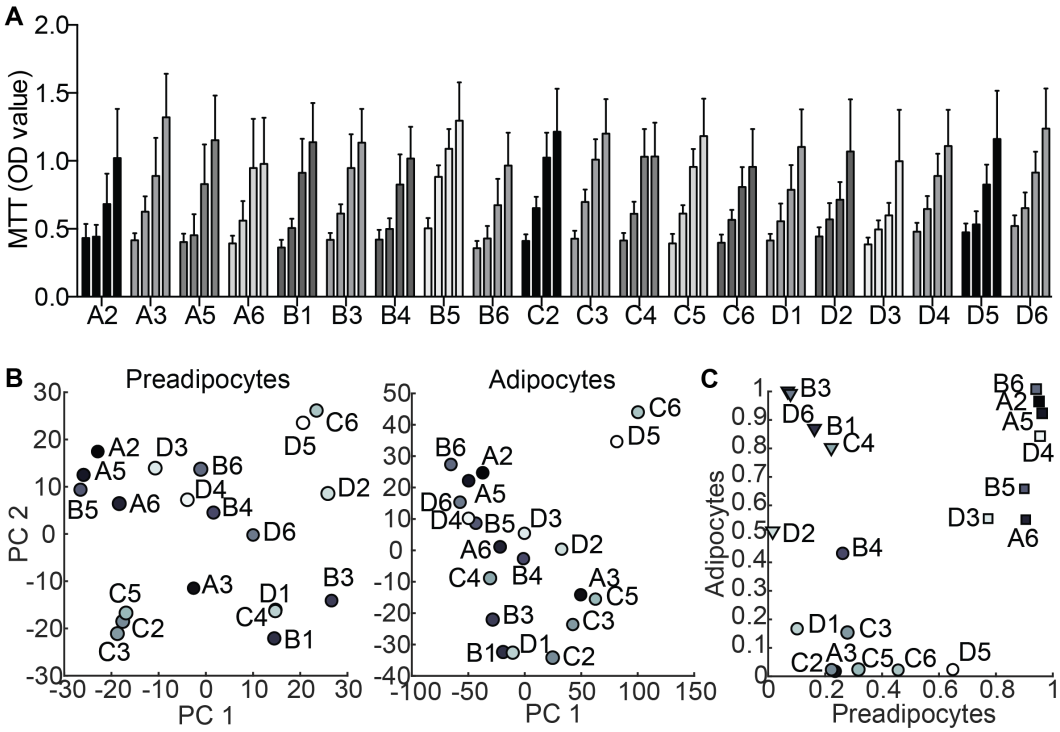

Figure 33: RNAseq profiling on preadipocytes and adipocytes of BAT1 clones showed distinct clusters when correlated to ProFAT database.
(A) MTT assay of 20 preadipocyte clones for 4 days (left to right bar, n= 3-5). (B) PCA plot of the first two PC of preadipocytes (left panel) and adipocytes (right panel) expression data. (C) Scatterplot comparison of the estimated BATness from preadipocyte and adipocyte clones. Dots, triangles and squares indicated three clusters identified by k-means clustering.

3.4.5 Dimensionality reduction using Laplacian Eigenmaps reveals distinct brown adipocyte gene expression signatures

According to the analysis above, there were groups of clones with different correlations to BATness. Nonetheless, these groups did not associate with clusters in the hierarchical clustering of the RNAseq data. Furthermore, we were not able to estimate the number of different brown adipocyte lineages in the clones and recognize marker genes allowing us to distinguish different lineages. In that quest, nonlinear dimensionality reduction techniques were applied to discover patterns to classify the clones. The analysis was restricted to the RNAseq data from preadipocytes to avoid bias caused by differences in differentiation capacity and to establish the precursor populations. Laplacian Eigenmaps revealed 7 distinct gene sets, which were generated into 7

gene expression modules (GEMs, M1-M7) with sizes ranging from 76 to 227 genes (Figure 34A). Most of the GEMs showed distinct gene expression patterns, only M6 was divided into small subgroups distributed across the clustering tree (Figure 34B). The following PCA analysis on the expression of preadipocytes and adipocytes did not show any clustering (Figure 34C).

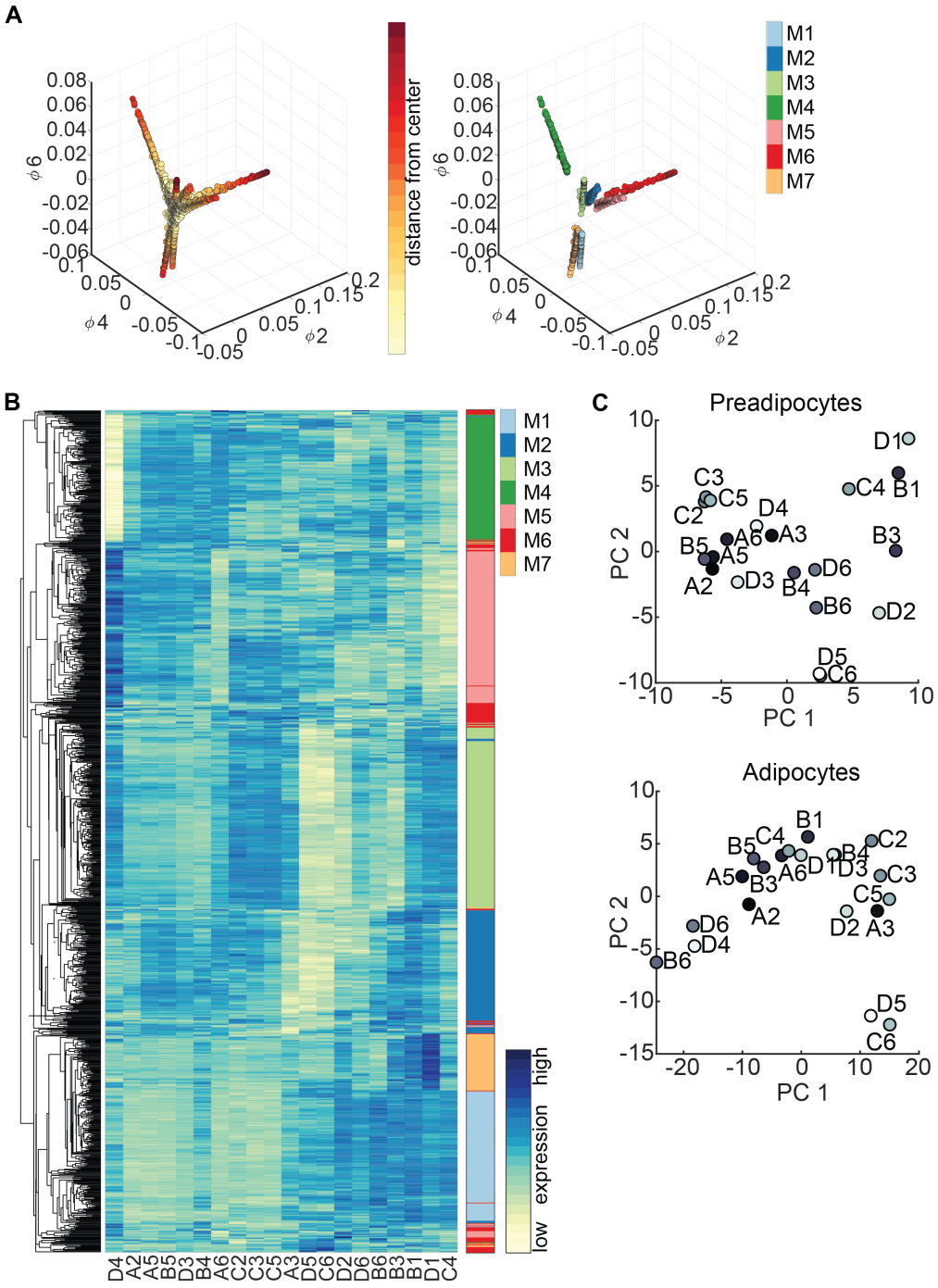

Figure 34: Laplacian Eigenmap approach revealed different GEMs.
(A) Brown preadipocyte gene expression of the three eigenvectors (ϕ2, ϕ4 and ϕ6) in Laplacian Eigenmap derived low dimensional space. Distance from estimated center is

color-coded (left panel). Genes with low variance were removed and remaining modules were coded in colors (right panel). (B) Heatmap od hierarchical clustered module genes in rows. Gene expression was z-score normalized. Module membership was indicated by the right color bar. (C) PCA plots for the first two PCs of GEM genes from preadipoctes (upper panel) and adipocytes (lower panel).

3.4.6 Eif5, Tcf25 and Bin1 mark subpopulations of brown preadipocytes and adipocytes *in vivo*

We isolated the genes that were expressed in both preadipocytes and adipocytes GEMs to enable the identification of potential brown lineage markers. There were 57 genes showing stable expression ($p < 0.05$, Pearson correlation) between preadipocyte and adipocyte clones (Figure 35A). Furthermore, stably expressed genes were correlated to the ProFAT database to estimate the BATness specific to the clones. Two genes from M4 (Bin1 and Phax) were identified as the least correlated with BATness, while genes from M2 were mostly correlated with BATness. Genes from other GEMs were evenly distributed with the BATness correlation (Figure 35B).

Among 57 stably expressed genes, eukaryotic translation initiation factor 5 (Eif5), transcription factor 25 (Tcf25) and Bridging integrator 1 (Bin1) were selected as the potential lineage markers, based on the BATness (Figure 35B), maximum expression and fold change in the clones (Figure 35C) and the availability of antibodies on the market. Eif5 was the most correlated with the classical BAT phenotype, while Tcf25 had no tendency to be more or less brown, and Bin1 was the least associated gene to the brown phenotype (Figure 35B).

The expression of the three marker genes was correlated to mRNA expression of Ucp1, Pparg, Ppargc1a and Prdm16, as the brown and differentiation markers of brown adipocytes. Eif5 was positively associated; Tcf25 showed no correlation and Bin1 was negatively correlated to the expression of Ucp1 and differentiation markers (Figure 36A). Further confirmation was performed *in vivo* by measuring the gene expression in mice chronically housed at either thermoneutrality (30°C) or at 5°C (Figure 36B, upper panels) and mice fed with chow or HFD (Figure 36B, lower panels).

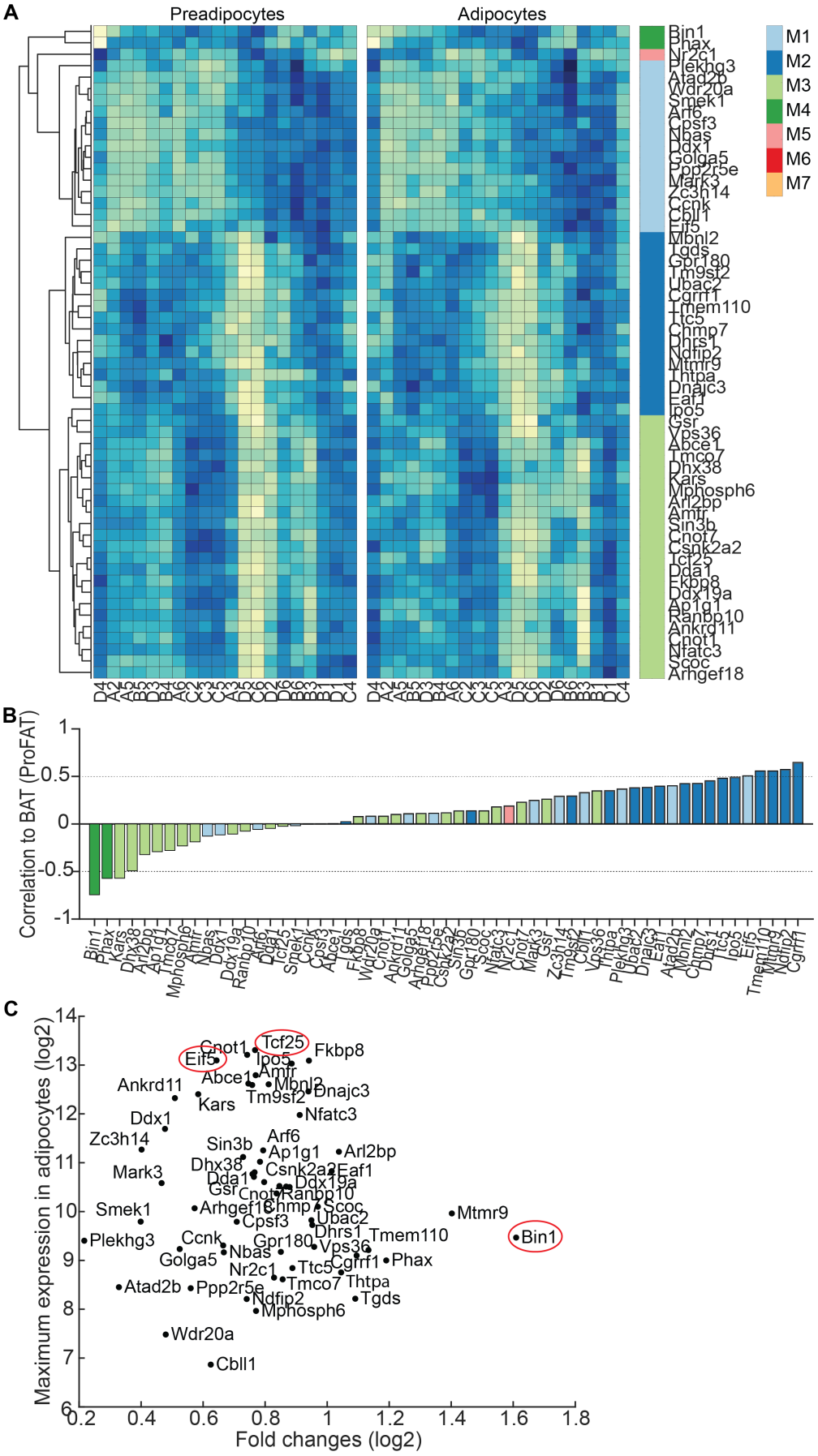

Figure 35: Eif5, Tcf25 and Bin1 marked subsets of brown adipocytes.

(A) Heatmaps of stably expressed genes of preadipocytes (left panel) and adipocytes (right panel). Module membership is indicated by the color bar. (B) Correlation coefficients for stable expressed genes compared with estimated BATness from ProFAT database. Color of bars indicated module membership. (C) Scatter plots of stable expressed genes in regards to their maximum expression in differentiated adipocytes and maximal fold change (log2) between differentiated adipocyte clones. These data based on RNAseq analysis.

Expression of Ucp1 was increased in BAT upon chronic cold exposure compared to its expression at thermoneutrality, while slightly decreased in BAT of obese HFD-fed mice compared to lean chow-fed mice. Similar to Ucp1, the expression of Eif5 was up regulated in the BAT of cold exposed mice and down regulated in the BAT of DIO-mice. The expression of Tcf25 was induced in BAT exposed to cold, while Bin1 expression was unaltered and upon HFD feeding, the expression of Tcf25 and Bin1 were stable (Figure 36B). In addition, our scRNAseq data showed a random distribution of Eif5, Tcf25 and Bin1 in the preadipocyte clusters, confirming the stable expression of these marker genes throughout brown adipocyte differentiation (Figure 36C).

Furthermore, immunofluorescence stainings of Eif5, Tcf25 and Bin1 were performed on murine BAT sections in order to observe the distribution of these markers in mature adipocytes *in vivo.* Comparable to Ucp1, Eif5 was detected in most brown adipocytes with different intensities (Figure 37A). Quantification of Eif5 intensities was performed with the same approach for Ucp1 quantification, and resulted in around a quarter of brown adipocytes expressing medium and high Eif5 (Figure 37B). Nuclear and perinuclear staining of Tcf25 and Bin1, respectively, was observed in ~ 25% of brown adipocytes (Figure 37A and B). Bin1 staining was also detected in endothelial cells. Comparative gene expression analysis in periadrenal (ADR), supraclavicular (SCLV) and subcutaneous (SCT) white and brown adipose tissue of humans confirmed the expression of Eif5, Tcf25 and Bin1 in human BAT and WAT as seen in mice (Figure 37C).

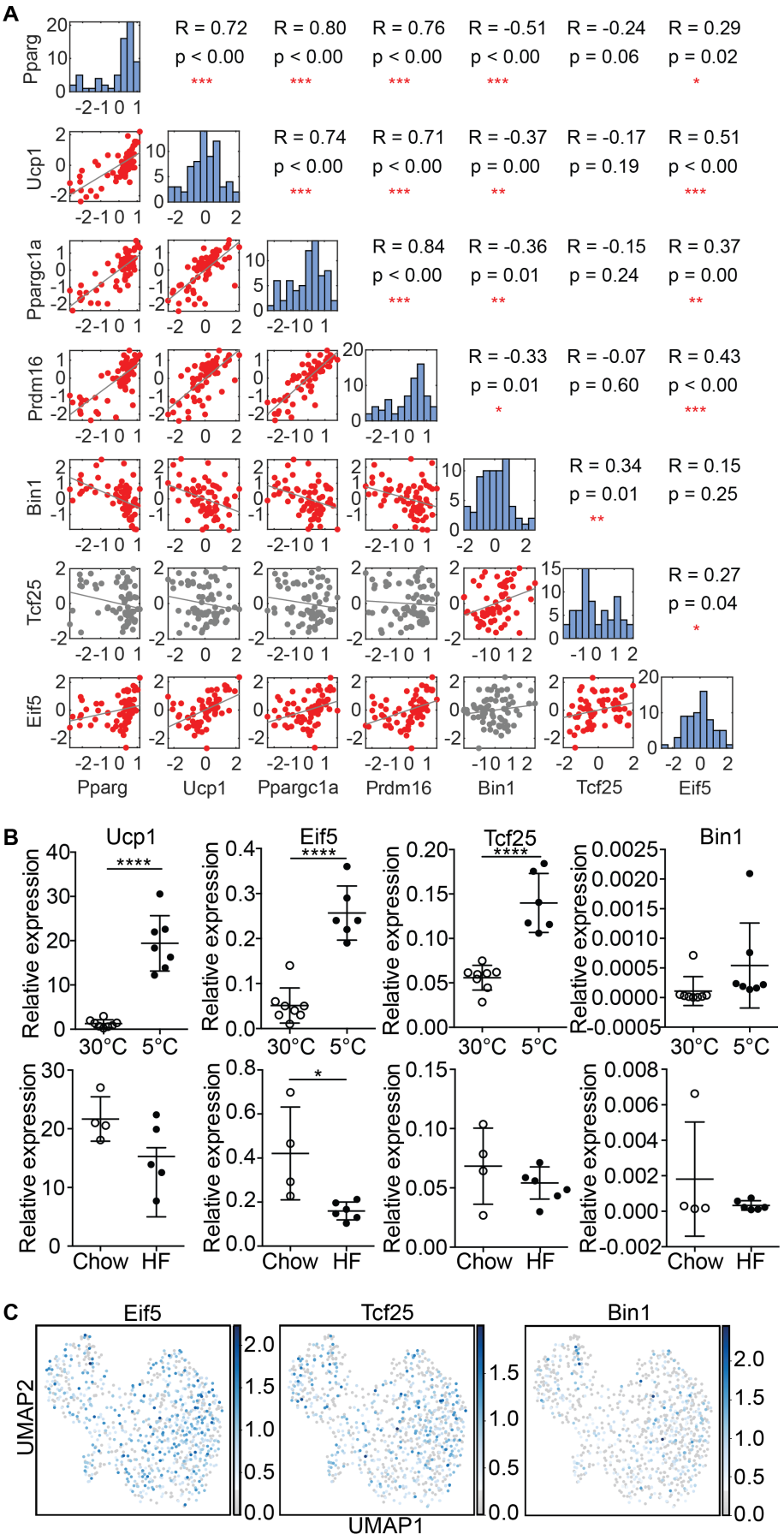
A
Pparg
Ucp1
Ppargc1a
Prdm16
Bin1
Tcf25
Eif5
R = 0.72
p < 0.00
R = 0.80
p < 0.00
R = 0.76
p < 0.00
R = -0.51
p < 0.00
R = -0.24
p = 0.06
R = 0.29
p = 0.02
R = 0.74
p < 0.00
R = 0.71
p < 0.00
R = -0.37
p = 0.00
R = -0.17
p = 0.19
R = 0.51
p < 0.00
R = 0.84
p < 0.00
R = -0.36
p = 0.01
R = -0.15
p = 0.24
R = 0.37
p = 0.00
R = -0.33
p = 0.01
R = -0.07
p = 0.60
R = 0.43
p < 0.00
R = 0.34
p = 0.01
R = 0.15
p = 0.25
R = 0.27
p = 0.04
B
Ucp1
Eif5
Tcf25
Bin1
Relative expression
30°C
5°C
Chow
HF
C
Eif5
Tcf25
Bin1
UMAP2
UMAP1

Figure 36: Character of Eif5 was closely related to Ucp1, Tcf25 was not correlated, while Bin1 was negatively correlated to Ucp1.
(A) Correlation plot for pairwise comparison of selected markers to selected stably expressed genes. Red plots denoted a significant correlation. (B) Expression of Ucp1, Tcf25 and Bin1 in mice kept in cold or thermoneutrality (upper panels, n= 6-8) and chow-fed ot HFD-fed mice (lower panels, n= 4-6). Data are mean expressions normalized to B2m ± SEM. (C) UMAP of all preadipocytes on the expression of Eif5, Tcf25 and Bin1 superimposed. The expression values shown were size factor normalized and log transformed.

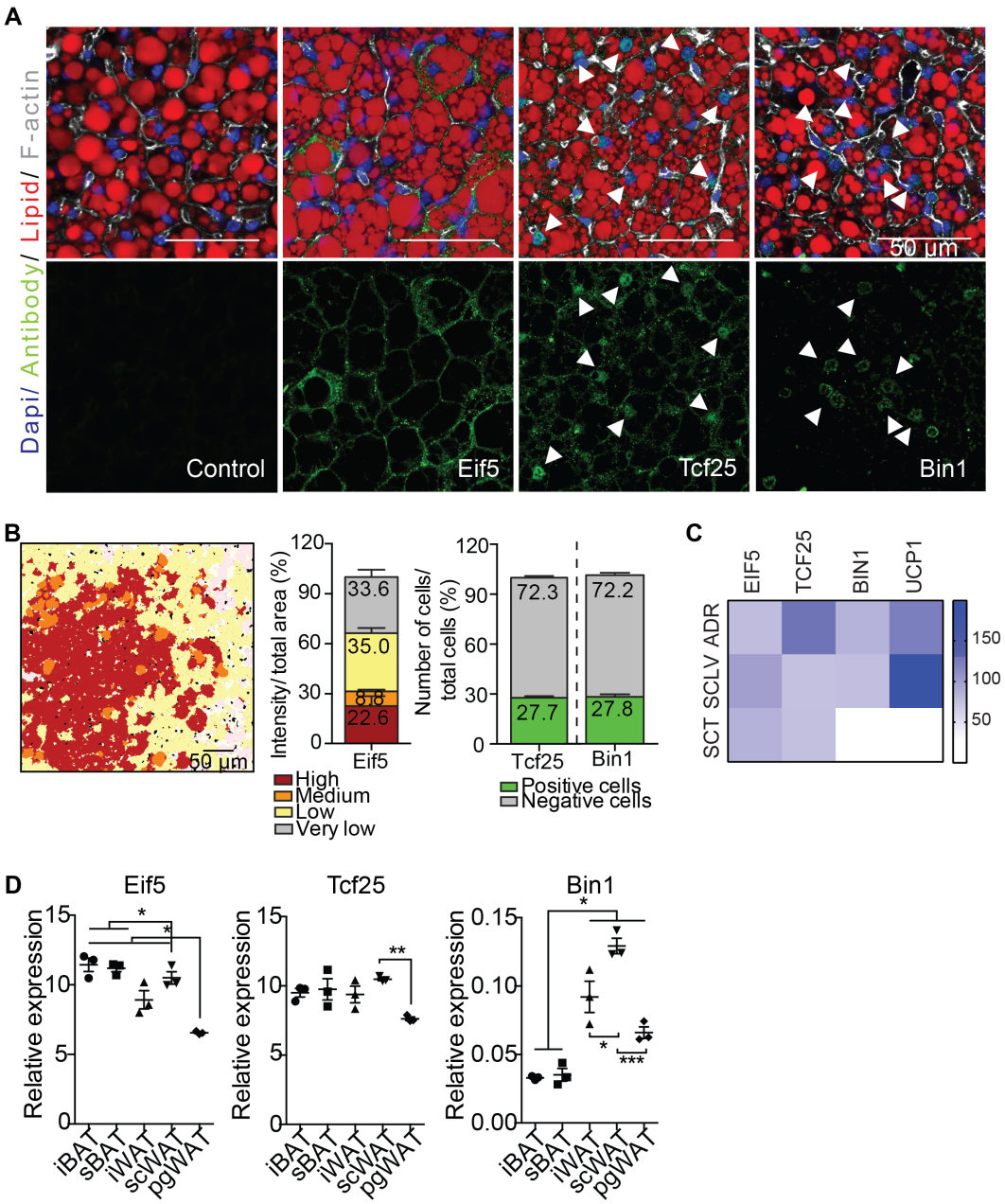

Figure 37: Eif5, Tcf25 and Bin1 were heterogeneously detected in mice and human BAT and WAT depots.
(A) BAT staining for Eif5, Tcf25 or Bin1 (green), lipid (red), Dapi (blue) and F-actin (gray) from wild type male C57BL/6J mice. (B) Representative color gradient picture for Eif5 quantification on BAT section (left panel) and percentage area of different Eif5 intensity (very low, low, medium and high) normalized to total area (middle panel, n= 9). Quantification of Tcf25- and Bin1-positive and -negative cells showed in percentage

total cells (right panel, n= 9-18). (C) Heatmap of mRNA expression in periadrenal (ADR), supraclavicular (SCLV) and subcutaneous (SCT) adipose tissue coming from six human donors. (D) Relative mRNA expression of Eif5, Tcf25 and Bin1 in iBAT, sBAT, iWAT, scWAT and pgWAT of wild type C57BL/6J mice (n= 3 data are mean expression normalized to B2m ± SEM).

3.4.7 Loss of Bin1 increases Ucp1 expression and oxygen consumption

Additionally, we characterized functional differences in the Eif5^{high}, Tcf25^{high} and Bin1^{high} brown adipocytes. Thus, representative clones were selected using hierarchical clustering from gene expression measured by qPCR (Figure 38A). Clone B1 was chosen as Eif5^{high}, D1 as Tcf25^{high} and D5 as Bin1^{high} expressing cells. To this end, we established stable knockdown cell lines of these genes in the respective clones, and confirmed the gene expressions by semi-quantitative PCR at day 0 (preadipocytes) and day 8 (adipocytes) of differentiation (Figure 38B). Knockdown of these genes did not impair adipogenesis, as confirmed by the expression of Pparg (Figure 38C).

Reduction of Eif5 in the B1 clone induced Ucp1 and P2rx5 at the mRNA level (Figure 38C, middle and right panel), with no significant effect on mitochondrial respiratory capacity (Figure 38D, left panel). Tcf25 knockdown in D1 clone reduced expression of Ucp1 and Prdm16, while inducing the expression of Cd137 and Asc1 (Figure 38C). Microplate-based oxygen consumption of the shTcf25 D1 clone showed a reduction in maximal respiratory capacity (Figure 38D, right panel), with no differences in mitochondrial uncoupling. Knockdown of Bin1 in the D5 clone induced Ucp1 mRNA level (Figure 38C) and showed a higher basal oxygen consumption rate (OCR). Furthermore, addition of oligomycin (ATP synthase inhibitor) to the wells did not change the OCR of shBin1 D5, indicating full mitochondrial uncoupling (Figure 38D, lower panel). Therefore, the presence of Bin1 in preadipocytes and adipocytes correlated with low thermogenic capacity and a reduction in Bin1 resulted in induction of thermogenic gene expression and full mitochondrial uncoupling, at least in clones with high Bin1 expression.

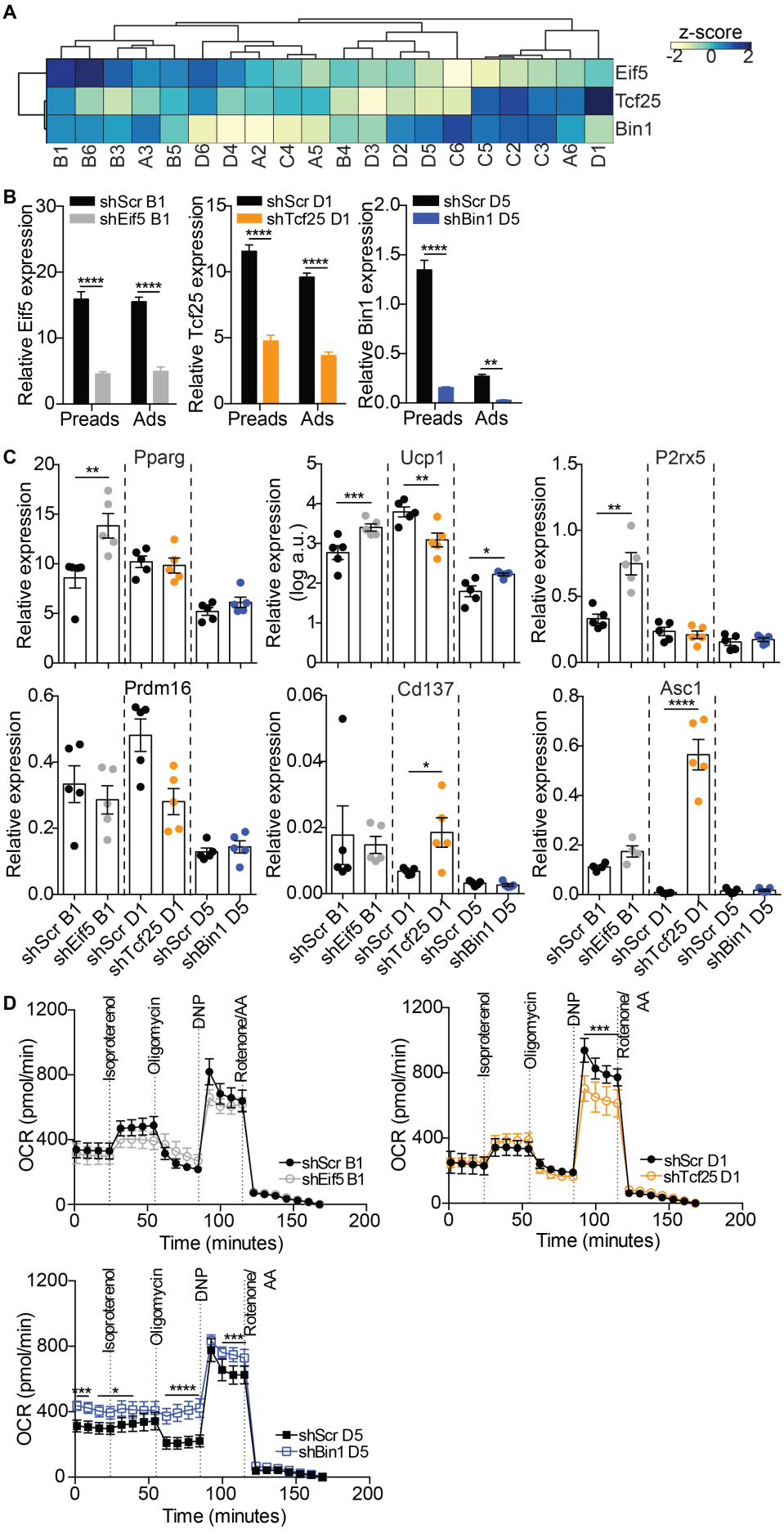
A
z-score
-2 0 2
Eif5
Tcf25
Bin1
B1 B6 B3 A3 B5 D6 D4 A2 C4 A5 B4 D3 D2 D5 C6 C5 C2 C3 A6 D1
B
shScr B1
shEif5 B1
Relative Eif5 expression
Preads Ads
shScr D1
shTcf25 D1
Relative Tcf25 expression
shScr D5
shBin1 D5
Relative Bin1 expression
C
Pparg
Ucp1
P2rx5
Prdm16
Cd137
Asc1
Relative expression
(log a.u.)
shScr B1
shEif5 B1
shScr D1
shTcf25 D1
shScr D5
shBin1 D5
D
OCR (pmol/min)
Isoproterenol
Oligomycin
DNP
Rotenone/AA
Time (minutes)
shScr B1
shEif5 B1
shScr D1
shTcf25 D1
shScr D5
shBin1 D5

Figure 38: Knockdown of Eif5, Tcf25 and Bin1 on clones high in the respective genes, showed different characteristics.
(A) Heatmap and hierarchical clustering of cell lines with regards to the mRNA expressions of Eif5, Tcf25 and Bin1. (B) Expression of Eif5, Tcf25 and Bin1 in control cells (shScr) of different clones (B1, D1 and D5) and the respective knockdown (shEif5 B1, shTcf25 D1 and shBin1 D5); Preads (d0 of differentiation) and Ads (d8 of differentiation) (n=5). (C) Relative mRNA expression of Pparg, Ucp1, P2rx5, Prdm16, Cd137 and Asc1at day 8 of differentiation and 3 hours treatment with 0.5 µM CL-316,243 in shScr B1, shEif5 B1, shScr D1, shTcf25 D1, shScr D5 and shBin1 D5 (n= 5). (D) OCR of shScr B1 and shEif5 B1 (left panel), shScr D1 and shTcf25 D1 (right panel) and shScr D5 and shBin1 D5 (lower panel) at day 8 of differentiation measured by Seahorse (n=4).

Next, we depleted these marker genes in a mixed brown preadipocyte population. Stable knockdown cell lines were established for Eif5 (shEif5), Tcf25 (shTcf25), Bin1 (shBin1) and scrambled shRNA-expressing cells (shScr) as the control. Successful knockdown was confirmed by qPCR analysis in preadipocytes and adipocytes (Figure 39A), reaffirmed by immunofluorescence staining on preadipocytes of the gene markers (Figure 39B). Similar to the clonal knockdown lines, there was no effect in differentiation capacity upon loss of these markers, in regards to their lipid accumulation (Figure 39C and D) and Pparg mRNA levels (Figure 39E).

In accordance with clonal knockdown lines, depletion of Tcf25 decreased the expression of brown adipocyte marker, P2rx5, and induced the expression of white adipocyte marker, Asc1. In general, Cd137 mRNA levels were higher in the knockdown cells compared to the control cells, while Prdm16 was lower in shEif5 and shTcf25 compared to shScr cells (Figure 40A). However, shEif5 and shBin1 cells had significantly higher Ucp1 mRNA or protein levels in adipocytes or adipocytes with CL-316,243 treatment compared to the shScr adipocytes, respectively (Figure 40A and B). Bin1 knockdown cells showed the highest P2rx5 level (Figure 40A), as well as highest OCR measured by seahorse analysis (Figure 40C). Thus, Bin1 marked a relatively white-like adipocyte in brown adipocyte population. Taken together, loss of Bin1 in the brown adipocytes increased thermogenic gene expression and mitochondrial activity, suggesting that Bin1 played a role in suppressing classical brown adipocyte identity.

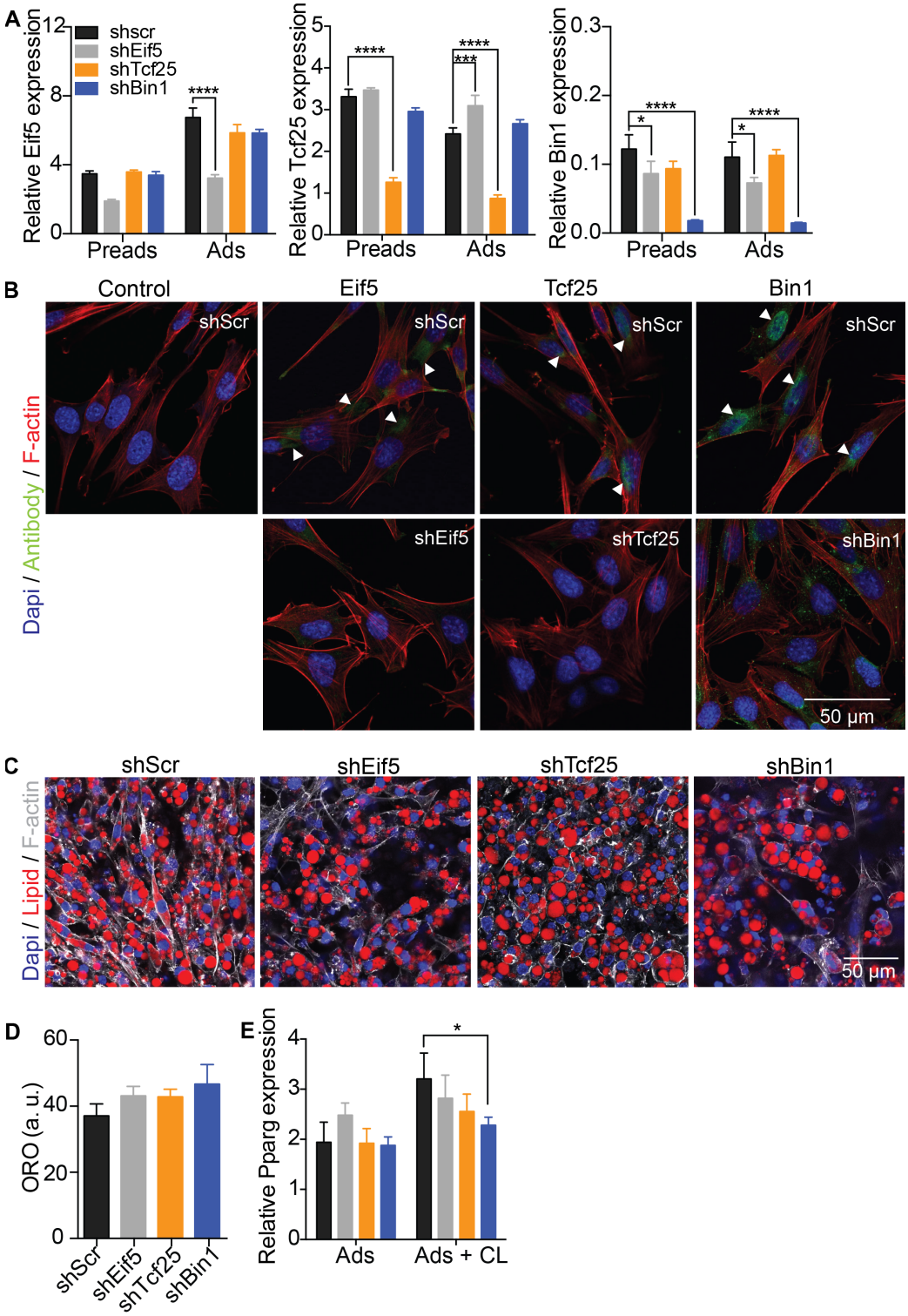

Figure 39: Validation of Eif5, Tcf25 and Bin1 knockdown in mix brown adipocyte population.

(A) Relative mRNA expression of Eif5, Tcf25 and Bin1 in control cells (shScr) and respective knockdown cells (shEif5, shTcf25 and shBin1) at day 0 (preadipocytes) and day 8 (adipocytes) of differentiation (n= 5). (B) Representative images of immunofluorescence staining of Eif5/Tcf25/Bin1 (green), F-actin (red and Dapi (blue) on shScr, shEif5, shTcf25 and shBin1 preadipocytes. (C) Representative images of differentiated shScr, shEif5, shTcf25 and shBin1 stained with F-actin (white), lipid (red) and Dapi (blue). (D) Quantification of relative lipid accumulation measured by ORO staining at day 8 of differentiation from knockdown cells (n= 3, mean OD normalized to

Dapi ± SEM). (E) Relative mRNA expression of Pparg in adipocytes without and with 3 hours CL-316,243 treatment from control and knockdown cells (n= 6).

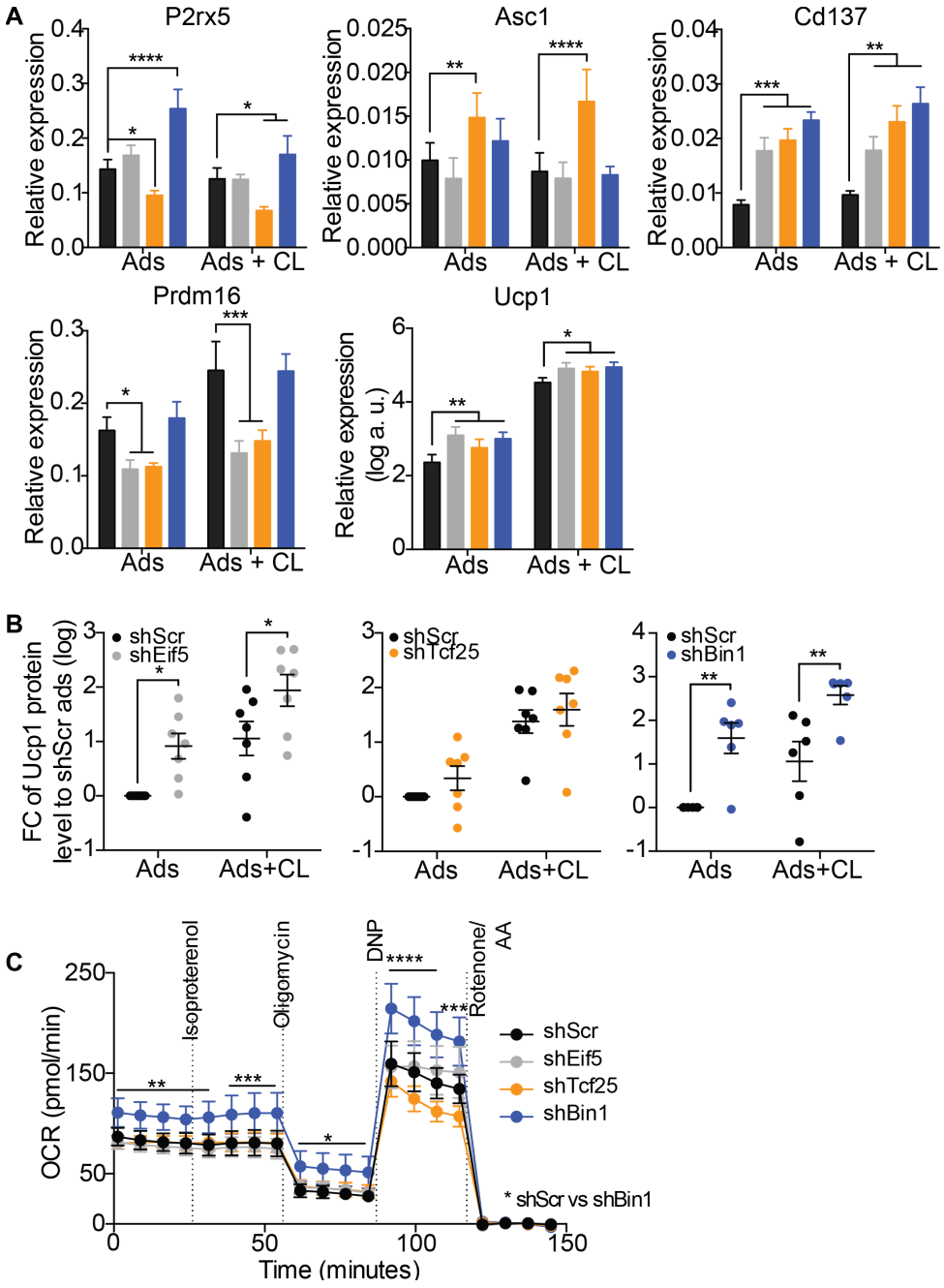

Figure 40: Loss of Bin1 led to an increase in thermogenic gene and mitochondrial activity.
(A) Relative mRNA expression of P2rx5, Asc1, Cd137, Prdm16 and Ucp1 on adipocytes without and with 3 hours CL-316,243 treatment from control and knockdown cells (n= 6). (B) Quantification of Western blots for Ucp1 in shScr, shEif5, shTcf25 and shBin1 adipocytes without and with 6 hours Cl-316,243 treatment normalized to β-actin (n= 6-7). (C) OCR for control and knockdown cell lines measured at day 8 of differentiation by Seahorse (n= 3).

4. Discussion

Obesity and the development of metabolic syndrome have been associated with the incidence of asthma. Almost 38% of asthmatic adults are also obese [212], and people who develop insulin resistance and systemic inflammation are known to have a higher prevalence of asthma [62]. The WHO defines asthma as inflammation in the air passages, which causes swelling of the airways, thus narrows and reduces the airflow in and out of the lungs. In addition, asthma can be categorized as allergic and non-allergic asthma [213, 214], with no or little difference in the immunopathology processes [215, 216]. However, early onset asthma has significantly higher sensitivity towards allergens [217]. Thus, the interaction between the development of metabolic syndrome, which induces asthma and lung allergic inflammation is rather complex and intriguing.

A suitable mouse strain is important to disentangle this intricate interaction. The female BALB/c strain is known to be more susceptible to develop immune response and airway inflammation upon allergen exposure [218], nevertheless our results showed a protective effect upon DIO in both sexes, as also reported by Montgomery, *et al*. [176]. Therefore, the C57BL/6J strain was assigned to study the interconnection between metabolic syndrome and lung allergic inflammation.

4.1 Less lung inflammation in obese sensitized mice

Studies showed that obesity and metabolic syndrome alter nitric oxide metabolism, a potential mechanistic link between asthma and obesity [219, 220], and contributes to a shift in HDM-induced airway cellular infiltration, which cause airway remodeling [221]. These changes in airway ultrastructure inhibit the action of glucocorticoids (drug treatments against airway hyperresponsiveness) to reduce airway inflammation and complicate the treatment [221, 222]. Additionally, HFD feeding was

previously shown to exacerbate airway allergy, upregulate eosinophils, Th17 and Th2 pulmonary profiles, especially via ILC2s and ILC3s [223]. In accordance, male and female C57BL/6J mice exhibited more eosinophils in BAL cells, Th17 and Th2 in the lungs upon acute HDM sensitization, which confirmed immune responses in C57Bl/6J mice upon HDM allergen with no sexual dimorphism.

In HDM-induced allergy, it is controversially discussed how $CD4^+$ and $CD8^+$ T cells play a role in the pathogenesis of airway inflammation. Some describe that airway inflammation and hyperresponsiveness is dependent on $CD4^+$ and $CD8^+$ T cells [224]. Meanwhile, a cross-sectional study comparing morbidly obese asthmatic and non-asthmatic obese subjects found no differences in $CD4^+$ T cells and even lower $CD8^+$ T cells count in bronchial biopsies of the asthmatic group [225]. Our results showed that the percentage of CD4 cells was increased upon acute HDM sensitization only, while prolonged HDM exposure did not change the percentage or CD4 or CD8, indicating prolonged and chronic HDM exposure did not exacerbate inflammatory responses in the lungs.

The *in vivo* studies showed that short- (2 weeks) and intermediate-term (5 weeks) HDM exposure induced lung allergic inflammation, while long-term exposure (11 weeks) suppressed lung inflammation, which is associated with an increase in $FoxP3^+$ T cells [226], as we observed in the chronic HDM sensitization. Although the percentage of CD4 was unaltered, the frequencies of $RORgt^+$, $FoxP3^+$ and $GATA3^+$ were increased upon chronic HDM sensitization. This indicates that there are differences in inflammatory cell infiltration in the lungs between acute and chronic HDM exposure, regardless of diet. However, this finding was attenuated in the HF group, which is in contrast to other studies, showing that DIO enhances and exacerbates allergen-induced airway inflammation, either via upregulation of ILCs or greater neutrophil infiltration [223, 227]. Moreover, other researchers showed a protective effect of short-term HFD on the development of allergic asthma [228]. The experimental setup for the feeding period was similar to ours, which

was 12 weeks. The attenuation is a consequence of changes in immune cell infiltration induced by alteration in metabolic parameters. For instance, RORgt, a transcription factor for Th-17 secreting IL-17, was reduced in HF CHDM. In the context of asthma, IL-17 has a profibrotic effect on lung fibroblasts [229], and enhances fibrocytes [230], an inflammatory cell type that promotes airway contraction and narrowing. In addition, IL-17 has a direct stimulating effect on epithelial cells to increase the expression of mucus-producing genes, like MUC5A [231]. Consistent with that, mucus secretion was attenuated in the lungs of obese sensitized mice.

IL-17 is known to trigger neutrophil infiltration [232], and inhibition of neutrophil recruitment is suggested to control allergic inflammation [233]. Although not as striking, the frequency of neutrophils in BAL cells tended to be reduced in HF CHDM. Moreover, obesity-induced metabolic impairment might have an impact on the immunopathology of airway allergy. Obesity suppresses neutrophil chemotaxis by lowering the expression of CXCR2, a chemokine receptor [234], and impairing neutrophil survival [235]. Therefore, IL-17 plays an important role in the inflammatory response in lungs upon chronic HDM exposure, and was attenuated with the metabolic changes caused by HFD feeding, resulting in less inflammation in the lungs.

4.2 Improvement in metabolic parameters caused by the interaction of HFD feeding and chronic lung allergic inflammation

Like other studies with a similar experimental setup, where mice were exposed to either control or HFD, followed by acute PBS or HDM sensitization, we did not observe differences in body weight gain between sensitized and non-sensitized mice [221, 222]. This indicates that additional inflammatory responses caused by HDM are not sufficient to elicit metabolic changes. However, with chronic exposure to HDM, body weight gain remained unaltered, yet there was a reduction in the

fat mass of obese mice. An *in vitro* study using 3T3-L1 cells showed that HDM extracts are able to induce triglyceride accumulation and preadipocyte proliferation [236]. Therefore, interaction between metabolic syndrome and lung allergic inflammation caused a reduction in fat mass of obese sensitized mice.

Many studies aim to understand the effect of being obese or having metabolic impairment on the progression of HDM allergy, whereas research regarding the effect of HDM allergy on the prognosis of obesity or metabolic syndrome is not well established. In obesity, the expansion of adipose tissue is associated with M1 macrophage infiltration [237]. Upon acute HDM exposure, the frequency of M1 macrophages was reduced in male and female HF HDM mice compared to their PBS controls. This finding demonstrates that acute HDM exposure dampens M1 macrophage infiltration in the pgWAT of obese mice, which may explain why there was a slight improvement in glucose tolerance.

Outside the lungs, neutrophils are also involved in the development of adipose tissue inflammation, by infiltrating adipose tissue and producing chemokines and cytokines, thereby inducing macrophage infiltration [238]. During chronic HDM exposure, the frequency of neutrophils was reduced in the pgWAT of HFD-fed mice compared to the HF CPBS group, indicating less inflammation driven by long-term HDM exposure. A further consequence of the reduction in neutrophils was the reduction in macrophages. Although the percentage of gated M1 and M2 macrophages was unaltered, the expression of Cd68, the total macrophages marker in adipose tissue, was greatly reduced in HF CHDM in comparison to HF CPBS. Obesity-induced inflammation in adipose tissue also leads to higher secretion of pro-inflammatory cytokines by pgWAT, like Tnfa and IL-6, which can cause systemic insulin resistance by promoting lipolysis or direct inhibition of the insulin pathway [239, 240]. On the other hand, we found that chronic exposure to HDM attenuated the expression levels of pro-inflammatory cytokines in the pgWAT of obese mice. This indicates that when metabolic syndrome and HDM allergy are progressing simultaneously, there is less

expansion of pgWAT. That causes less infiltration of pro-inflammatory cells, further leading to the dampening of the inflammation in obese sensitized mice. This might be one of many factors contributing to the improvement in glucose tolerance and decreased hyperinsulinemia in obese sensitized mice.

Metabolic improvements in obese sensitized mice with chronic HDM sensitization indicate that the interaction and simultaneous development of these diseases may provide a protective effect on each other's conditions. The improvements were also supported by less triglyceride content in the liver of obese sensitized mice. This reduction of hepatic triglyceride might be due to less expansion and inflammation in the pgWAT of obese sensitized mice. Massive expansion of WAT in obesity, exceeding the capacity to store lipids, results in lipid spillover to other organs, including the liver [241]. Less lipid accumulation in the liver of obese sensitized mice might be caused by a reduction in *de novo* lipogenesis in the liver, which is still associated with less discharge of free fatty acids from WAT. Decreased delivery of FFA to the liver is beneficial for liver metabolism and insulin sensitivity [242], thereby less hyperinsulinemia is found in obese sensitized mice accordingly. FFA-induced hepatic insulin resistance and HFD-induced Kupffer cells, resident macrophages in the liver, also activate pro-inflammatory cytokines (e.g., Tnfa) [243, 244]. In contrast, we found no changes in pro-inflammatory and Kupffer cells mRNA levels in the liver of obese sensitized mice. Therefore, the beneficial interaction of these diseases is reflected in less inflammation and expansion of WAT, by which improves glucose and liver metabolism.

4.3 Vascularization in BAT and beiging in WAT are responsible for the increase in EE

Back to the theory of energy balance, this phenomenon in pgWAT might only be caused by alteration in energy intake and/or energy expenditure. Metabolic cages measurements showed an increase in food intake in

the HF CHDM mice compared to its control. Moreover, we observed a higher BMR and EE, both in dark and light phase, in the obese sensitized mice correspond to their individual body weight. Several factors affecting EE, including physical activity, were unaltered in obese sensitized mice, thus exercise is not the major contributor in this case, that is responsible for the increase in EE. Browning of WAT might contribute to the increase in EE via induction of thermogenic capacity, especially in scWAT [245]. Upon chronic HDM exposure, scWAT of obese mice expressed higher Cidea and Prdm16, both of which are known as specific brown and beige adipocyte markers [145]. During beiging in human fat cells, Cidea expression escalates and translocates into the nucleus to transcriptionally regulate Ucp1 expression by interacting with liver x receptor α (LXRα) and diminishes its binding to Ucp1 enhancer [246]. Meanwhile, Prdm16 functions in maintaining brown adipocyte identity and its depletion inhibits beige adipocyte development [247]. Moreover, a specific beige fat marker, Tmem26 [147], was also upregulated in obese sensitized mice, indicating browning in the scWAT. There are two possible mechanisms that contribute to browning in scWAT of mice with allergen-induced asthma, which are via the AMPK/Ppargc1a and IL-33/ILC2/AAMac pathways [248]. The AMPK/Ppargc1a signal can directly promote thermogenic genes in white and brown adipocytes [249], and we observed an up-regulation of Ppargc1a in the scWAT of obese sensitized mice. Meanwhile, asthma-induced IL-33 activates ILC2, further sustains alternatively activated macrophages (AAMac), which contribute to energy metabolism in scWAT [248]. Moreover, the expressions of IL-13 and IL-4 were increased in the scWAT of obese sensitized mice. ILC2s secreted IL-13 that activated eosinophils to secrete IL-4. IL-4 induced differentiation of M2 macrophages, which serves as an important source of catecholamines for beige fat activation. Alternatively, IL-4 acts directly on $Pdgfra^{+}$ precursor cells to increase the proliferation and differentiation into beige adipocytes [145]. Therefore, exposing mice chronically to

HDM and HFD promotes beiging in scWAT contributing to the increase in EE and BMR.

Furthermore, activation of BAT is known to promote metabolic health and combat obesity by increasing EE [250, 251]. The same browning pathway as in scWAT, AMPK/Ppargc1a, was suggested to drive more browning in BAT of ovalbumin-induced asthmatic mice [248]. In contrast, we did not find induction of Ucp1 mRNA or protein levels in HF CHDM group, as also seen in histology images. However, thermogenesis in BAT can be induced by creatine, which is independent from Ucp1 thermogenesis pathway. BAT of obese sensitized mice had higher expressions of GATM and GAMT, both are key enzymes to synthesize creatine. GATM synthesizes guanidinoacetate (creatine precursor) from arginine and glycine, then GAMT catalysis the synthesis of creatine [252]. Fat-specific deletion of GATM blunted the capacity of β3-adrenergic activation resulting in lower metabolic rate, thus more prone to develop obesity on a HFD. Impairment in the adrenergic thermogenesis was rescued by dietary creatine supplementation in the KO mice [253]. Creatine increased EE via stimulation of mitochondrial ATP turnover, and its reduction decreased EE *in vivo* and in human brown adipocytes [254]. Therefore, the increase of creatine synthesis may contribute to the increase of EE and BMR via creatine energetic and metabolism in BAT.

There was also an increase in Vegfa expression exclusively in BAT, not in pgWAT and scWAT, indicating more vascularization upon chronic HDM administration in obese mice. *In vitro*, Vegf induces proliferation in brown preadipocytes by 70%, whereas blocking Vegf signaling increases brown adipocyte apoptosis [255]. *In vivo*, adipose-specific overexpression of Vegf protects against DIO and improves insulin sensitivity [154], while adipose-specific deletion of Vegfa results in BAT whitening [155]. Therefore, we observed an improvement in glucose tolerance, which was partly supported by the increase in Glut1 expression in BAT of obese sensitized mice. Brown fat regulates glucose uptake via Glut1, which is stimulated by β-adrenoreceptor,

either via cAMP-dependent pathway or *de novo* synthesis [256], or Glut4, which is regulated by insulin [257]. In addition, Vegf deficiency represses the expression of β3-adrenergic receptor in BAT [155]. Thus, this leads us to hypothesize that the increase in vascularization in BAT of obese sensitized mice enables β3-adrenergic signaling to permeate in BAT, thereby stimulating Glut1 to increase glucose uptake. Taken together, interconnection of metabolic syndrome and lung allergic inflammation provides a beneficial effect on metabolic health by increasing browning in scWAT and stimulating Glut1 in BAT.

4.4 Eif5, Tcf25 and Bin1 are marker genes to distinguish distinct brown adipocyte lineages with different function in BAT thermogenesis

As discussed above, BAT is appealing as a target to improve metabolic health. However, it is a complex tissue and translation from murine study to human application is rather uncertain, since cellular differences between murine and human BAT have been controversially discussed. However, a recent study showed the existence of different subpopulation of brown adipocytes with high and low thermogenic capacity in murine [205], thus confirming our findings in which the Ucp1 expression greatly differs in individual brown adipocytes throughout the tissue. Although at room temperature murine BAT seems morphologically uniform. Therefore, the differences in Ucp1 content is considered as our reference to test if this is the result of developmental heterogeneity in murine brown adipocytes and not due to environmental or anatomical differences. The scRNAseq from SVF of murine BAT showed various types of cells, including immune cells, erythrocytes and preadipocyte clusters. Preadipocyte clustering is driven by distinct differentiation stages of preadipocytes, rather than distinct developmental lineages. Thus, this scRNAseq result could not identify potentially different brown preadipocyte lineages, yet still provides a valuable source for cellular composition studies within murine BAT. To this end, we overcome the

limitation of scRNAseq by using 67 immortalized brown preadipocyte clones from adult male C57BL/6J mice kept at room temperature. In contrast to isolated preadipocytes from human BAT [258], all preadipocytes isolated from murine BAT were believed to give rise or differentiate only to mature brown adipocytes. Opposite to that, the clones were differentiated into various degrees, such as in lipid accumulation and the expression of adipogenic markers, like Pparg. However, the heterogeneous expression of Ucp1 in mature adipocyte clones was not highly associated with their differentiation capacity and lipid accumulation. In addition, we observed a heterogeneous response to β3-adrenergic stimulation and the expression of classical brown, beige and white adipocyte markers on the clones. Similar to the human study [258], we found strong differences in gene expression between brown adipocyte clones.

RNAseq was performed from undifferentiated and differentiated cell lines focusing on clones derived from one mouse in order to get a more detailed insight about differences between clones. Moreover, selecting clones coming from one mouse is crucial to study the differences between individual cellular lineages and exclude inter-individual bias between mice. Analysis of RNAseq shown in hierarchical clustering and PCA were unable to conserve structure between preadipocytes and adipocytes, and in consequence we were not able to distinguish or cluster the clones into lineages. As seen in scRNAseq, this finding indicates there are plenty of subtle differences between the clones that complicate the assignment into lineages and might be influenced by cell cycle state, proliferation capacity etc., which generate transcriptional noise. To get an overview of the browning capacity in the clones, we correlated the RNAseq profile of each preadipocyte and adipocyte sample with the ProFat database. This enables us to identify three distinct clusters of cells that exhibited either characteristics of classical BAT in undifferentiated or differentiated states, BAT characteristic upon differentiation only or no BAT characteristics in undifferentiated and differentiated clones. Although the clones were all derived from the SVF

of BAT, this result showed group distinction between clones, thus indicating that the clones were derived from different lineages.

To visualize distinct lineages in the clones, we implemented Laplacian eigenmaps to identify lineage markers. Using this approach to structure our data, we were able to extract unique and stable gene expression between preadipocytes and adipocytes coming from seven distinct gene expression modules, and correlated each of them with the ProFat database. Among 57 conserved genes, we selected Eif5, Tcf25 and Bin1 as representative genes to distinguish brown adipocytes according to their similarity to classical, intermediate or distant brown adipocyte, respectively. Immunofluorescence staining of mature brown adipocytes in BAT sections for Eif5, Tcf25 and Bin1 revealed a contribution of each population to around 25% of brown adipocytes, thus reinforcing our *in vitro* findings. Furthermore, in contrast to what has been identified as specific surface proteins for white, beige and brown adipocytes [259], none of these genes are selective for brown fat. However, these three genes showed a broad tissue expression pattern and different responses upon challenge, such as chronic cold exposure and HFD feeding. When challenged, the expression of Eif5 and Tcf25 showed a similar trend with Ucp1 expression, whereas Bin1 expression was not affected in BAT *in vivo*. This indicates that the three marker genes might have different functions and regulatory effects in murine BAT.

In general, Eif5 interacts with the 40S ribosomal unit to initiate protein synthesis [260, 261]; Tcf25, also known as nuclear localized protein 1 (Nulp1), is a member of the basic helix-loop-helix family of transcription factors that plays an important role during early embryonic organogenesis [262, 263]; Bin1 or amphiphysin 2 has been shown to regulate muscle differentiation, and is highly expressed in skeletal muscle and brain [264]. However, the function of these genes in BAT has not been studied yet. We observed that the loss of Eif5 had no significant impact on the characteristics of brown adipocytes, whereas the loss of Tcf25 shifted the cellular identity to white-like adipocytes, supported by the increase of white adipocyte marker, Asc1, and a

decrease in maximum respiratory capacity. On the other hand, Bin1 expression was negatively correlated with thermogenic genes and high-Bin1 cells expressed low Ucp1. Moreover, loss of Bin1 increased Ucp1 expression and mitochondrial activity, indicating that Bin1 is not only a marker of “quiescent” brown adipocytes, but actively suppresses thermogenic capacity (Figure 41).

Additionally, we confirmed the existence of these marker genes, Eif5, Tcf25 and Bin1, in human BAT. The result strongly supports that human BAT is comprised of distinct brown adipocyte populations. However, it is inevitable that there might be other lineage markers, which need to be discovered in order to create an overall picture of brown adipocyte lineage determination and functional development interspecies. Since the activation of BAT remains an attractive pharmacological target to increase EE and combat obesity and metabolic syndrome, it is important to note that differences in anatomy, morphology and potentially function and development between rodent and human BAT [143] can complicate the translation from rodents to human physiology.

Morphology of murine BAT seems homogeneous when they are kept at room temperature [265], whereas human BAT shows a heterogeneous mixture of unilocular and multilocular adipocytes [266]. Meanwhile, in thermoneutral conditions and upon prolonged HFD feeding, murine BAT resembles the morphology of human BAT [265]. The appearance of unilocular adipocytes may indicate that individual brown adipocytes in murine BAT are heterogeneously responding to environmental changes, such as temperature and diet, thus supporting the existence of distinct brown adipocyte lineages with potentially different function. However, if human BAT is also comprised of distinct lineages in brown adipocytes, differences in the relative contribution of these lineages could help to explain the differences in BAT activity between individuals and the difficulties in translating research from murine housed at room temperature to human physiology.

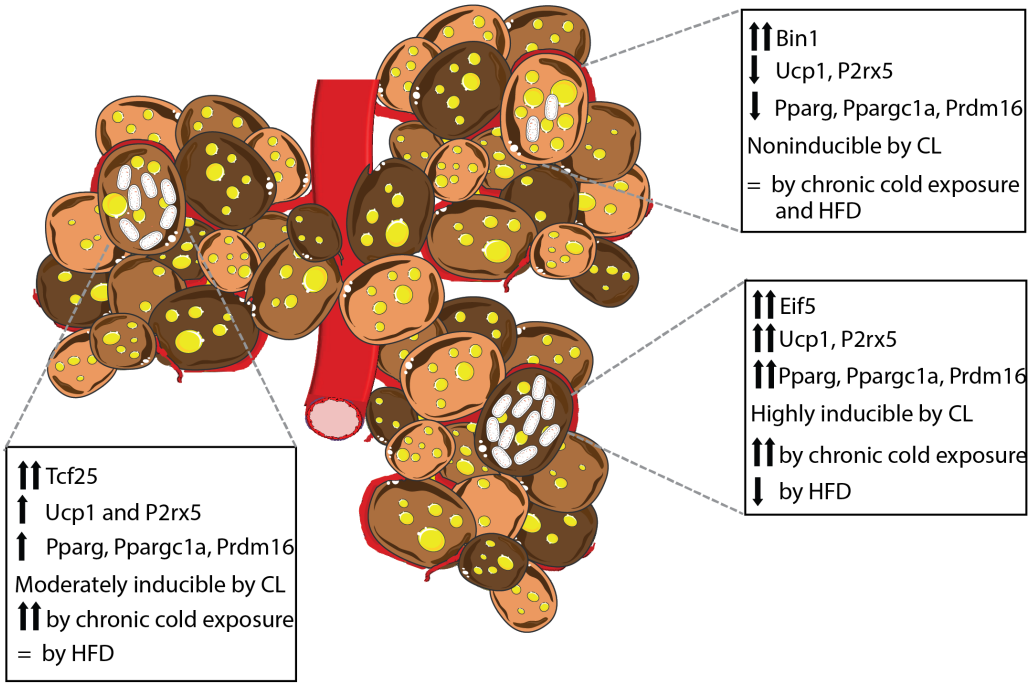

Figure 41: Schematic illustration of brown adipose tissue heterogeneity.
Murine BAT is composed of functionally distinct brown adipocytes. Eif5 expressing brown adipocytes is identified as classical brown adipocytes, characterized by high Ucp1 content and mitochondrial uncoupling. Tcf25 expression brown adipocytes are similar to Eif5 expressing brown adipocytes, although with a lower Ucp1 expression. In contrast, Bin1 expressing brown adipocytes appear in dormant state, characterized by low Ucp1 content with little response to beta-adrenergic stimulation. Additionally, loss of Bin1 results in an up-regulation of thermogenic capacity. Subpopulations of brown adipocytes are color-coded, based on their thermogenic capacity, with dark brown as the highest ($Eif5^{high}$), brown ($Tcf25^{high}$) and light brown ($Bin1^{high}$) (= indicates unchanged expression).

5. Conclusion and perspectives

In summary, the work of this thesis opens up a new perspective on the interconnection of obesity and metabolic syndrome with lung allergy inflammation, in the context of energy balance. The known correlation between obesity and/or metabolic disease with allergic asthma are mostly exacerbation with one another. A more detailed setup of study, conjoining simultaneous development of metabolic disorder and HDM-induced lung allergy inflammation reveals a favorable interaction. It appears that HFD feeding and chronic exposure to HDM attenuated the inflammatory reaction in the lungs by decreasing the frequency of RORgt^{+}, thus reducing mucus secretion and neutrophil infiltration to the lungs. In the scope of adipose tissue inflammation upon HFD feeding, the interconnection with prolonged HDM exposure reduced the expansion of pgWAT, therefore dampening inflammation by decreasing neutrophil infiltration, total macrophage and pro-inflammatory cytokine expressions. The attenuation of pgWAT expansion in obese sensitized mice also resulted in less triglyceride accumulation in the liver, which increased insulin sensitivity and improved glucose tolerance. And as a consequence, the liver showed less inflammation and an improvement in both insulin sensitivity and glucose metabolism. The observed advantages in the metabolic phenotype of obese sensitized mice were the result of increased energy expenditure and basal metabolic rate. The improvement in energy expenditure and basal metabolic rate were driven by browning in scWAT and increased vascularization and creatine synthesis in BAT. Further, stimulation of Glut1 to increase glucose uptake also explained the refinement in glucose metabolism. Therefore, it is inevitable that interconnection between this two diseases attenuates the progression of each other's prognosis.

However, a deeper molecular interaction and mechanism to better explain the positive traits needs to be carried out, notably in the browning of scWAT and the association with lung allergy inflammation in the development of obesity. In addition, crosstalk between lung, brain

and adipose tissue, in the expansion of beta-adrenergic signaling might be worth investigating, since beta-adrenergic agonists are used as bronchodilators in asthma medication to relax the airway muscles. A more comprehensive study to understand the main molecule that intercedes the mechanism benefiting in both lung inflammation and metabolic syndrome, is appealing as a pharmacological target.

Although a lot of positive contributions of BAT in the development of obesity and other metabolic-related diseases have been discovered, the cellular distinction in murine BAT is far from being understood in the context of its lineages, particularly in order to translate murine breakthrough research into humans. Using scRNAseq, we characterized the composition of the stromal vascular fraction of murine BAT. However, computational analysis of scRNAseq data in the brown preadipocyte clusters revealed distinct differentiation stages of adipocytes rather than different preadipocyte lineages. Furthermore, we performed a detailed phenotypic and computational analysis of immortalized brown preadipocyte and adipocyte clones derived from murine interscapular BAT. Using nonlinear manifold approaches, a set of potential lineage markers for brown adipocytes were identified, along with their relative correlations to various markers known for BAT. We characterized Eif5, Tcf25 and Bin1 as markers for precursors and brown adipocyte subsets, which functionally differ in their capacity to induce browning in BAT. In particular, loss of Bin1 increased mitochondrial uncoupling and thermogenic gene expression. Thus, our data suggests the existence of multiple murine brown adipocyte lineages.

These genes were detected in different fat depots in humans, thus we provide novel approaches to “humanize” murine BAT, fostering translation into human physiology. However, specific functions of the selected marker genes need to be addressed. Therefore, future studies on adipose-selective deletion of these putative lineage markers will provide a more precise and broad spectrum of the function and underlying mechanism.

References

[1] WHO. (2020). *Obesity and overweight*. Available: https://www.who.int/news-room/fact-sheets/detail/obesity-and-overweight

[2] J. C. Wells and M. Siervo, "Obesity and energy balance: is the tail wagging the dog?," *Eur J Clin Nutr,* vol. 65, pp. 1173-89, Nov 2011.

[3] T. Christian and I. Rashad, "Trends in U.S. food prices, 1950-2007," *Econ Hum Biol,* vol. 7, pp. 113-20, Mar 2009.

[4] J. O. Hill, H. R. Wyatt, and J. C. Peters, "Energy balance and obesity," *Circulation,* vol. 126, pp. 126-32, Jul 3 2012.

[5] K. D. Hall, "Did the Food Environment Cause the Obesity Epidemic?," *Obesity (Silver Spring),* vol. 26, pp. 11-13, Jan 2018.

[6] J. E. Blundell and J. I. MacDiarmid, "Fat as a risk factor for overconsumption: satiation, satiety, and patterns of eating," *J Am Diet Assoc,* vol. 97, pp. S63-9, Jul 1997.

[7] M. Vadiveloo, M. Scott, P. Quatromoni, P. Jacques, and N. Parekh, "Trends in dietary fat and high-fat food intakes from 1991 to 2008 in the Framingham Heart Study participants," *Br J Nutr,* vol. 111, pp. 724-34, Feb 2014.

[8] K. M. Flegal, M. D. Carroll, C. L. Ogden, and L. R. Curtin, "Prevalence and trends in obesity among US adults, 1999-2008," *JAMA,* vol. 303, pp. 235-41, Jan 20 2010.

[9] M. Vanhala, P. Vanhala, E. Kumpusalo, P. Halonen, and J. Takala, "Relation between obesity from childhood to adulthood and the metabolic syndrome: population based study," *BMJ,* vol. 317, p. 319, Aug 1 1998.

[10] P. L. Huang, "A comprehensive definition for metabolic syndrome," *Dis Model Mech,* vol. 2, pp. 231-7, May-Jun 2009.

[11] M. G. Saklayen, "The Global Epidemic of the Metabolic Syndrome," *Curr Hypertens Rep,* vol. 20, p. 12, Feb 26 2018.

[12] L. K. Phillips and J. B. Prins, "The link between abdominal obesity and the metabolic syndrome," *Current Hypertension Reports,* vol. 10, pp. 156-164, 2008.

[13] K. G. M. M. Alberti, P. Z. Zimmet, and W. Consultation, "Definition, diagnosis and classification of diabetes mellitus and its complications part 1: Diagnosis and classification of diabetes mellitus - Provisional report of a WHO consultation," *Diabetic Medicine,* vol. 15, pp. 539-553, Jul 1998.

[14] J. Ye, "Mechanisms of insulin resistance in obesity," *Frontiers of Medicine,* vol. 7, pp. 14-24, 2013.

[15] J. A. Kim, M. Montagnani, K. K. Koh, and M. J. Quon, "Reciprocal relationships between insulin resistance and endothelial dysfunction - Molecular and pathophysiological mechanisms," *Circulation,* vol. 113, pp. 1888-1904, Apr 18 2006.

[16] P. L. Huang, "A comprehensive definition for metabolic syndrome," *Disease Models & Mechanisms,* vol. 2, pp. 231-237, 2009.

[17] M. T. Hudda, C. M. Nightingale, A. S. Donin, C. G. Owen, A. R. Rudnicka, J. C. K. Wells*, et al.*, "Patterns of childhood body mass index (BMI), overweight

and obesity in South Asian and black participants in the English National child measurement programme: effect of applying BMI adjustments standardising for ethnic differences in BMI-body fatness associations," *Int J Obes (Lond),* vol. 42, pp. 662-670, Apr 2018.

[18] M. B. Chalk, "Obesity: addressing a multifactorial disease," *Case Manager,* vol. 15, pp. 47-9; quiz 50, Nov-Dec 2004.

[19] C. E. Elks, M. den Hoed, J. H. Zhao, S. J. Sharp, N. J. Wareham, R. J. Loos*, et al.*, "Variability in the heritability of body mass index: a systematic review and meta-regression," *Front Endocrinol (Lausanne),* vol. 3, p. 29, 2012.

[20] G. S. H. Yeo, "Genetics of obesity: can an old dog teach us new tricks?," *Diabetologia,* vol. 60, pp. 778-783, May 2017.

[21] I. S. Farooqi and S. O'Rahilly, "Monogenic human obesity syndromes," *Recent Prog Horm Res,* vol. 59, pp. 409-24, 2004.

[22] M. Pigeyre, F. T. Yazdi, Y. Kaur, and D. Meyre, "Recent progress in genetics, epigenetics and metagenomics unveils the pathophysiology of human obesity," *Clin Sci (Lond),* vol. 130, pp. 943-86, Jun 1 2016.

[23] A. Hinney, C. I. Vogel, and J. Hebebrand, "From monogenic to polygenic obesity: recent advances," *Eur Child Adolesc Psychiatry,* vol. 19, pp. 297-310, Mar 2010.

[24] A. Hinney and J. Hebebrand, "Polygenic obesity in humans," *Obes Facts,* vol. 1, pp. 35-42, 2008.

[25] R. K. Singh, P. Kumar, and K. Mahalingam, "Molecular genetics of human obesity: A comprehensive review," *C R Biol,* vol. 340, pp. 87-108, Feb 2017.

[26] A. Scuteri, S. Sanna, W. M. Chen, M. Uda, G. Albai, J. Strait*, et al.*, "Genome-wide association scan shows genetic variants in the FTO gene are associated with obesity-related traits," *PLoS Genet,* vol. 3, p. e115, Jul 2007.

[27] L. J. Scott, K. L. Mohlke, L. L. Bonnycastle, C. J. Willer, Y. Li, W. L. Duren*, et al.*, "A genome-wide association study of type 2 diabetes in Finns detects multiple susceptibility variants," *Science,* vol. 316, pp. 1341-5, Jun 1 2007.

[28] F. Stutzmann, V. Vatin, S. Cauchi, A. Morandi, B. Jouret, O. Landt*, et al.*, "Non-synonymous polymorphisms in melanocortin-4 receptor protect against obesity: the two facets of a Janus obesity gene," *Hum Mol Genet,* vol. 16, pp. 1837-44, Aug 1 2007.

[29] S. Li, W. Chen, S. R. Srinivasan, E. Boerwinkle, and G. S. Berenson, "Influence of lipoprotein lipase gene Ser447Stop and beta1-adrenergic receptor gene Arg389Gly polymorphisms and their interaction on obesity from childhood to adulthood: the Bogalusa Heart Study," *Int J Obes (Lond),* vol. 30, pp. 1183-8, Aug 2006.

[30] M. S. Corbalan, A. Marti, L. Forga, M. A. Martinez-Gonzalez, and J. A. Martinez, "Beta(2)-adrenergic receptor mutation and abdominal obesity risk: effect modification by gender and HDL-cholesterol," *Eur J Nutr,* vol. 41, pp. 114-8, Jun 2002.

[31] A. Marti, M. S. Corbalan, M. A. Martinez-Gonzalez, and J. A. Martinez, "TRP64ARG polymorphism of the beta 3-adrenergic receptor gene and obesity risk: effect modification by a sedentary lifestyle," *Diabetes Obes Metab,* vol. 4, pp. 428-30, Nov 2002.

[32] H. S. Park, Y. Kim, and C. Lee, "Single nucleotide variants in the beta2-adrenergic and beta3-adrenergic receptor genes explained 18.3% of adolescent obesity variation," *J Hum Genet,* vol. 50, pp. 365-369, 2005.

[33] R. Zurbano, M. C. Ochoa, M. J. Moreno-Aliaga, J. A. Martinez, A. Marti, and i. Grupo de Estudio Navarro de la obesidad, "[Influence of the -866G/A polymorphism of the UCP2 gene on an obese pediatric population]," *Nutr Hosp,* vol. 21, pp. 52-6, Jan-Feb 2006.

[34] S. Chathoth, M. H. Ismail, C. Vatte, C. Cyrus, Z. Al Ali, K. A. Ahmed*, et al.*, "Association of Uncoupling Protein 1 (UCP1) gene polymorphism with obesity: a case-control study," *BMC Med Genet,* vol. 19, p. 203, Nov 20 2018.

[35] C. V. Musa, A. Mancini, A. Alfieri, G. Labruna, G. Valerio, A. Franzese*, et al.*, "Four novel UCP3 gene variants associated with childhood obesity: effect on fatty acid oxidation and on prevention of triglyceride storage," *Int J Obes (Lond),* vol. 36, pp. 207-17, Feb 2012.

[36] G. Taubes, "As obesity rates rise, experts struggle to explain why," *Science,* vol. 280, pp. 1367-8, May 29 1998.

[37] T. W. Winkler, A. E. Justice, M. Graff, L. Barata, M. F. Feitosa, S. Chu*, et al.*, "Correction: The Influence of Age and Sex on Genetic Associations with Adult Body Size and Shape: A Large-Scale Genome-Wide Interaction Study," *PLoS Genet,* vol. 12, p. e1006166, Jun 2016.

[38] M. O. Goodarzi, "Genetics of obesity: what genetic association studies have taught us about the biology of obesity and its complications," *Lancet Diabetes Endocrinol,* vol. 6, pp. 223-236, Mar 2018.

[39] P. Kaushik and J. T. Anderson, "Obesity: epigenetic aspects," *Biomol Concepts,* vol. 7, pp. 145-55, Jun 1 2016.

[40] H. Reddon, J. L. Gueant, and D. Meyre, "The importance of gene-environment interactions in human obesity," *Clin Sci (Lond),* vol. 130, pp. 1571-97, Sep 1 2016.

[41] E. Sonestedt, C. Roos, B. Gullberg, U. Ericson, E. Wirfalt, and M. Orho-Melander, "Fat and carbohydrate intake modify the association between genetic variation in the FTO genotype and obesity," *Am J Clin Nutr,* vol. 90, pp. 1418-25, Nov 2009.

[42] S. Li, J. H. Zhao, J. Luan, U. Ekelund, R. N. Luben, K. T. Khaw*, et al.*, "Physical activity attenuates the genetic predisposition to obesity in 20,000 men and women from EPIC-Norfolk prospective population study," *PLoS Med,* vol. 7, Aug 31 2010.

[43] W. Johnson, K. K. Ong, C. E. Elks, N. J. Wareham, A. Wong, G. Muniz-Terrera*, et al.*, "Modification of genetic influences on adiposity between 36 and 63 years of age by physical activity and smoking in the 1946 British Birth Cohort Study," *Nutr Diabetes,* vol. 4, p. e136, Sep 8 2014.

[44] A. E. Justice, T. W. Winkler, M. F. Feitosa, M. Graff, V. A. Fisher, K. Young*, et al.*, "Genome-wide meta-analysis of 241,258 adults accounting for smoking behaviour identifies novel loci for obesity traits," *Nat Commun,* vol. 8, p. 14977, Apr 26 2017.

[45] H. Liu and G. Guo, "Lifetime Socioeconomic Status, Historical Context, and Genetic Inheritance in Shaping Body Mass in Middle and Late Adulthood," *Am Sociol Rev,* vol. 80, pp. 705-737, Aug 2015.

[46] J. Wakefield, "Fighting obesity through the built environment," *Environ Health Perspect,* vol. 112, pp. A616-8, Aug 2004.
[47] A. Lee, M. Cardel, and W. T. Donahoo, "Social and Environmental Factors Influencing Obesity," in *Endotext*, K. R. Feingold, B. Anawalt, A. Boyce, G. Chrousos, W. W. de Herder, K. Dungan*, et al.*, Eds., ed South Dartmouth (MA), 2000.
[48] J. P. Block, R. A. Scribner, and K. B. DeSalvo, "Fast food, race/ethnicity, and income: a geographic analysis," *Am J Prev Med,* vol. 27, pp. 211-7, Oct 2004.
[49] M. A. Martinez-Gonzalez, J. A. Martinez, F. B. Hu, M. J. Gibney, and J. Kearney, "Physical inactivity, sedentary lifestyle and obesity in the European Union," *Int J Obes Relat Metab Disord,* vol. 23, pp. 1192-201, Nov 1999.
[50] M. A. McQueen, "Exercise aspects of obesity treatment," *Ochsner J,* vol. 9, pp. 140-3, Fall 2009.
[51] A. S. Barnes, "Obesity and sedentary lifestyles: risk for cardiovascular disease in women," *Tex Heart Inst J,* vol. 39, pp. 224-7, 2012.
[52] D. R. Moellering and D. L. Smith, "Ambient Temperature and Obesity," *Current Obesity Reports,* vol. 1, pp. 26-34, 2012.
[53] C. D. Davis, "The Gut Microbiome and Its Role in Obesity," *Nutrition Today,* vol. 51, pp. 167-174, 2016.
[54] A. A. J. Vaillant, Vashisht, R., Zito, P. M., *Immediate Hypersensitivity Reactions*. Treasure Island: StatPearls Publishing, 2020.
[55] D. B. Corry and F. Kheradmand, "Toeard a comprehensive understanding of allergic lung disease," *Trans Am Clin Climatol Assoc,* vol. 120, pp. 33-48, 2009.
[56] G. Passalacqua and G. Ciprandi, "Allergy and the lung," *Clinical & Experimental Immunology,* vol. 153, pp. 12-16, 2008.
[57] F. Fassio and F. Guagnini, "House dust mite-related respiratory allergies and probiotics: a narrative review," *Clinical and Molecular Allergy,* vol. 16, 2018.
[58] W. R. Thomas, "Geography of house dust mite allergens," *Asian Pacific Journal of Allergy and Immunology,* vol. 28, pp. 211-224, Dec 2010.
[59] J. Portnoy, J. D. Miller, P. B. Williams, G. L. Chew, J. D. Miller, F. Zaitoun*, et al.*, "Environmental assessment and exposure control of dust mites: a practice parameter," *Annals of Allergy Asthma & Immunology,* vol. 111, pp. 465-507, Dec 2013.
[60] S. Illi, E. von Mutius, S. Lau, B. Niggemann, C. Grüber, and U. Wahn, "Perennial allergen sensitisation early in life and chronic asthma in children: a birth cohort study," *The Lancet,* vol. 368, pp. 763-770, 2006.
[61] U. Peters, A. E. Dixon, and E. Forno, "Obesity and asthma," *Journal of Allergy and Clinical Immunology,* vol. 141, pp. 1169-1179, 2018.
[62] S. Park, N.-K. Choi, S. Kim, and C.-H. Lee, "The relationship between metabolic syndrome and asthma in the elderly," *Scientific Reports,* vol. 8, 2018.
[63] W. H. Organization. (2020). *Obesity and overweight*. Available: https://www.who.int/news-room/fact-sheets/detail/obesity-and-overweight

[64] W. A. Organization. (2011). *White Book on Allergy*. Available: https://www.worldallergy.org/UserFiles/file/WAO-White-Book-on-Allergy_web.pdf

[65] AAAAI. *Allergy Statistics*. Available: https://www.aaaai.org/about-aaaai/newsroom/allergy-statistics -:~:text=Worldwide%2C%20allergic%20rhinitis%20affects%20between,and%2030%20%25%20of%20the%20population.&text=Worldwide%2C%20sensitization%20(IgE%20antibodies),to%2040%25%20of%20the%20population.&text=In%202012%2C%207.5%25%20or%2017.6,in%20the%20past%2012%20months.

[66] L. G. Hersoug and A. Linneberg, "The link between the epidemics of obesity and allergic diseases: does obesity induce decreased immune tolerance?," *Allergy,* vol. 62, pp. 1205-1213, 2007.

[67] F. Holguin, M. Rojas, L. A. Brown, and A. M. Fitzpatrick, "Airway and plasma leptin and adiponectin in lean and obese asthmatics and controls," *J Asthma,* vol. 48, pp. 217-23, Apr 2011.

[68] N. L. Lugogo, J. W. Hollingsworth, D. L. Howell, L. G. Que, D. Francisco, T. D. Church*, et al.*, "Alveolar macrophages from overweight/obese subjects with asthma demonstrate a proinflammatory phenotype," *Am J Respir Crit Care Med,* vol. 186, pp. 404-11, Sep 1 2012.

[69] O. Sideleva, B. T. Suratt, K. E. Black, W. G. Tharp, R. E. Pratley, P. Forgione*, et al.*, "Obesity and asthma: an inflammatory disease of adipose tissue not the airway," *Am J Respir Crit Care Med,* vol. 186, pp. 598-605, Oct 1 2012.

[70] K. Matsuda, Y. Nishi, Y. Okamatsu, M. Kojima, and T. Matsuishi, "Ghrelin and leptin: A link between obesity and allergy?," *Journal of Allergy and Clinical Immunology,* vol. 117, pp. 705-706, 2006.

[71] M. Tschop, C. Weyer, P. A. Tataranni, V. Devanarayan, E. Ravussin, and M. L. Heiman, "Circulating Ghrelin Levels Are Decreased in Human Obesity," *Diabetes,* vol. 50, pp. 707-709, 2001.

[72] C. M. Visness, S. J. London, J. L. Daniels, J. S. Kaufman, K. B. Yeatts, A.-M. Siega-Riz*, et al.*, "Association of obesity with IgE levels and allergy symptoms in children and adolescents: Results from the National Health and Nutrition Examination Survey 2005-2006," *Journal of Allergy and Clinical Immunology,* vol. 123, pp. 1163-1169.e4, 2009.

[73] K. E. Wellen and G. S. Hotamisligil, "Inflammation, stress, and diabetes," *Journal of Clinical Investigation,* vol. 115, pp. 1111-1119, 2005.

[74] J.-A. Shin, J.-H. Lee, S.-Y. Lim, H.-S. Ha, H.-S. Kwon, Y.-M. Park*, et al.*, "Metabolic syndrome as a predictor of type 2 diabetes, and its clinical interpretations and usefulness," *Journal of Diabetes Investigation,* vol. 4, pp. 334-343, 2013.

[75] M. Kasuga, "Insulin resistance and pancreatic cell failure," *Journal of Clinical Investigation,* vol. 116, pp. 1756-1760, 2006.

[76] P. E. Scherer and J. A. Hill, "Obesity, Diabetes, and Cardiovascular Diseases," *Circulation Research,* vol. 118, pp. 1703-1705, 2016.

[77] R. A. DeFronzo, "Insulin resistance, lipotoxicity, type 2 diabetes and atherosclerosis: the missing links. The Claude Bernard Lecture 2009," *Diabetologia,* vol. 53, pp. 1270-1287, Jul 2010.

[78] F. D. Fuchs and P. K. Whelton, "High Blood Pressure and Cardiovascular Disease," *Hypertension,* vol. 75, pp. 285-292, 2020.

[79] S. Kofler, T. Nickel, and M. Weis, "Role of cytokines in cardiovascular diseases: a focus on endothelial responses to inflammation," *Clinical Science,* vol. 108, pp. 205-213, 2005.
[80] B. Isomaa, P. Almgren, T. Tuomi, B. Forsen, K. Lahti, M. Nissen*, et al.*, "Cardiovascular Morbidity and Mortality Associated With the Metabolic Syndrome," *Diabetes Care,* vol. 24, pp. 683-689, 2001.
[81] S. Fujihara, H. Mori, H. Kobara, N. Nishiyama, M. Kobayashi, M. Oryu*, et al.*, "Metabolic Syndrome, Obesity, and Gastrointestinal Cancer," *Gastroenterology Research and Practice,* 2012.
[82] G.-M. Zhang, Y. Zhu, and D.-W. Ye, "Metabolic syndrome and renal cell carcinoma," *World Journal of Surgical Oncology,* vol. 12, p. 236, 2014.
[83] A. W. Hsing, L. C. Sakoda, and S. C. Chua, "Obesity, metabolic syndrome, and prostate cancer," *The American Journal of Clinical Nutrition,* vol. 86, pp. 843S-857S, 2007.
[84] Y. R. Li, V. Ro, and J. C. Tchou, "Obesity, Metabolic Syndrome, and Breast Cancer: From Prevention to Intervention," *Current Surgery Reports,* vol. 6, 2018.
[85] E. Giovannucci, "Insulin, Insulin-Like Growth Factors and Colon Cancer: A Review of the Evidence," *The Journal of Nutrition,* vol. 131, pp. 3109S-3120S, 2001.
[86] L. W. Bowers, E. L. Rossi, C. H. Oâ€™Flanagan, L. A. deGraffenried, and S. D. Hursting, "The Role of the Insulin/IGF System in Cancer: Lessons Learned from Clinical Trials and the Energy Balance-Cancer Link," *Frontiers in Endocrinology,* vol. 6, 2015.
[87] Y. Gizem and Y. Abdullah, "Metabolic Syndrome and Neurodegenerative Diseases," *Journal of Geriatric Medicine and Gerontology,* vol. 4, 2018.
[88] H. Ashrafian, L. Harling, A. Darzi, and T. Athanasiou, "Neurodegenerative disease and obesity: what is the role of weight loss and bariatric interventions?," *Metabolic Brain Disease,* vol. 28, pp. 341-353, 2013.
[89] A. F. Godoy-Matos, W. S. Silva Júnior, and C. M. Valerio, "NAFLD as a continuum: from obesity to metabolic syndrome and diabetes," *Diabetology & Metabolic Syndrome,* vol. 12, 2020.
[90] G. Petrovic, G. Bjelakovic, D. Benedeto-Stojanov, A. Nagorni, V. Brzacki, and B. Markovic-Zivkovic, "Obesity and metabolic syndrome as risk factors for the development of non-alcoholic fatty liver disease as diagnosed by ultrasound," *Vojnosanitetski pregled,* vol. 73, pp. 910-920, 2016.
[91] J. Steier, A. Lunt, N. Hart, M. I. Polkey, and J. Moxham, "Observational study of the effect of obesity on lung volumes," *Thorax,* vol. 69, pp. 752-759, 2014.
[92] N. Leone, D. Courbon, F. Thomas, K. Bean, B. Jégo, B. Leynaert*, et al.*, "Lung Function Impairment and Metabolic Syndrome," *American Journal of Respiratory and Critical Care Medicine,* vol. 179, pp. 509-516, 2009.
[93] Y.-Y. Lee, Y.-C. Tsao, C.-K. Yang, C.-H. Chuang, W. Yu, J.-C. Chen*, et al.*, "Association between risk factors of metabolic syndrome with lung function," *European Journal of Clinical Nutrition,* vol. 74, pp. 811-817, 2019.
[94] S. Bhatia and A. Sood, "Obesity and obstructive lung disease: An epidemiologic review," pp. 67-87, 2019.

[95] A. E. Dixon, S. E. Johnson, L. V. Griffes, D. M. Raymond, R. Ramdeo, A. Soloveichik*, et al.*, "Relationship of Adipokines with Immune Response and Lung Function in Obese Asthmatic and Non-Asthmatic Women," *Journal of Asthma,* vol. 48, pp. 811-817, 2011.
[96] A. Bruno, E. Pace, P. Chanez, D. Gras, I. Vachier, G. Chiappara*, et al.*, "Leptin and leptin receptor expression in asthma," *Journal of Allergy and Clinical Immunology,* vol. 124, pp. 230-237.e4, 2009.
[97] L. Khaodhiar, K. C. McCowen, and G. L. Blackburn, "Obesity and its comorbid conditions," *Clin Cornerstone,* vol. 2, pp. 17-31, 1999.
[98] C. W. Baffi, L. Wood, D. Winnica, P. J. Strollo, M. T. Gladwin, L. G. Que*, et al.*, "Metabolic Syndrome and the Lung," *Chest,* vol. 149, pp. 1525-1534, 2016.
[99] P. Trayhurn and J. H. Beattie, "Physiological role of adipose tissue: white adipose tissue as an endocrine and secretory organ," *Proceedings of the Nutrition Society,* vol. 60, pp. 329-339, Aug 2001.
[100] S. Gancheva, T. Jelenik, E. Alvarez-Hernandez, and M. Roden, "Interorgan Metabolic Crosstalk in Human Insulin Resistance," *Physiological Reviews,* vol. 98, pp. 1371-1415, Jul 2018.
[101] I. Harman-Boehm, M. Bluher, H. Redel, N. Sion-Vardy, S. Ovadia, E. Avinoach*, et al.*, "Macrophage infiltration into omental versus subcutaneous fat across different populations: Effect of regional adiposity and the comorbidities of obesity," *Journal of Clinical Endocrinology & Metabolism,* vol. 92, pp. 2240-2247, Jun 2007.
[102] I. K. Lesna, A. Kralova, S. Cejkova, J. Fronek, M. Petras, A. Sekerkova*, et al.*, "Characterisation and comparison of adipose tissue macrophages from human subcutaneous, visceral and perivascular adipose tissue," *Journal of Translational Medicine,* vol. 14, Jul 11 2016.
[103] K. Y. Lee, Q. Luong, R. Sharma, J. M. Dreyfuss, S. Ussar, and C. R. Kahn, "Developmental and functional heterogeneity of white adipocytes within a single fat depot," *Embo Journal,* vol. 38, Feb 1 2019.
[104] T. Schoettl, I. P. Fischer, and S. Ussar, "Heterogeneity of adipose tissue in development and metabolic function," *The Journal of Experimental Biology,* vol. 221, p. jeb162958, 2018.
[105] R. V. Shah, V. L. Murthy, S. A. Abbasi, R. Blankstein, R. Y. Kwong, A. B. Goldfine*, et al.*, "Visceral Adiposity and the Risk of Metabolic Syndrome Across Body Mass Index," *JACC: Cardiovascular Imaging,* vol. 7, pp. 1221-1235, 2014.
[106] L. Fontana, J. C. Eagon, M. E. Trujillo, P. E. Scherer, and S. Klein, "Visceral fat adipokine secretion is associated with systemic inflammation in obese humans," *Diabetes,* vol. 56, pp. 1010-1013, Apr 2007.
[107] P. Trayhurn, "Hypoxia and Adipose Tissue Function and Dysfunction in Obesity," *Physiological Reviews,* vol. 93, pp. 1-21, Jan 2013.
[108] R. W. O'Rourke, A. E. White, M. D. Metcalf, A. S. Olivas, P. Mitra, W. G. Larison*, et al.*, "Hypoxia-induced inflammatory cytokine secretion in human adipose tissue stromovascular cells," *Diabetologia,* vol. 54, pp. 1480-1490, Jun 2011.
[109] M. Feuerer, L. Herrero, D. Cipolletta, A. Naaz, J. Wong, A. Nayer*, et al.*, "Lean, but not obese, fat is enriched for a unique population of regulatory T cells that affect metabolic parameters," *Nature Medicine,* vol. 15, pp. 930-939, 2009.

[110] A. B. Molofsky, J. C. Nussbaum, H. E. Liang, S. J. Van Dyken, L. E. Cheng, A. Mohapatra*, et al.*, "Innate lymphoid type 2 cells sustain visceral adipose tissue eosinophils and alternatively activated macrophages," *Journal of Experimental Medicine,* vol. 210, pp. 535-549, Mar 11 2013.

[111] J. M. Han, S. J. Patterson, M. Speck, J. A. Ehses, and M. K. Levings, "Insulin Inhibits IL-10-Mediated Regulatory T Cell Function: Implications for Obesity," *Journal of Immunology,* vol. 192, pp. 623-629, Jan 15 2014.

[112] S. Winer, Y. Chan, G. Paltser, D. Truong, H. Tsui, J. Bahrami*, et al.*, "Normalization of obesity-associated insulin resistance through immunotherapy," *Nature Medicine,* vol. 15, pp. 921-929, 2009.

[113] F. Villarroya, R. Cereijo, A. Gavalda-Navarro, J. Villarroya, and M. Giralt, "Inflammation of brown/beige adipose tissues in obesity and metabolic disease," *Journal of Internal Medicine,* vol. 284, pp. 492-504, Nov 2018.

[114] K. R. Westerterp, "Control of energy expenditure in humans," *Eur J Clin Nutr,* vol. 71, pp. 340-344, Mar 2017.

[115] F. Zurlo, K. Larson, C. Bogardus, and E. Ravussin, "Skeletal muscle metabolism is a major determinant of resting energy expenditure," *J Clin Invest,* vol. 86, pp. 1423-7, Nov 1990.

[116] K. I. Stanford, R. J. W. Middelbeek, K. L. Townsend, D. An, E. B. Nygaard, K. M. Hitchcox*, et al.*, "Brown adipose tissue regulates glucose homeostasis and insulin sensitivity," *Journal of Clinical Investigation,* vol. 123, pp. 215-223, 2012.

[117] D. Cota, C. Wu, W. Cheng, Y. Sun, Y. Dang, F. Gong*, et al.*, "Activating Brown Adipose Tissue for Weight Loss and Lowering of Blood Glucose Levels: A MicroPET Study Using Obese and Diabetic Model Mice," *PLoS ONE,* vol. 9, p. e113742, 2014.

[118] K. I. Stanford, R. J. W. Middelbeek, K. L. Townsend, D. An, E. B. Nygaard, K. M. Hitchcox*, et al.*, "Brown adipose tissue regulates glucose homeostasis and insulin sensitivity," *Journal of Clinical Investigation,* vol. 123, pp. 215-223, Jan 2013.

[119] M. Chondronikola, E. Volpi, E. Borsheim, C. Porter, P. Annamalai, S. Enerback*, et al.*, "Brown Adipose Tissue Improves Whole-Body Glucose Homeostasis and Insulin Sensitivity in Humans," *Diabetes,* vol. 63, pp. 4089-4099, Dec 2014.

[120] A. M. Cypess, S. Lehman, G. Williams, I. Tal, D. Rodman, A. B. Goldfine*, et al.*, "Identification and Importance of Brown Adipose Tissue in Adult Humans," *New England Journal of Medicine,* vol. 360, pp. 1509-1517, 2009.

[121] K. A. Virtanen, M. E. Lidell, J. Orava, M. Heglind, R. Westergren, T. Niemi*, et al.*, "Functional Brown Adipose Tissue in Healthy Adults," *New England Journal of Medicine,* vol. 360, pp. 1518-1525, 2009.

[122] M. C. Zingaretti, F. Crosta, A. Vitali, M. Guerrieri, A. Frontini, B. Cannon*, et al.*, "The presence of UCP1 demonstrates that metabolically active adipose tissue in the neck of adult humans truly represents brown adipose tissue," *The FASEB Journal,* vol. 23, pp. 3113-3120, 2009.

[123] W. D. van Marken Lichtenbelt, J. W. Vanhommerig, N. M. Smulders, J. M. A. F. L. Drossaerts, G. J. Kemerink, N. D. Bouvy*, et al.*, "Cold-Activated Brown Adipose Tissue in Healthy Men," *New England Journal of Medicine,* vol. 360, pp. 1500-1508, 2009.

[124] J. Nedergaard, T. Bengtsson, and B. Cannon, "Unexpected evidence for active brown adipose tissue in adult humans," *American Journal of Physiology-Endocrinology and Metabolism,* vol. 293, pp. E444-E452, 2007.
[125] Aaron M. Cypess, Lauren S. Weiner, C. Roberts-Toler, Elisa F. Elía, Skyler H. Kessler, Peter A. Kahn*, et al.*, "Activation of Human Brown Adipose Tissue by a β3-Adrenergic Receptor Agonist," *Cell Metabolism,* vol. 21, pp. 33-38, 2015.
[126] M. Klingenberg and S.-G. Huang, "Structure and function of the uncoupling protein from brown adipose tissue," *Biochimica et Biophysica Acta (BBA) - Biomembranes,* vol. 1415, pp. 271-296, 1999.
[127] D. Ricquier, "UCP1, the mitochondrial uncoupling protein of brown adipocyte: A personal contribution and a historical perspective," *Biochimie,* vol. 134, pp. 3-8, 2017.
[128] J. Orava, P. Nuutila, Martin E. Lidell, V. Oikonen, T. Noponen, T. Viljanen*, et al.*, "Different Metabolic Responses of Human Brown Adipose Tissue to Activation by Cold and Insulin," *Cell Metabolism,* vol. 14, pp. 272-279, 2011.
[129] V. Ouellet, S. M. Labbe, D. P. Blondin, S. Phoenix, B. Guerin, F. Haman*, et al.*, "Brown adipose tissue oxidative metabolism contributes to energy expenditure during acute cold exposure in humans," *Journal of Clinical Investigation,* vol. 122, pp. 545-552, Feb 2012.
[130] K. L. Townsend and Y.-H. Tseng, "Brown fat fuel utilization and thermogenesis," *Trends in Endocrinology & Metabolism,* vol. 25, pp. 168-177, 2014.
[131] T. Yoneshiro, Q. Wang, K. Tajima, M. Matsushita, H. Maki, K. Igarashi*, et al.*, "BCAA catabolism in brown fat controls energy homeostasis through SLC25A44," *Nature,* vol. 572, pp. 614-+, Aug 29 2019.
[132] H. M. Feldmann, V. Golozoubova, B. Cannon, and J. Nedergaard, "UCP1 Ablation Induces Obesity and Abolishes Diet-Induced Thermogenesis in Mice Exempt from Thermal Stress by Living at Thermoneutrality," *Cell Metabolism,* vol. 9, pp. 203-209, 2009.
[133] L. Z. Sharp, K. Shinoda, H. Ohno, D. W. Scheel, E. Tomoda, L. Ruiz*, et al.*, "Human BAT Possesses Molecular Signatures That Resemble Beige/Brite Cells," *Plos One,* vol. 7, Nov 16 2012.
[134] J. Wu, P. Bostrom, L. M. Sparks, L. Ye, J. H. Choi, A. H. Giang*, et al.*, "Beige Adipocytes Are a Distinct Type of Thermogenic Fat Cell in Mouse and Human," *Cell,* vol. 150, pp. 366-376, Jul 20 2012.
[135] Naja Z. Jespersen, Therese J. Larsen, L. Peijs, S. Daugaard, P. Homøe, A. Loft*, et al.*, "A Classical Brown Adipose Tissue mRNA Signature Partly Overlaps with Brite in the Supraclavicular Region of Adult Humans," *Cell Metabolism,* vol. 17, pp. 798-805, 2013.
[136] R. D. Xue, M. D. Lynes, J. M. Dreyfuss, F. Shamsi, T. J. Schulz, H. B. Zhang*, et al.*, "Clonal analyses and gene profiling identify genetic biomarkers of the thermogenic potential of human brown and white preadipocytes," *Nature Medicine,* vol. 21, pp. 760-+, Jul 2015.
[137] N. Z. Jespersen, A. Feizi, E. S. Andersen, S. Heywood, H. B. Hattel, S. Daugaard*, et al.*, "Heterogeneity in the perirenal region of humans suggests presence of dormant brown adipose tissue that contains brown fat precursor cells," *Molecular Metabolism,* vol. 24, pp. 30-43, Jun 2019.

[138] N. Z. Jespersen, T. J. Larsen, L. Peijs, S. Daugaard, P. Homoe, A. Loft*, et al.*, "A Classical Brown Adipose Tissue mRNA Signature Partly Overlaps with Brite in the Supraclavicular Region of Adult Humans," *Cell Metabolism,* vol. 17, pp. 798-805, May 7 2013.
[139] J. Nedergaard and B. Cannon, "How brown is brown fat? It depends where you look," *Nature Medicine,* vol. 19, pp. 540-541, 2013.
[140] A. M. Cypess, A. P. White, C. Vemochet, T. J. Schulz, R. D. Xue, C. A. Sass*, et al.*, "Anatomical localization, gene expression profiling and functional characterization of adult human neck brown fat," *Nature Medicine,* vol. 19, pp. 635-639, May 2013.
[141] P. Seale, B. Bjork, W. L. Yang, S. Kajimura, S. Chin, S. H. Kuang*, et al.*, "PRDM16 controls a brown fat/skeletal muscle switch," *Nature,* vol. 454, pp. 961-U27, Aug 21 2008.
[142] A. Song, W. Dai, M. J. Jang, L. Medrano, Z. Li, H. Zhao*, et al.*, "Low- and high-thermogenic brown adipocyte subpopulations coexist in murine adipose tissue," *Journal of Clinical Investigation,* vol. 130, pp. 247-257, 2019.
[143] B. Cannon and J. Nedergaard, "Nonshivering thermogenesis and its adequate measurement in metabolic studies," *Journal of Experimental Biology,* vol. 214, pp. 242-253, 2010.
[144] M. Harms and P. Seale, "Brown and beige fat: development, function and therapeutic potential," *Nature Medicine,* vol. 19, pp. 1252-1263, Oct 2013.
[145] W. Wang and P. Seale, "Control of brown and beige fat development," *Nature Reviews Molecular Cell Biology,* vol. 17, pp. 691-702, 2016.
[146] T. Yoneshiro, S. Aita, M. Matsushita, T. Kayahara, T. Kameya, Y. Kawai*, et al.*, "Recruited brown adipose tissue as an antiobesity agent in humans," *Journal of Clinical Investigation,* vol. 123, pp. 3404-3408, Aug 2013.
[147] J. Wu, P. Bostrom, L. M. Sparks, L. Ye, J. H. Choi, A. H. Giang*, et al.*, "Beige adipocytes are a distinct type of thermogenic fat cell in mouse and human," *Cell,* vol. 150, pp. 366-76, Jul 20 2012.
[148] N. J. Rothwell and M. J. Stock, "Effects of denervating brown adipose tissue on the responses to cold, hyperphagia and noradrenaline treatment in the rat," *The Journal of Physiology,* vol. 355, pp. 457-463, 1984.
[149] A. Takahashi, T. Shimazu, and Y. Maruyama, "Importance of Sympathetic-Nerves for the Stimulatory Effect of Cold-Exposure on Glucose-Utilization in Brown Adipose-Tissue," *Japanese Journal of Physiology,* vol. 42, pp. 653-664, 1992.
[150] A. Vitali, I. Murano, M. C. Zingaretti, A. Frontini, D. Ricquier, and S. Cinti, "The adipose organ of obesity-prone C57BL/6J mice is composed of mixed white and brown adipocytes," *Journal of Lipid Research,* vol. 53, pp. 619-629, Apr 2012.
[151] A. Asano, M. Morimatsu, H. Nikami, T. Yoshida, and M. Saito, "Adrenergic activation of vascular endothelial growth factor mRNA expression in rat brown adipose tissue: implication in cold-induced angiogenesis," *Biochemical Journal,* vol. 328, pp. 179-183, Nov 15 1997.
[152] J. M. Fredriksson, H. Nikami, and J. Nedergaard, "Cold-induced expression of the VEGF gene in brown adipose tissue is independent of thermogenic oxygen consumption," *Febs Letters,* vol. 579, pp. 5680-5684, Oct 24 2005.
[153] M. Bagchi, L. A. Kim, J. Boucher, T. E. Walshe, C. R. Kahn, and P. A. D'Amore, "Vascular endothelial growth factor is important for brown

adipose tissue development and maintenance," *Faseb Journal,* vol. 27, pp. 3257-3271, Aug 2013.

[154] I. Elias, S. Franckhauser, T. Ferre, L. Vila, S. Tafuro, S. Munoz*, et al.*, "Adipose Tissue Overexpression of Vascular Endothelial Growth Factor Protects Against Diet-Induced Obesity and Insulin Resistance," *Diabetes,* vol. 61, pp. 1801-1813, 2012.

[155] I. Shimizu, T. Aprahamian, R. Kikuchi, A. Shimizu, K. N. Papanicolaou, S. MacLauchlan*, et al.*, "Vascular rarefaction mediates whitening of brown fat in obesity," *Journal of Clinical Investigation,* vol. 124, pp. 2099-2112, 2014.

[156] W. P. Cawthorn, F. Heyd, K. Hegyi, and J. K. Sethi, "Tumour necrosis factor-α inhibits adipogenesis via a β-catenin/TCF4(TCF7L2)-dependent pathway," *Cell Death & Differentiation,* vol. 14, pp. 1361-1373, 2007.

[157] E. Nisoli, L. Briscini, A. Giordano, C. Tonello, S. M. Wiesbrock, K. T. Uysal*, et al.*, "Tumor necrosis factor alpha mediates apoptosis of brown adipocytes and defective brown adipocyte function in obesity," *Proceedings of the National Academy of Sciences,* vol. 97, pp. 8033-8038, 2000.

[158] C. N. Lumeng, J. B. DelProposto, D. J. Westcott, and A. R. Saltiel, "Phenotypic Switching of Adipose Tissue Macrophages With Obesity Is Generated by Spatiotemporal Differences in Macrophage Subtypes," *Diabetes,* vol. 57, pp. 3239-3246, Dec 2008.

[159] D. Wu, A. B. Molofsky, H. E. Liang, R. R. Ricardo-Gonzalez, H. A. Jouihan, J. K. Bando*, et al.*, "Eosinophils Sustain Adipose Alternatively Activated Macrophages Associated with Glucose Homeostasis," *Science,* vol. 332, pp. 243-247, Apr 8 2011.

[160] M. W. Lee, J. I. Odegaard, L. Mukundan, Y. F. Qiu, A. B. Molofsky, J. C. Nussbaum*, et al.*, "Activated Type 2 Innate Lymphoid Cells Regulate Beige Fat Biogenesis," *Cell,* vol. 160, pp. 74-87, Jan 15 2015.

[161] J. R. Brestoff, B. S. Kim, S. A. Saenz, R. R. Stine, L. A. Monticelli, G. F. Sonnenberg*, et al.*, "Group 2 innate lymphoid cells promote beiging of white adipose tissue and limit obesity," *Nature,* vol. 519, pp. 242-+, Mar 12 2015.

[162] F. Alessandrini, H. Schulz, S. Takenaka, B. Lentner, E. Karg, H. Behrendt*, et al.*, "Effects of ultrafine carbon particle inhalation on allergic inflammation of the lung," *J Allergy Clin Immunol,* vol. 117, pp. 824-30, Apr 2006.

[163] A. Feuchtinger, T. Stiehler, U. Jutting, G. Marjanovic, B. Luber, R. Langer*, et al.*, "Image analysis of immunohistochemistry is superior to visual scoring as shown for patient outcome of esophageal adenocarcinoma," *Histochem Cell Biol,* vol. 143, pp. 1-9, Jan 2015.

[164] T. B. Haack, R. Kopajtich, P. Freisinger, T. Wieland, J. Rorbach, T. J. Nicholls*, et al.*, "ELAC2 mutations cause a mitochondrial RNA processing defect associated with hypertrophic cardiomyopathy," *Am J Hum Genet,* vol. 93, pp. 211-23, Aug 8 2013.

[165] A. Dobin, C. A. Davis, F. Schlesinger, J. Drenkow, C. Zaleski, S. Jha*, et al.*, "STAR: ultrafast universal RNA-seq aligner," *Bioinformatics,* vol. 29, pp. 15-21, Jan 1 2013.

[166] S. Anders, P. T. Pyl, and W. Huber, "HTSeq--a Python framework to work with high-throughput sequencing data," *Bioinformatics,* vol. 31, pp. 166-9, Jan 15 2015.

[167] M. I. Love, W. Huber, and S. Anders, "Moderated estimation of fold change and dispersion for RNA-seq data with DESeq2," *Genome Biol,* vol. 15, p. 550, 2014.
[168] F. A. Wolf, P. Angerer, and F. J. Theis, "SCANPY: large-scale single-cell gene expression data analysis," *Genome Biol,* vol. 19, p. 15, Feb 6 2018.
[169] M. Belkin, Niyogi, P., "Laplacian Eigenmaps for Dimensionality Reducation and Data Representation," *Neural Computation,* vol. 15, pp. 1373-1396, 2003.
[170] B. N. Melgert, D. S. Postma, I. Kuipers, M. Geerlings, M. A. Luinge, B. W. van der Strate*, et al.*, "Female mice are more susceptible to the development of allergic airway inflammation than male mice," *Clin Exp Allergy,* vol. 35, pp. 1496-503, Nov 2005.
[171] Y. S. Yang, M. J. Yang, K. H. Cho, K. Lee, Y. B. Kim, J. S. Kim*, et al.*, "Study of a BALB/c Mouse Model for Allergic Asthma," *Toxicol Res,* vol. 24, pp. 253-261, Dec 2008.
[172] A. T. Nials and S. Uddin, "Mouse models of allergic asthma: acute and chronic allergen challenge," *Dis Model Mech,* vol. 1, pp. 213-20, Nov-Dec 2008.
[173] S. Oeder, F. Alessandrini, O. F. Wirz, A. Braun, M. Wimmer, U. Frank*, et al.*, "Pollen-derived nonallergenic substances enhance Th2-induced IgE production in B cells," *Allergy,* vol. 70, pp. 1450-60, Nov 2015.
[174] S. Nishikawa, A. Yasoshima, K. Doi, H. Nakayama, and K. Uetsuka, "Involvement of sex, strain and age factors in high fat diet-induced obesity in C57BL/6J and BALB/cA mice," *Exp Anim,* vol. 56, pp. 263-72, Jul 2007.
[175] J. Li, H. Wu, Y. Liu, and L. Yang, "High fat diet induced obesity model using four strainsof mice: Kunming, C57BL/6, BALB/c and ICR," *Exp Anim,* vol. 69, pp. 326-335, Aug 5 2020.
[176] M. K. Montgomery, N. L. Hallahan, S. H. Brown, M. Liu, T. W. Mitchell, G. J. Cooney*, et al.*, "Mouse strain-dependent variation in obesity and glucose homeostasis in response to high-fat feeding," *Diabetologia,* vol. 56, pp. 1129-39, May 2013.
[177] I. P. Fischer, M. Irmler, C. W. Meyer, S. J. Sachs, F. Neff, M. Hrabe de Angelis*, et al.*, "A history of obesity leaves an inflammatory fingerprint in liver and adipose tissue," *Int J Obes (Lond),* vol. 42, pp. 507-517, Mar 2018.
[178] S. Andrikopoulos, A. R. Blair, N. Deluca, B. C. Fam, and J. Proietto, "Evaluating the glucose tolerance test in mice," *Am J Physiol Endocrinol Metab,* vol. 295, pp. E1323-32, Dec 2008.
[179] M. Bielohuby, S. Sisley, D. Sandoval, N. Herbach, A. Zengin, M. Fischereder*, et al.*, "Impaired glucose tolerance in rats fed low-carbohydrate, high-fat diets," *Am J Physiol Endocrinol Metab,* vol. 305, pp. E1059-70, Nov 1 2013.
[180] J. H. Ellenbroek, L. van Dijck, H. A. Tons, T. J. Rabelink, F. Carlotti, B. E. Ballieux*, et al.*, "Long-term ketogenic diet causes glucose intolerance and reduced beta- and alpha-cell mass but no weight loss in mice," *Am J Physiol Endocrinol Metab,* vol. 306, pp. E552-8, Mar 1 2014.
[181] M. S. Winzell and B. Ahren, "The high-fat diet-fed mouse: a model for studying mechanisms and treatment of impaired glucose tolerance and type 2 diabetes," *Diabetes,* vol. 53 Suppl 3, pp. S215-9, Dec 2004.
[182] J. M. Poret, F. Souza-Smith, S. J. Marcell, D. A. Gaudet, T. H. Tzeng, H. D. Braymer*, et al.*, "High fat diet consumption differentially affects adipose

tissue inflammation and adipocyte size in obesity-prone and obesity-resistant rats," *Int J Obes (Lond),* vol. 42, pp. 535-541, Mar 2018.
[183] H. Kwon and J. E. Pessin, "Adipokines mediate inflammation and insulin resistance," *Front Endocrinol (Lausanne),* vol. 4, p. 71, 2013.
[184] N. Ouchi, J. L. Parker, J. J. Lugus, and K. Walsh, "Adipokines in inflammation and metabolic disease," *Nat Rev Immunol,* vol. 11, pp. 85-97, Feb 2011.
[185] D. Wu, A. B. Molofsky, H. E. Liang, R. R. Ricardo-Gonzalez, H. A. Jouihan, J. K. Bando*, et al.*, "Eosinophils sustain adipose alternatively activated macrophages associated with glucose homeostasis," *Science,* vol. 332, pp. 243-7, Apr 8 2011.
[186] R. A. van der Heijden, F. Sheedfar, M. C. Morrison, P. P. Hommelberg, D. Kor, N. J. Kloosterhuis*, et al.*, "High-fat diet induced obesity primes inflammation in adipose tissue prior to liver in C57BL/6j mice," *Aging (Albany NY),* vol. 7, pp. 256-68, Apr 2015.
[187] L. G. Hersoug and A. Linneberg, "The link between the epidemics of obesity and allergic diseases: does obesity induce decreased immune tolerance?," *Allergy,* vol. 62, pp. 1205-13, Oct 2007.
[188] N. M. Lainez, C. R. Jonak, M. G. Nair, I. M. Ethell, E. H. Wilson, M. J. Carson*, et al.*, "Diet-Induced Obesity Elicits Macrophage Infiltration and Reduction in Spine Density in the Hypothalami of Male but Not Female Mice," *Front Immunol,* vol. 9, p. 1992, 2018.
[189] Y. Yang, D. L. Smith, Jr., K. D. Keating, D. B. Allison, and T. R. Nagy, "Variations in body weight, food intake and body composition after long-term high-fat diet feeding in C57BL/6J mice," *Obesity (Silver Spring),* vol. 22, pp. 2147-55, Oct 2014.
[190] L. L. Hwang, C. H. Wang, T. L. Li, S. D. Chang, L. C. Lin, C. P. Chen*, et al.*, "Sex differences in high-fat diet-induced obesity, metabolic alterations and learning, and synaptic plasticity deficits in mice," *Obesity (Silver Spring),* vol. 18, pp. 463-9, Mar 2010.
[191] I. J. Neeland, A. T. Turer, C. R. Ayers, T. M. Powell-Wiley, G. L. Vega, R. Farzaneh-Far*, et al.*, "Dysfunctional adiposity and the risk of prediabetes and type 2 diabetes in obese adults," *JAMA,* vol. 308, pp. 1150-9, Sep 19 2012.
[192] J. Lu, J. Zhao, H. Meng, and X. Zhang, "Adipose Tissue-Resident Immune Cells in Obesity and Type 2 Diabetes," *Front Immunol,* vol. 10, p. 1173, 2019.
[193] Ivanov, II, B. S. McKenzie, L. Zhou, C. E. Tadokoro, A. Lepelley, J. J. Lafaille*, et al.*, "The orphan nuclear receptor RORgammat directs the differentiation program of proinflammatory IL-17+ T helper cells," *Cell,* vol. 126, pp. 1121-33, Sep 22 2006.
[194] J. Zhu, H. Yamane, J. Cote-Sierra, L. Guo, and W. E. Paul, "GATA-3 promotes Th2 responses through three different mechanisms: induction of Th2 cytokine production, selective growth of Th2 cells and inhibition of Th1 cell-specific factors," *Cell Res,* vol. 16, pp. 3-10, Jan 2006.
[195] S. Thunberg, G. Gafvelin, M. Nord, R. Gronneberg, J. Grunewald, A. Eklund*, et al.*, "Allergen provocation increases TH2-cytokines and FOXP3 expression in the asthmatic lung," *Allergy,* vol. 65, pp. 311-8, Mar 2010.

[196] C. N. Lumeng, J. L. Bodzin, and A. R. Saltiel, "Obesity induces a phenotypic switch in adipose tissue macrophage polarization," *J Clin Invest,* vol. 117, pp. 175-84, Jan 2007.
[197] M. C. Petersen, D. F. Vatner, and G. I. Shulman, "Regulation of hepatic glucose metabolism in health and disease," *Nat Rev Endocrinol,* vol. 13, pp. 572-587, Oct 2017.
[198] M. Harms and P. Seale, "Brown and beige fat: development, function and therapeutic potential," *Nat Med,* vol. 19, pp. 1252-63, Oct 2013.
[199] B. Cannon and J. Nedergaard, "Brown adipose tissue: function and physiological significance," *Physiol Rev,* vol. 84, pp. 277-359, Jan 2004.
[200] L. Burysek and J. Houstek, "beta-Adrenergic stimulation of interleukin-1alpha and interleukin-6 expression in mouse brown adipocytes," *FEBS Lett,* vol. 411, pp. 83-6, Jul 7 1997.
[201] B. J. Nieves, P. A. D'Amore, and B. A. Bryan, "The function of vascular endothelial growth factor," *BioFactors,* vol. 35, pp. 332-337, 2009.
[202] L. Kazak and P. Cohen, "Creatine metabolism: energy homeostasis, immunity and cancer biology," *Nature Reviews Endocrinology,* vol. 16, pp. 421-436, 2020.
[203] A. M. Cypess and C. R. Kahn, "The role and importance of brown adipose tissue in energy homeostasis," *Curr Opin Pediatr,* vol. 22, pp. 478-84, Aug 2010.
[204] C. Porter, D. N. Herndon, M. Chondronikola, T. Chao, P. Annamalai, N. Bhattarai*, et al.*, "Human and Mouse Brown Adipose Tissue Mitochondria Have Comparable UCP1 Function," *Cell Metab,* vol. 24, pp. 246-55, Aug 9 2016.
[205] A. Song, W. Dai, M. J. Jang, L. Medrano, Z. Li, H. Zhao*, et al.*, "Low- and high-thermogenic brown adipocyte subpopulations coexist in murine adipose tissue," *J Clin Invest,* vol. 130, pp. 247-257, Jan 2 2020.
[206] Z. Wu, P. Puigserver, and B. M. Spiegelman, "Transcriptional activation of adipogenesis," *Curr Opin Cell Biol,* vol. 11, pp. 689-94, Dec 1999.
[207] A. Than, H. L. He, S. H. Chua, D. Xu, L. Sun, M. K. Leow*, et al.*, "Apelin Enhances Brown Adipogenesis and Browning of White Adipocytes," *J Biol Chem,* vol. 290, pp. 14679-91, Jun 5 2015.
[208] Y. Onogi, A. Khalil, and S. Ussar, "Identification and characterization of adipose surface epitopes," *Biochem J,* vol. 477, pp. 2509-2541, Jul 17 2020.
[209] S. E. Ross, N. Hemati, K. A. Longo, C. N. Bennett, P. C. Lucas, R. L. Erickson*, et al.*, "Inhibition of adipogenesis by Wnt signaling," *Science,* vol. 289, pp. 950-3, Aug 11 2000.
[210] W. Pawlina, L. H. Larkin, S. Ogilvie, and S. C. Frost, "Human relaxin inhibits division but not differentiation of 3T3-L1 cells," *Mol Cell Endocrinol,* vol. 72, pp. 55-61, Jul 30 1990.
[211] Y. Cheng, L. Jiang, S. Keipert, S. Zhang, A. Hauser, E. Graf*, et al.*, "Prediction of Adipose Browning Capacity by Systematic Integration of Transcriptional Profiles," *Cell Rep,* vol. 23, pp. 3112-3125, Jun 5 2018.
[212] C. W. Baffi, D. E. Winnica, and F. Holguin, "Asthma and obesity: mechanisms and clinical implications," *Asthma Res Pract,* vol. 1, p. 1, 2015.
[213] F. M. Rackemann, "A working classification of asthma," *The American Journal of Medicine,* vol. 3, pp. 601-606, 1947.

[214] S. Romanet-Manent, D. Charpin, A. Magnan, A. Lanteaume, and D. Vervloet, "Allergicvsnonallergic asthma: what makes the difference?," *Allergy,* vol. 57, pp. 607-613, 2002.

[215] M. Humbert, S. R. Durham, S. Ying, P. Kimmitt, J. Barkans, B. Assoufi*, et al.*, "IL-4 and IL-5 mRNA and protein in bronchial biopsies from patients with atopic and nonatopic asthma: evidence against "intrinsic" asthma being a distinct immunopathologic entity," *American Journal of Respiratory and Critical Care Medicine,* vol. 154, pp. 1497-1504, 1996.

[216] M. Humbert, J. A. Grant, L. Taborda-Barata, S. R. Durham, R. Pfister, G. Menz*, et al.*, "High-affinity IgE receptor (FcepsilonRI)-bearing cells in bronchial biopsies from atopic and nonatopic asthma," *American Journal of Respiratory and Critical Care Medicine,* vol. 153, pp. 1931-1937, 1996.

[217] C. Miranda, A. Busacker, S. Balzar, J. Trudeau, and S. E. Wenzel, "Distinguishing severe asthma phenotypes☆Role of age at onset and eosinophilic inflammation," *Journal of Allergy and Clinical Immunology,* vol. 113, pp. 101-108, 2004.

[218] B. N. Melgert, D. S. Postma, I. Kuipers, M. Geerlings, M. A. Luinge, B. W. A. Strate*, et al.*, "Female mice are more susceptible to the development of allergic airway inflammation than male mice," *Clinical <html_ent glyph="@amp;" ascii="&"/> Experimental Allergy,* vol. 35, pp. 1496-1503, 2005.

[219] K. M. de Winter–de Groot, C. K. van der Ent, I. Prins, J. M. Tersmette, and C. S. P. M. Uiterwaal, "Exhaled nitric oxide: The missing link between asthma and obesity?," *Journal of Allergy and Clinical Immunology,* vol. 115, pp. 419-420, 2005.

[220] B. Ryffel, V. P. Singh, R. Aggarwal, S. Singh, A. Banik, T. Ahmad*, et al.*, "Metabolic Syndrome Is Associated with Increased Oxo-Nitrative Stress and Asthma-Like Changes in Lungs," *Plos One,* vol. 10, p. e0129850, 2015.

[221] J. Diaz, L. Warren, L. Helfner, X. Xue, P. K. Chatterjee, M. Gupta*, et al.*, "Obesity shifts house dust mite-induced airway cellular infiltration from eosinophils to macrophages: effects of glucocorticoid treatment," *Immunologic Research,* vol. 63, pp. 197-208, 2015.

[222] V. P. Singh, U. Mabalirajan, K. Pratap, D. Bahal, D. Maheswari, A. Gheware*, et al.*, "House dust mite allergen causes certain features of steroid resistant asthma in high fat fed obese mice," *International Immunopharmacology,* vol. 55, pp. 20-27, 2018.

[223] L. Everaere, S. Ait-Yahia, O. Molendi-Coste, H. Vorng, S. Quemener, P. LeVu*, et al.*, "Innate lymphoid cells contribute to allergic airway disease exacerbation by obesity," *Journal of Allergy and Clinical Immunology,* vol. 138, pp. 1309-1318.e11, 2016.

[224] K. Raemdonck, K. Baker, N. Dale, E. Dubuis, F. Shala, M. G. Belvisi*, et al.*, "CD4+ and CD8+ T cells play a central role in a HDM driven model of allergic asthma," *Respiratory Research,* vol. 17, 2016.

[225] A. van Huisstede, A. Rudolphus, A. van Schadewijk, M. C. Cabezas, G. H. H. Mannaerts, C. Taube*, et al.*, "Bronchial and Systemic Inflammation in Morbidly Obese Subjects with Asthma: A Biopsy Study," *American Journal of Respiratory and Critical Care Medicine,* vol. 190, pp. 951-954, Oct 15 2014.

[226] S. J. Bracken, A. J. Adami, S. M. Szczepanek, M. Ehsan, P. Natarajan, L. A. Guernsey*, et al.*, "Long-Term Exposure to House Dust Mite Leads to the Suppression of Allergic Airway Disease Despite Persistent Lung Inflammation," *International Archives of Allergy and Immunology,* vol. 166, pp. 243-258, 2015.

[227] R. Bagadood, C. Stover, and Y. Amrani, "Obesity enhances allergen-induced airway inflammation in a murine model of asthma," p. PA4361, 2019.

[228] T. Schröder, A. V. Wiese, F. Ender, K. M. Quell, T. Vollbrandt, J. Duhn*, et al.*, "Short‐term high‐fat diet feeding protects from the development of experimental allergic asthma in mice," *Clinical & Experimental Allergy,* vol. 49, pp. 1245-1257, 2019.

[229] M. Peters, S. Kohler-Bachmann, T. Lenz-Habijan, and A. Bufe, "Influence of an Allergen-Specific Th17 Response on Remodeling of the Airways," *American Journal of Respiratory Cell and Molecular Biology,* vol. 54, pp. 350-358, Mar 2016.

[230] H. Hayashi, A. Kawakita, S. Okazaki, M. Yasutomi, H. Murai, and Y. Ohshima, "IL-17A/F Modulates Fibrocyte Functions in Cooperation with CD40-Mediated Signaling," *Inflammation,* vol. 36, pp. 830-838, Aug 2013.

[231] W. T. Xia, J. Bai, X. M. Wu, Y. Wei, S. Y. Feng, L. Li*, et al.*, "Interleukin-17A Promotes MUC5AC Expression and Goblet Cell Hyperplasia in Nasal Polyps via the Act1-Mediated Pathway," *Plos One,* vol. 9, Jun 3 2014.

[232] D. C. Newcomb and R. S. Peebles, "Th17-mediated inflammation in asthma," *Current Opinion in Immunology,* vol. 25, pp. 755-760, 2013.

[233] K. Hosoki, T. Itazawa, I. Boldogh, and S. Sur, "Neutrophil recruitment by allergens contribute to allergic sensitization and allergic inflammation," *Current Opinion in Allergy and Clinical Immunology,* vol. 16, pp. 45-50, 2016.

[234] L. L. Kordonowy, E. Burg, C. C. Lenox, L. M. Gauthier, J. M. Petty, M. Antkowiak*, et al.*, "Obesity Is Associated with Neutrophil Dysfunction and Attenuation of Murine Acute Lung Injury," *American Journal of Respiratory Cell and Molecular Biology,* vol. 47, pp. 120-127, 2012.

[235] N. D. J. Ubags, E. Burg, M. Antkowiak, A. M. Wallace, E. Dilli, J. Bement*, et al.*, "A Comparative Study of Lung Host Defense in Murine Obesity Models. Insights into Neutrophil Function," *American Journal of Respiratory Cell and Molecular Biology,* vol. 55, pp. 188-200, 2016.

[236] C. D. Kassotis, K. Hoffman, and H. M. Stapleton, "Characterization of Adipogenic Activity of House Dust Extracts and Semi-Volatile Indoor Contaminants in 3T3-L1 Cells," *Environmental Science & Technology,* vol. 51, pp. 8735-8745, 2017.

[237] S. P. Weisberg, D. McCann, M. Desai, M. Rosenbaum, R. L. Leibel, and A. W. Ferrante, "Obesity is associated with macrophage accumulation in adipose tissue," *Journal of Clinical Investigation,* vol. 112, pp. 1796-1808, Dec 2003.

[238] S. Talukdar, D. Y. Oh, G. Bandyopadhyay, D. Li, J. Xu, J. McNelis*, et al.*, "Neutrophils mediate insulin resistance in mice fed a high-fat diet through secreted elastase," *Nature Medicine,* vol. 18, pp. 1407-1412, 2012.

[239] G. S. Hotamisligil, D. L. Murray, L. N. Choy, and B. M. Spiegelman, "Tumor necrosis factor alpha inhibits signaling from the insulin receptor," *Proceedings of the National Academy of Sciences,* vol. 91, pp. 4854-4858, 1994.
[240] M. Hoene and C. Weigert, "The role of interleukin-6 in insulin resistance, body fat distribution and energy balance," *Obesity Reviews,* vol. 0, pp. 071024234852001-???, 2007.
[241] F. Bril, D. Barb, P. Portillo-Sanchez, D. Biernacki, R. Lomonaco, A. Suman*, et al.*, "Metabolic and histological implications of intrahepatic triglyceride content in nonalcoholic fatty liver disease," *Hepatology,* vol. 65, pp. 1132-1144, 2017.
[242] S. Bevilacqua, R. Bonadonna, G. Buzzigoli, C. Boni, D. Ciociaro, F. Maccari*, et al.*, "Acute elevation of free fatty acid levels leads to hepatic insulin resistance in obese subjects," *Metabolism,* vol. 36, pp. 502-506, 1987.
[243] G. Boden, P. She, M. Mozzoli, P. Cheung, K. Gumireddy, P. Reddy*, et al.*, "Free Fatty Acids Produce Insulin Resistance and Activate the Proinflammatory Nuclear Factor- B Pathway in Rat Liver," *Diabetes,* vol. 54, pp. 3458-3465, 2005.
[244] A. Alisi, T. Tang, Y. Sui, M. Lian, Z. Li, and J. Hua, "Pro-Inflammatory Activated Kupffer Cells by Lipids Induce Hepatic NKT Cells Deficiency through Activation-Induced Cell Death," *PLoS ONE,* vol. 8, p. e81949, 2013.
[245] J. Wu, P. Cohen, and B. M. Spiegelman, "Adaptive thermogenesis in adipocytes: Is beige the new brown?," *Genes & Development,* vol. 27, pp. 234-250, 2013.
[246] S. Jash, S. Banerjee, M.-J. Lee, S. R. Farmer, and V. Puri, "CIDEA Transcriptionally Regulates UCP1 for Britening and Thermogenesis in Human Fat Cells," *iScience,* vol. 20, pp. 73-89, 2019.
[247] P. Cohen, Julia D. Levy, Y. Zhang, A. Frontini, Dmitriy P. Kolodin, Katrin J. Svensson*, et al.*, "Ablation of PRDM16 and Beige Adipose Causes Metabolic Dysfunction and a Subcutaneous to Visceral Fat Switch," *Cell,* vol. 156, pp. 304-316, 2014.
[248] X. Song, B. Li, H. Wang, X. Zou, R. Gao, W. Zhang*, et al.*, "Asthma alleviates obesity in males through regulating metabolism and energy expenditure," *Biochimica et Biophysica Acta (BBA) - Molecular Basis of Disease,* vol. 1865, pp. 350-359, 2019.
[249] X. Zhang, Q. X. Zhang, X. Wang, L. Zhang, W. Qu, B. Bao*, et al.*, "Dietary luteolin activates browning and thermogenesis in mice through an AMPK/PGC1α pathway-mediated mechanism," *International Journal of Obesity,* vol. 40, pp. 1841-1849, 2016.
[250] A. M. Cypess and C. R. Kahn, "Brown fat as a therapy for obesity and diabetes," *Current Opinion in Endocrinology, Diabetes and Obesity,* vol. 17, pp. 143-149, 2010.
[251] S. H. Kim and J. Plutzky, "Brown Fat and Browning for the Treatment of Obesity and Related Metabolic Disorders," *Diabetes & Metabolism Journal,* vol. 40, p. 12, 2016.
[252] R. P. da Silva, K. Clow, J. T. Brosnan, and M. E. Brosnan, "Synthesis of guanidinoacetate and creatine from amino acids by rat pancreas," *British Journal of Nutrition,* vol. 111, pp. 571-577, 2013.

[253] L. Kazak, E. T. Chouchani, G. Z. Lu, M. P. Jedrychowski, C. J. Bare, A. I. Mina*, et al.*, "Genetic Depletion of Adipocyte Creatine Metabolism Inhibits Diet-Induced Thermogenesis and Drives Obesity," *Cell Metabolism,* vol. 26, pp. 660-671.e3, 2017.

[254] L. Kazak, Edward T. Chouchani, Mark P. Jedrychowski, Brian K. Erickson, K. Shinoda, P. Cohen*, et al.*, "A Creatine-Driven Substrate Cycle Enhances Energy Expenditure and Thermogenesis in Beige Fat," *Cell,* vol. 163, pp. 643-655, 2015.

[255] M. Bagchi, L. A. Kim, J. Boucher, T. E. Walshe, C. R. Kahn, and P. A. D'Amore, "Vascular endothelial growth factor is important for brown adipose tissue development and maintenance," *The FASEB Journal,* vol. 27, pp. 3257-3271, 2013.

[256] O. S. Dallner, E. Chernogubova, K. A. Brolinson, and T. Bengtsson, "β3-Adrenergic Receptors Stimulate Glucose Uptake in Brown Adipocytes by Two Mechanisms Independently of Glucose Transporter 4 Translocation," *Endocrinology,* vol. 147, pp. 5730-5739, 2006.

[257] S. Huang and M. P. Czech, "The GLUT4 Glucose Transporter," *Cell Metabolism,* vol. 5, pp. 237-252, 2007.

[258] K. Shinoda, I. H. N. Luijten, Y. Hasegawa, H. Hong, S. B. Sonne, M. Kim*, et al.*, "Genetic and functional characterization of clonally derived adult human brown adipocytes," *Nature Medicine,* vol. 21, pp. 389-+, Apr 2015.

[259] S. Ussar, K. Y. Lee, S. N. Dankel, J. Boucher, M.-F. Haering, A. Kleinridders*, et al.*, "ASC-1, PAT2, and P2RX5 are cell surface markers for white, beige, and brown adipocytes," *Science Translational Medicine,* vol. 6, pp. 247ra103-247ra103, 2014.

[260] D. T. Peterson, Safer, B., Merrick, W.C., "Role of eukaryotic initiation factor 5 in the formation of 80 S initiation complexes," *J Biol Chem,* vol. 254, pp. 7730-7735, 1979.

[261] H. Trachsel and T. Staehelin, "Initiation of mammalian protein synthesis The multiple functions of the initiation factor eIF-3," *Biochimica et Biophysica Acta (BBA) - Nucleic Acids and Protein Synthesis,* vol. 565, pp. 305-314, 1979.

[262] J. E. Lee, "Basic helix-loop-helix genes in neural development," *Current Opinion in Neurobiology,* vol. 7, pp. 13-20, 1997.

[263] M. Olsson, M. Durbeej, P. Ekblom, and T. Hjalt, "Nulp1, a novel basic helix-loop-helix protein expressed broadly during early embryonic organogenesis and prominently in developing dorsal root ganglia," *Cell and Tissue Research,* vol. 308, pp. 361-370, Jun 2002.

[264] R. J. Wechsler-Reya, K. J. Elliott, and G. C. Prendergast, "A role for the putative tumor suppressor Bin1 in muscle cell differentiation," *Molecular and Cellular Biology,* vol. 18, pp. 566-575, Jan 1998.

[265] X. Cui, N. L. T. Nguyen, E. Zarebidaki, Q. Cao, F. Li, L. Zha*, et al.*, "Thermoneutrality decreases thermogenic program and promotes adiposity in high-fat diet-fed mice," *Physiological Reports,* vol. 4, p. e12799, 2016.

[266] C. Porter, David N. Herndon, M. Chondronikola, T. Chao, P. Annamalai, N. Bhattarai*, et al.*, "Human and Mouse Brown Adipose Tissue Mitochondria Have Comparable UCP1 Function," *Cell Metabolism,* vol. 24, pp. 246-255, 2016.

References